University of Southern Queensland

USQ

PER STUDIA MENS NOVA

AUSTRALIA

Numerical Evaluation of the Performance of an Indirect Heating Integrated Collector Storage Solar Water Heating System

A Dissertation submitted by

Marwaan Awad Hamad AL-Khaffajy

B.Sc. Eng.

Supervised by

Dr. Ruth Mossad

Dr. Ahmad Sharifian-Barforoush

For the award of

Master of Engineering Research

Major Subject: Mechanical Engineering

Minor Subject: Thermal Fluid

2012

Abstract

Due to the impact of energy usage on the environment and the increase in the price of fossil fuel, people must be encouraged to use renewable energy sources such as solar energy, wind power, hydraulic energy, geothermal energy and biomass energy. The indirect heating integrated collector storage solar water heating system is one of the compact systems for domestic water heating. It incorporates a solar energy collection component and a hot water storage component into one unit. The indirect heating type is characterized by service water passing through a serpentine tube (a heat exchanger) that is immersed in the stored fluid. The objectives of this study were to investigate ways to reduce heat losses from the system and enhance heat gained by the service water with the aim of reducing both the initial and the running costs.

The continuity, momentum and energy equations were solved in a steady state condition, using ANSYS 13.0-FLUENT software and using the pressure-based type solver. The results for particular system using the realizable k-ϵ and standard k-ω turbulence models were compared to available experimental results to determine the appropriateness of the turbulence model choice. The percentage error for the numerical simulation of k-ϵ model was higher than for the k-ω model. The error varied between zero (no errors) and 15 per cent for k-ϵ, and zero to 8.5 per cent for k-ω model. The radiation heat transfer was also included by using a surface-to-surface radiation model.

To minimise the heat loss from the system, a parametric study was conducted in a system of double glass covers. The air gap spacing between the absorber and the lower glass cover (L_1) and the gap between the upper and lower glass covers (L_2) for the system were varied within the range of 15-50 mm to investigate which combination of gap sizes (L_1, L_2) would result in minimum total heat losses, i.e. including radiation and convection losses. Three-dimensional CFD models for the absorber, the double glass covers and the air in between (i.e. the storage and service water were not included) were developed. The results showed that when the gap size was small, the heat loss through the gap was mainly due to conduction, while as the gap size increased, the velocity of the air in the gap increased and this increased the convection contribution to the heat loss. The optimum lower gap spacing was found in the range of 15 and 20 mm, while the optimum upper gap was found in the range of 30 and 35 mm.

To enhance the heat gained by the service water, important parameters of the heat exchanger were investigated. These parameters are tube length, shape, positioning and the cross sectional area of the pipe. The tube length was 16.2 m for the double row heat exchanger and it was varied to 8.1 and 10.8 m for the single row heat exchanger. Circular and elliptical tubes were also examined. The mass flow rate was chosen as 500 and 650 L/h. The outlet service water temperature was used as a measure of the performance, since it is a measure of the energy acquired from the solar radiation. Three-dimensional CFD models were developed and validated using the experimental results of Gertzos, Pnevmatikakis and Caouris (2008). A standard k-ω turbulence model was used in the optimization of the heat exchanger because it gave good agreement with the experimental results.

The results showed an increase in the outlet temperature of the system, and a significant reduction in the initial and operating costs of the system. The outlet temperature of the elliptical tube system was higher than the circular tube of similar length and cross-sectional area. The single row heat exchanger (HX) with 10.8 m length and elliptical cross sectional area gave a high service water outlet temperature of 57.9^{o} C with low pumping power. The outlet temperature of the system with tube length of 10.8 m (single row heat exchanger) was higher than those of 16.2 m (double row heat exchanger). These resulted in an increase in the thermal performance and a significant reduction in both the initial and operating costs of the system.

The study was conducted in steady state condition assuming that the circulating water mass flow rate was 900 L/h, the storage water temperature was constant at 60^{o}C and for two service water inlet temperatures'; 15 and 20 ^{o} C.

Certification of Dissertation

I certify that the ideas, numerical work, results, analysis, and conclusions reported in this dissertation are entirely my own effort, except where otherwise acknowledged. I also certify that the work is original and has not been previously submitted for any award, except where otherwise acknowledged.

……………………………………. / /2012

Signature of candidature Date

Marwaan Awad Hamad AL-Khaffajy

ENDORSEMENT

……………………………………. / /2012

Signature of supervisor/s

Date

……………………………………. / /2012

Signature of supervisor/s Date

ACKNOWLEDGEMENT

This dissertation would not have been possible without the guidance, encouragement and support of several individuals who, in one way or another contributed and extended their valuable assistance in the preparation and completion of this study.

First and foremost I offer my sincerest gratitude to my father who passed away after four months of starting my study (after I arrived in Australia). He encouraged me to study my Master's degree and he was very proud of me telling his relatives and friends that "Marwaan started his study in a developed country". I would like to acknowledge my mother for her patience while I have been away from her for three years, and for her prayers to finish this work. I would like to acknowledge my wife and my daughter "Sadane" for their endless love, continuous support and encouragement. I gratefully acknowledge my brothers and sisters phoning me and asking about my progress day-by-day. I would like to express my special acknowledgment to my wife's family who supported and encouraged me to provide a valuable contribution to this field of research. I thank my friends in Australia and Iraq and my relatives. Special thanks go to all the Iraqi students at USQ who shared with me, from the early stages, their experience of study and life in Australia.

I would like to record my gratitude to Dr. Ruth Mossad for her supervision, advice, and guidance from the very early stage of this research as well as giving me extraordinary experiences throughout the work. I will always remember the time we spent on research and publications. I am indebted to her more than she knows.

Many thanks go, in particular, to my associate supervisor Dr. Ahmad Sharifian-Barforoush. I am much indebted to him for using his precious time to read this thesis and provide his critical comments.

I would also like to acknowledge the support of the Faculty of Engineering. Also, I thank FoES Associate Dean (Research) Assoc. Prof. Armando Apan and his assistant Juanita Ryan for their support. Many thanks go to the English for Academic Purposes programs staff at USQ who taught me the English language. I am indebted to Ms Angela Windsor, Dr. Lindsay Henderson, Mrs Rosemary Taylor and Dr Sang-Soon Park. Finally, my thanks go to Ms Sandra Cochrane, who helps me in editing the thesis.

Associated publications[1]

Journal papers

Mossad, R & Al-Khaffajy, M 2012, 'Investigating two configurations of a heat exchanger in an Indirect Heating Integrated Collector Storage Solar Water Heating System (IHICSSWHS)', *Renewable Energies and Power Quality*, vol. 10, no. 11, p. 716.

Journal paper under review

Al-Khaffajy, M & Mossad, R 2012, 'Optimization of the Heat Exchanger in an Indirect Heating Integrated Collector Storage Solar Water Heater System', *Renewable Energies*.

Refereed conference proceedings

AL-Khaffajy, M & Mossad, R 2011, 'Optimization of the Air Gap Spacing: in a Solar Water Heater with Double Glass Cover', paper presented to 9th Ausralasian Heat and Mass Transfer Conference - 9AHMTC, Monash University, Melbourne, Vectoria, Australia 2-4 November.

[1] Some of the above publications are available through USQ - *ePrint*: http://eprints.usq.edu.au/view/people/Al-Khaffajy=3AM=2E=3A=3A.html

Table of Content

CHAPTER 1: Introduction

CHAPTER 2: Literature Review and Research Gap

CHAPTER 3: Mathematical Model

CHAPTER 4: System Modifications using the CFD Approach

CHAPTER 5: Results and Discussion

CHAPTER 6: Conclusion

List of Figures

Chapter1: Introduction

Chapter 2: Literature Review and Research Gap

Chapter 3: Mathematical Model

Chapter 4: System Modifications Using the CFD Approach

Chapter 5: Results and Discussion

List of Tables

Nomenclature

English Symbols

a	Speed of sound
F_{jk}	View factor between surface j and k
g	Acceleration due to gravity
L_1	Lower air gap spacing
L_2	Upper air gap spacing
N	Number of surrounding faces in the radiation
M_t	Turbulent Mach number
p	Fluid pressure
Pr	Turbulent Prandtl number
$\dot{q}$	Heat flux due to radiation
$q_{in,k}$	Radiation energy flux incident on surface k from the surrounding surfaces
$q_{out,j}$	Radiation energy flux leaving surface j
Q_k	Heat transfer rate to unit k [W]
T_a	Ambient temperature
$\boldsymbol{U}$	Main fluid velocity
U_k	Overall heat transfer coefficient of unit k [W/ (m^2K)]
$\bar{\mathbf{V}}_j$	Tensor notation of mean velocity vector of the fluid

Greek symbols

μ	Viscosity
ρ	Density
$\boldsymbol{\rho}$	Reflectivity in the radiation
υ	Kinematic viscosity
β	Thermal expansion coefficient
k	Turbulent kinetic energy
ϵ	Turbulent dissipation
$\boldsymbol{\varepsilon}_k$	Emissivity of surface k in the radiation
u	Velocity component in x direction
v	Velocity component in y direction
w	Velocity component in z direction
$\bar{u}$	Mean velocity component in x direction
$\bar{v}$	Mean velocity component in y direction
$\bar{w}$	Mean velocity component in z direction
u', v' and w'	Components of the random velocities fluctuation in x, y and z direction
$\boldsymbol{\alpha}$	Absorptivity in the radiation
α	Thermal diffusivity
α^*	low-Reynolds number correction
$\boldsymbol{\sigma}$	Boltzmann's constant
σ_k	Turbulent Prandtl number for kinetic energy
f_x, f_y, f_z	X, Y, Z component of body force

$\overline{u_j' T'}$	Turbulent heat flux
$\rho\overline{V'}_i\overline{V'}_j$	Reynolds stresses tensor
S_k	kinetic energy source term
S_ε	Energy dissipation source term
$\overline{\Omega}_{ij}$	Mean rate of rotation tensor
Γ_k	Effective diffusivity of k
Γ_ω	effective diffusivity of ω

CHAPTER 1: Introduction

- ***Background***
- ***Solar Resources***
- ***Solar Collectors***
- ***Flat Plate Collectors***
- ***Integrated Collector Storage Solar Water Heating System***
- ***Research Focus and Scop***

1.1 Background

Energy resources are classified into two types: renewable resources including solar energy, wind power, hydraulic energy, geothermal energy and biomass energy, and non-renewable resources that cannot be replenished, such as petrol, nuclear energy, coal and natural gas. Figure 1.1 presents the world's energy consumption in 2006 by fuel type (286W 2009). The world's energy usage from non-renewable resources adds up to 91.88% while 8.12% of the energy is generated from renewable resources.

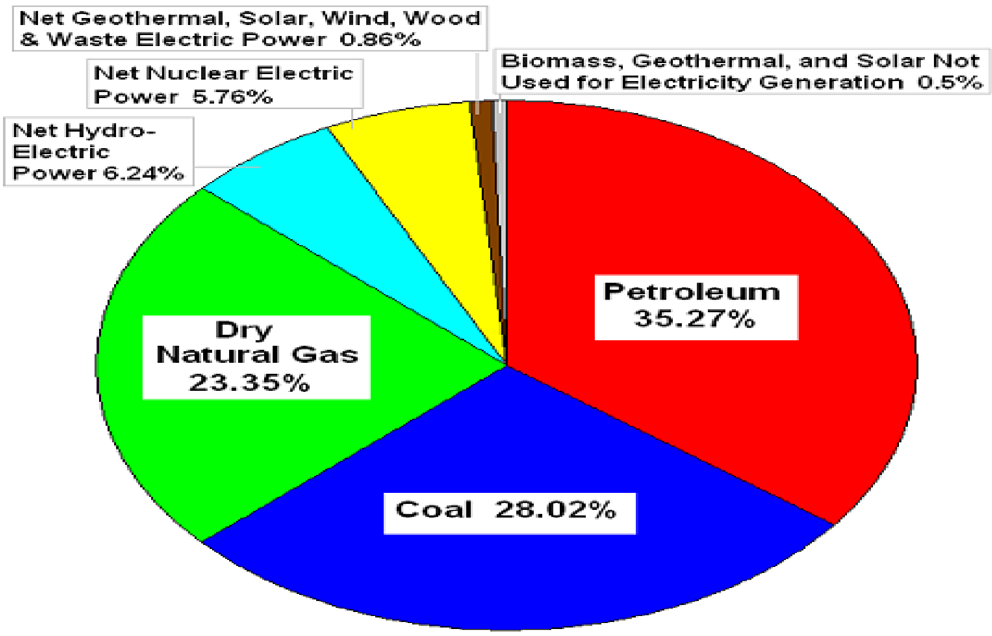

Figure 1.1: World Energy Consumption 2006 by Fuel Type (286W 2009)

Due to the massive increase in the non-renewable fuel prices and the increase in public awareness of its negative impact on the environment, the growth of renewable energy has accelerated over the past few years. According to British Petroleum (BP) (2011), power generated from renewable resources has increased to 14% of the total growth in global power generation. However, because of the enormous growth in the energy consumption, this growth is not enough to reduce the level of carbon emissions and to meet the Millennium Development Goals in 2030, that is the carbon emissions cap to be 30 $GtCO_2$ (Chakravarty et al. 2009).

As a consequence of the increase in the world's population, human development, the increase in individual income, and the aspiration for more comfortable life styles, the power consumption has increased significantly over the last three decades resulting in an increase in carbon emissions. In 1985, one kilowatt per capita was more than enough for basic needs; while in 2005 the primary need of energy was estimated for the Swiss to be two kilowatt per capita (Steinberger & Roberts 2010). The world's carbon emissions also increased from 21.2 $GtCO_2$/year in 1990 to 25.5 $GtCO_2$/year in 2003. The United States contributes by far the highest emissions of 5.8 $GtCO_2$/year which is equivalent to 16.8 tCO_2 per year per capita. Furthermore, the world's population is expected to increase to 8.1 billion by 2030 and hence, the average carbon emissions cap for each individual must be reduced to 3.7 tCO_2/year to achieve the Millennium Development Goals by 2030 (Chakravarty et al. 2009). Therefore, carbon emissions must be reduced, and this can be achieved by reducing power consumption and/or increasing the percentage of the energy generated by using the clean resources like solar, wind, geothermal and hydraulic energy.

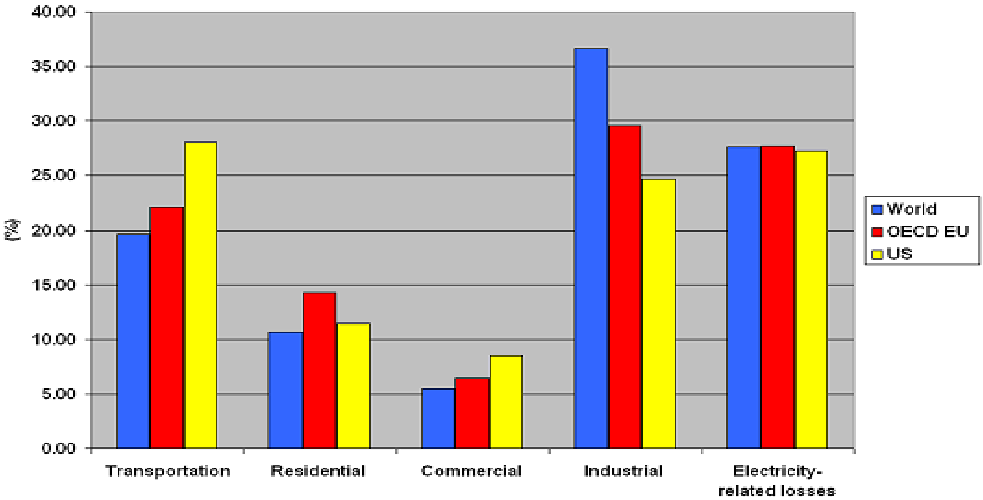

Figure 1.2: Energy Consumption by Sector (2006) – World and Selected Regions (286W 2009)

Increasing the investment of the clean resources involves four sectors: industrial, transportation, residential and commercial. Figure 1.2 presents the energy consumption by sector and region (286W 2009). The highest energy consumption occurs in the industrial sector. Therefore, much research has been conducted to reduce the energy consumption in this sector (Ang & Zhang 2000). The lowest consumption occurs in the commercial sector. The contribution of the present study will be in the residential sector. This study will focus on using the solar energy for domestic applications to reduce burning fossil fuel and hence carbon emission.

Research involving cheap and clean sources of energy such as solar energy, has increased significantly over the last four decades. US research in the solar energy was initially discouraged by the discovery of natural gas and oil in 1930's. However, after the World Oil Crisis in 1973, its research increased (Smyth, Eames & Norton 2006). Recently, the use of solar energy for electricity generation, air conditioning and water heating has grown. In the domestic applications, households consume energy by using air conditioning, heating, water heating, lighting and other applications (Figure 1.3). An environmentally and economically important and costly use, occurs in the production of domestic hot water, which accounts for approximately 14% of the domestic energy consumption in the United States (Department of Energy 2010). Domestic hot water is generally heated to around 60^{o} C, a temperature which can be easily produced by using solar energy rather than burning fossil fuel. Therefore, an economic and efficient system is required to encourage households to use solar water heating.

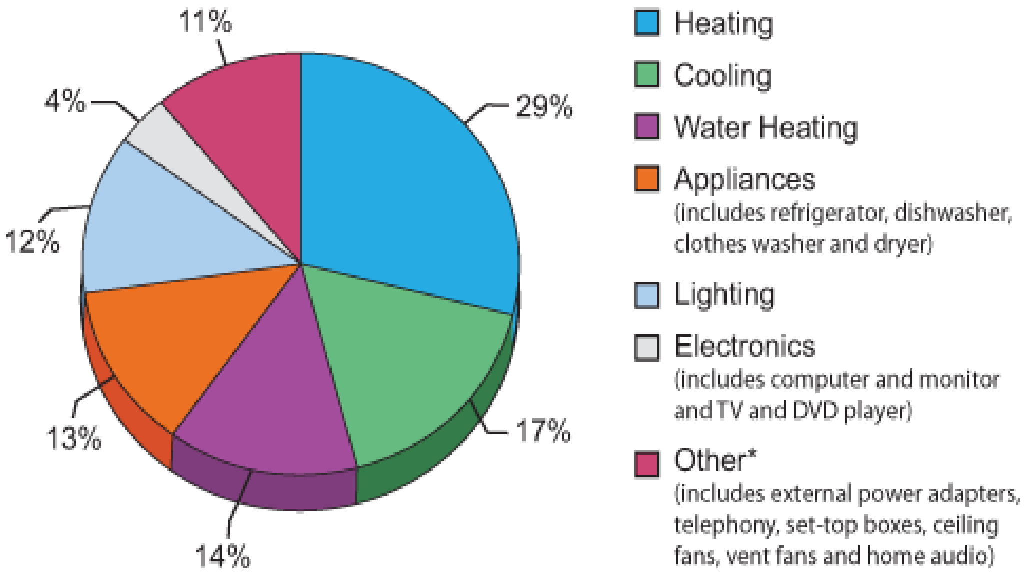

Figure 1.3: Annual energy bill for typical single family home (Department of Energy 2010)

1.2 Solar Resources

The sun's diameter is approximately 1.4 million km and it is 150 million km away from the earth. It has an effective black body temperature of 5777 Kelvin (Duffie 1991, p. 3) and hence the radiation is emitted from the sun at a rate of 3.8×10^{23} kW. Moreover, solar energy is readily available, friendly to the environment and renewable. During the day time, it is available anywhere in the globe. Solar energy is expected to continue for very long time due to endless nuclear reactions that are occurring at the core of the sun. These reactions are estimated to continue several billion years (Lovegrove & Luzzi 2001).

To produce the average world electricity consumption using solar radiation, an area of 35,000 km^2 (roughly the size of Taiwan) is required. To estimate this area, the following factors have been taken into consideration (Lovegrove & Luzzi 2001):

1. Only a small part of the solar energy reaches the earth: 1.7×10^{14} kW reaches the earth's atmosphere which is 4.5×10^{-8} per cent of total solar radiation. This energy is more than 1000 times the average world electricity expenditure of 1.6×10^{11} kW (Lovegrove & Luzzi 2001)
2. Solar intensity is affected by several factors: the position of the sun in the sky, the season and location on the globe. The maximum intensity of solar radiation on a clear sunny day at noon is around 1100 W/ m^2 (Duffie & Beckman 2006, p. 238)
3. The efficiency of converting solar radiation to electricity: the efficiency is assumed to be 20% for the 35,000 km^2 area (Lovegrove & Luzzi 2001).

1.3 Solar Collectors

The solar collectors are devices which transfer solar energy into thermal energy that increases the internal energy in the fluids, and hence increases their temperature. They are used to capture the solar energy. According to Lovegrove and Luzzi (2001), the simplest solar collector is a plate painted black and placed in the sun. The plate heats up until reaches the stagnation temperature when the heat gained from solar radiation equals the heat loss to the surrounding by convection and radiation. If water is sent through the plate, the water will extract energy from the plate, reducing its stagnation temperature. The water temperature increases and this energy can be used in many applications. Nowadays, many types of solar collectors are used.

There are several types of solar collectors, including the flat plate collector, evacuated tube, parabolic trough, central receiver and dish concentrator (Figures 1.4, 1.5 and 1.6). The temperature that the different types produce is a key indicator of their relevance to a particular use. For example, the evacuated tube type of collector can produce 90-200^{o} C and the parabolic trough can produce outlet fluid temperatures between 260-400^{o} C, while the central receiver can produce 500-800^{o} C. According to Lovegrove and Luzzi (2001), the highest outlet fluid temperature (500-1200^{o} C) is produced by the dish concentrator type. The flat plate collector is used for applications that require a temperature lower than 100^{o} C. As mentioned earlier, households generally have lower temperature requirements. Consequently, in order to study an economic system for household use, this research will focus on the flat plate collector.

A **B**

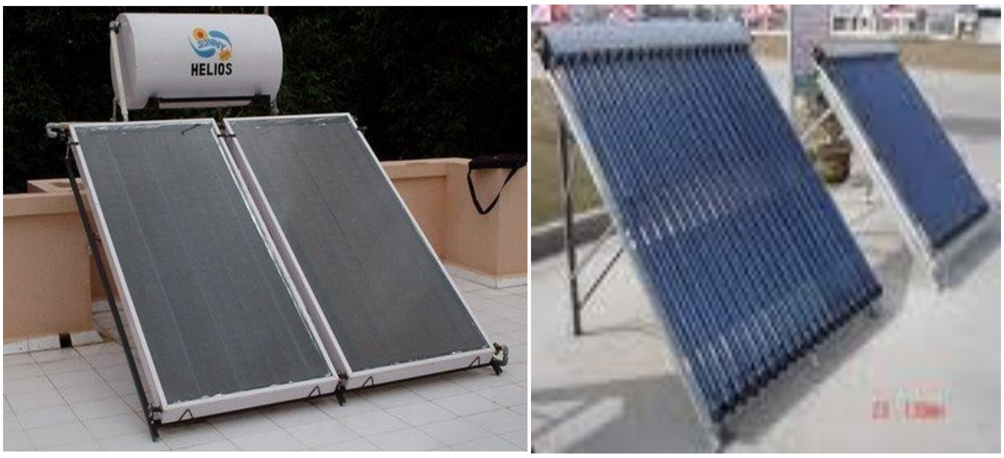

Figure 1.4: Solar collector type (A) Flat plate; (B) Evacuated tube (Fotosearch 2010)

A **B**

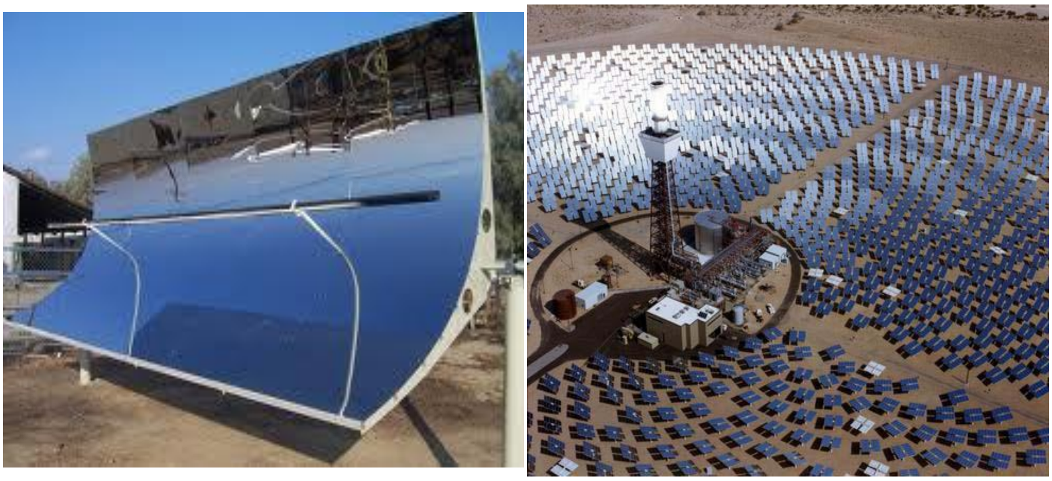

Figure 1.5: Solar collector types (A) Parabolic trough (B) Central receiver (Fotosearch 2010)

Figure 1.6: Dish concentrator collector (Dreamstime 2012)

1.4 Flat Plate Collectors

Flat plate collectors are the cheapest type of collectors. They are classified into two main types: conventional and integrated collectors. According to Duffie (2006, pp. 238-9), the conventional flat plate collector consists of:

1. A black surface that absorbs radiation and transfers the heat to the fluid
2. A glass cover that allows the solar radiation to reach the absorber surface and reduce convection and radiation losses
3. Tubes in which the fluid flows
4. Back insulation to reduce the conduction losses (Figure 1.7).

Since demand for hot water may not be continuous and solar energy is not available at night, a storage tank is needed to store the hot water (Figure 1.8).

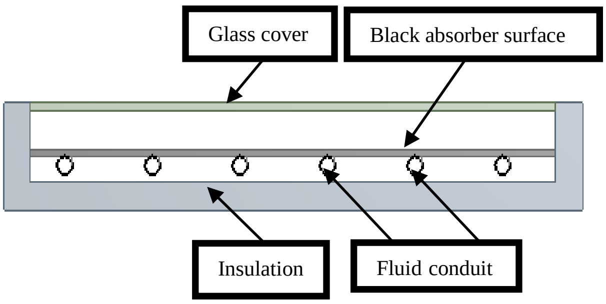

Figure 1. 7: Cross-section of a basic flat-plate collector (Duffie 2006, p. 239)

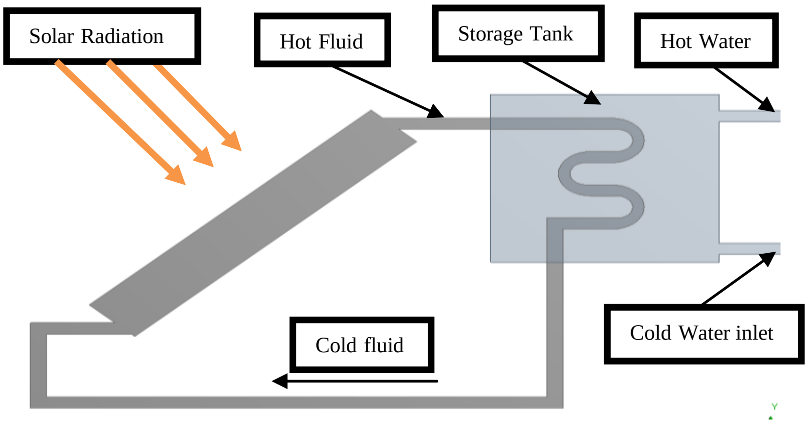

Figure 1. 8: Conventional type flat plate collector water heating system with storage tank

The integrated collector storage solar water heating systems differ from the conventional type by incorporating a solar energy collection component and a hot water storage component into one unit. This reduces the cost of the system as there are no connection pipes and only a small area is required for installation (Gertzos, Caouris & Panidis 2010; Khalifa & Abdul Jabbar 2010) . Therefore, this study will focus on the integrated collector storage solar water heating system.

1.5 Integrated Collector Storage Solar Water Heating System (ICSSWH)

In the late 1800s, some practical individuals in the southwest of the USA produced warm water for showering by leaving a water tank exposed to the sun. This was considered to be the first Integrated Collector Storage Solar Water Heating (ICSSWH) system (Smyth, Eames & Norton 2006). However, there are two types of ICSSWH. One is the direct heating system in which the service water flows into the storage tank and is directly heated through the collector (Figure 1.9). The other is the indirect heating type in which the service water passes through a serpentine tube (a heat exchanger) that is immersed in the stored fluid (Figures 1.10 and 1.11).

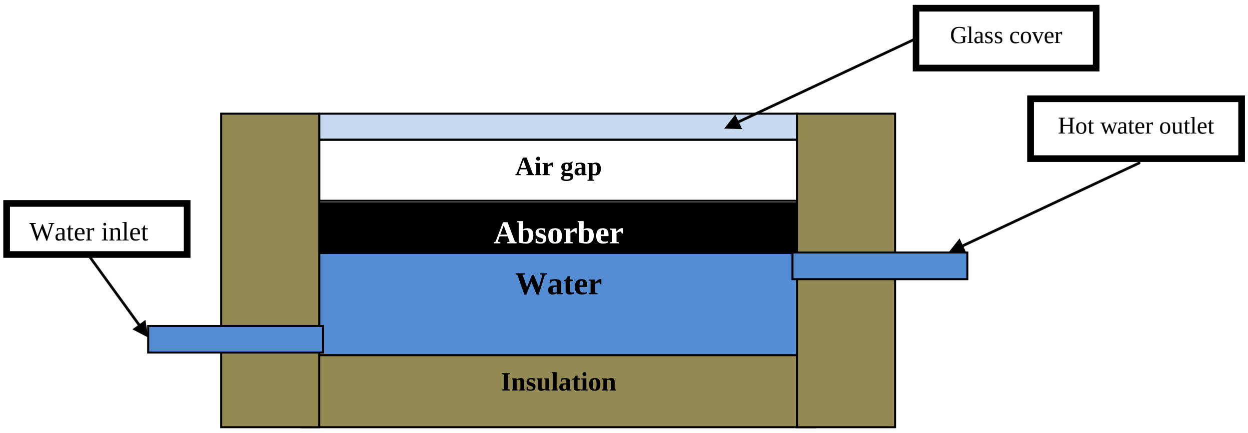

Figure 1.9: Integrated Collector Direct Heating System

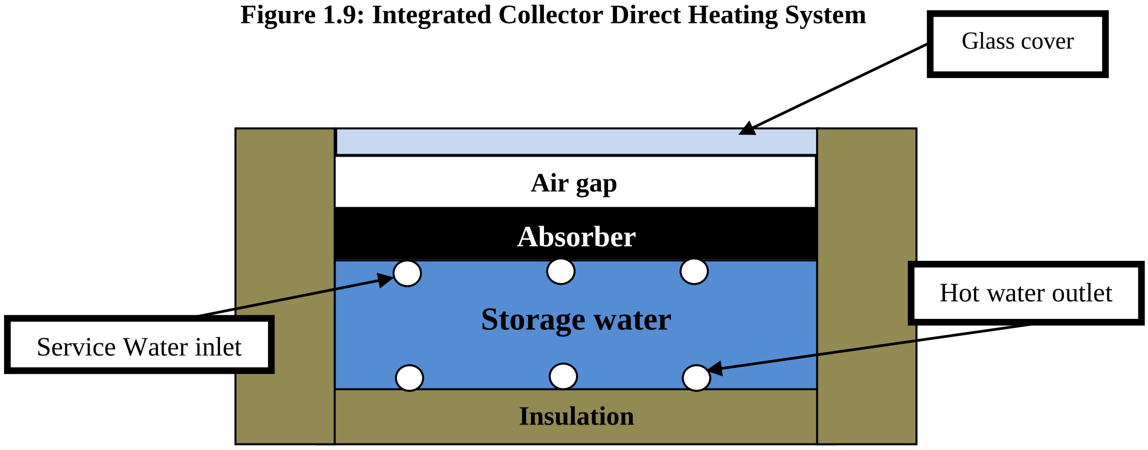

Figure 1.10: Integrated Collector Indirect Heating System

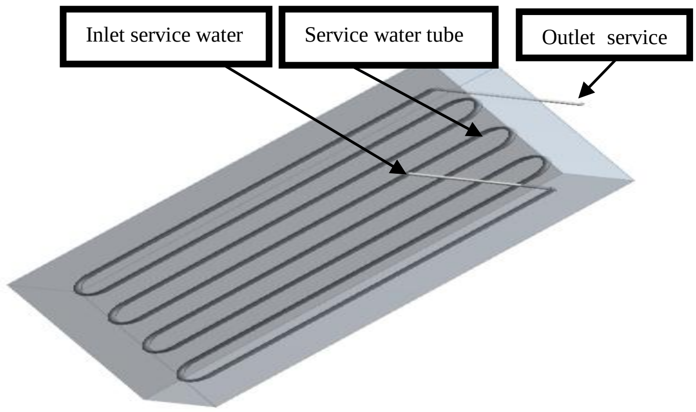

Figure 1.11: Storage tank and service water tube in the Indirect Heating System

Construction of the storage tank in the direct heating type is relatively expensive. Since the storage tank is connected directly to municipal water pressure, the pressure inside the tank is relatively high. Therefore, the storage tank in this type needs to be manufactured from a high corrosion resistance material that is able to withstand high pressures. This leads to increased tank construction costs to more than 50 percent of the total system price (Gertzos & Caouris 2007).

Since the storage tank in the indirect heating system is not exposed to municipal pressure, its capital cost is lower than the direct heating system (Gertzos & Caouris 2007). However, the storage fluid is static in the indirect heating system, which results in a low heat transfer rate between the storage fluid and the service water. Enhancing the heat gained by the service water will improve the system's efficiency so that it provides an acceptable outlet service water temperature.

The aim of the present study is to show that the thermal performance of the indirect heating integrated collector storage solar water heating system can be improved, while keeping the collector construction costs low. This can be achieved by enhancing the heat gained by the service water and reducing heat loss from the system.

In order to identify a way to maximize the heat gained by the service water and to minimize the heat loss, it is important to understand heat balance in the indirect heating integrated collector storage solar water heating system. The absorber surface is heated from the solar radiation which has been transmitted through the glass covers. During the daytime, the heat flows from the absorber to the storage and service water. When there is no solar radiation, the energy in the storage water flows to the absorber and service water. In both cases, the absorber loses some of the heat due to convection to the air in the gap spacing, radiation to the side walls (the side-wall surrounding the air gap spacing, Figure 1.10) and radiation to the top glass cover. The top glass cover loses heat due to convection to the ambient air and due to radiation to the sky.

1.6 Research Focus and Scope

There are different ways to improve the performance of the indirect heating integrated collector storage solar water heating system. These are:

1. Increasing the heat gained by the service water (Chen et al. 2010; Gertzos & Caouris 2008; Gertzos, Pnevmatikakis & Caouris 2008; Kumar & Rosen 2010).
2. Reducing heat losses to the environment (Kumar & Rosen 2011).
3. Increasing the system's ability to store energy (Smyth, Eames & Norton 2006).
4. Optimizing the angle of the collector for the reference point (Elminir et al. 2006; Gunerhan & Hepbasli 2007).

The present study will investigate ways to reduce heat losses from the system and enhance heat gained by the service water.

A. Heat Loss Reduction

Using a double glass cover instead of single one is an efficient strategy to reduce the heat loss (Kumar & Rosen 2011). The present study investigated the optimum air gap spacing between the upper and lower glass cover and between the lower glass and the absorber surface (Figure 1.12). A parametric study has been conducted in a system with double glass cover. The lower air gap spacing (L_1) and the upper air gap spacing (L_2) for the system with 0.7 m x 1.35 m absorber area were varied within the range of 15-50 mm to investigate which combination of gap sizes (L_1, L_2) would result in minimum total heat losses, i.e. including radiation and convection losses.

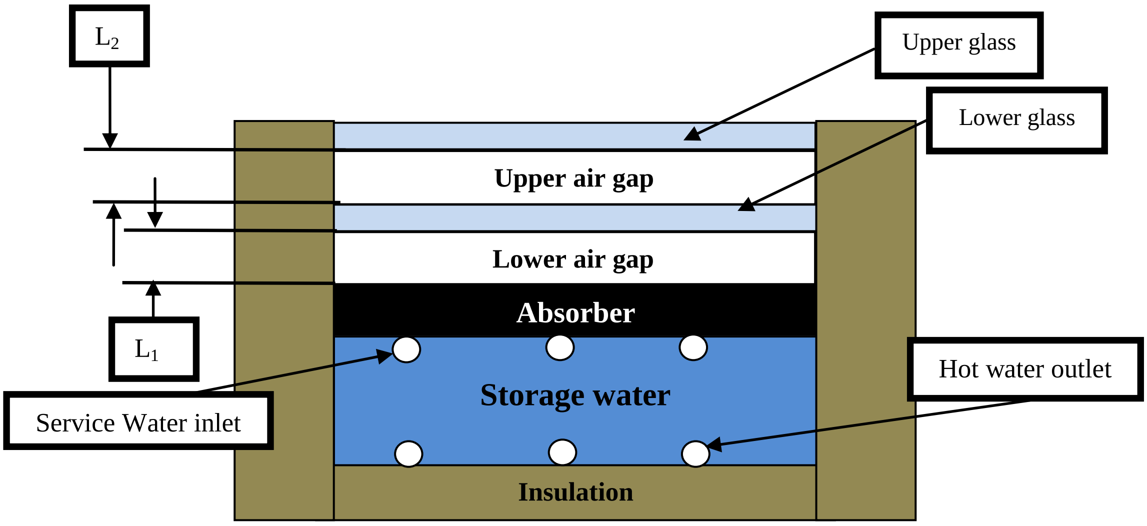

Figure 1.12: Indirect Heating System with double glass covers

B. Heat Transfer Enhancement

The heat gained by the service water can be enhanced by methods such as:

1. Agitating the storage water using a circulating pump. This will not be investigated in the present study because using a circulating pump increases the capital and running costs of the system. The pump requires electricity and continuous maintenance

2. Using the phase change material technique. Chen et al (2010) studied an indirect collector that is operated with paraffin instead of storage water. Their objective was to increase the thermal conductivity of the paraffin by adding aluminum foam with high thermal conductivity, 202.4 W/mK. Adding aluminum foam enhanced the heat transfer between the storage fluid and the service water. This method is out of the scope of the present study.
3. Changing the heat transfer surface design which includes adding fins, surface roughness, twisted-tape inserts and coiled tubes. The surface treatment technique enhances the heat transfer because it increases the turbulence, increases the surface area and improves the mixing or flow swirl (Kreith, Frank & Bohn 2001, pp. 514-7). This technique will not be used in this study because it increases the cost of the system.

The present study focuses on changing the length and cross sectional area of the service water tube to enhance the heat gained by the service water. The outlet service water temperature is used as a measure of the performance as it is a measure of the energy acquired from solar radiation. Single and double raw heat exchangers with different lengths are investigated. Circular and elliptic tube cross section pipes are also examined. The service water mass flow rate is chosen as 500 and 650 L/h, as average flow rates used in the investigation of the indirect heating system (Gertzos & Caouris 2008; Gertzos, Caouris & Panidis 2010; Gertzos, Pnevmatikakis & Caouris 2008).

CHAPTER 2: Literature Review and Research Gap

- ***Introduction***
- ***Collector Angle and Inlet Position***
- ***Storage Tank Construction***
- ***Glass Cover***
- ***Heat Transfer Enhancement***
- ***The Heat Exchanger in other Applications***
- ***Research Gap***

2.1 Introduction

This chapter provides a review of the previous work aimed at investigating the parameters that have an effect on the collector performance. These parameters are the collector angle, the service water inlet position, storage tank construction, glass cover, and methods of heat transfer enhancement. As the heat exchanger is a major component in the indirect heating system, the last section of this chapter is devoted to summarising the research conducted on general heat exchangers.

2.2 Collector Angle and Service Water Inlet Position

Gertzos, Pnevmatikakis & Caouris (2008) conducted an experimental and numerical study investigating the heat transfer between the service and storage water in the indirect heating system. Their main objectives were to study the effect of the inlet position and the slope of the collector on the outlet service water temperature. They built the heat exchanger (storage tank and service water tube) for the system. The storage water was heated, using successive passages through the external heater. When the temperature of the storage water reached 80^{o} C, they stopped the heating process, allowed the service water to flow through the tube, and measured the outlet and the average storage water temperature for one hour period of the energy withdrawal (Figure 2.1).

In the numerical simulation, they developed a 3D CFD model (using CFD package FLUENT 6.3) and solved the continuity momentum and energy equation in transient condition, using a standard k-omega turbulence model. They used the SIMPLE algorithm (Semi-Implicit Method for Pressure Linked equation) for the velocity-pressure coupling and the second order upwind scheme for momentum, turbulent kinetic energy, specific turbulent dissipation ratio and energy. They examined the case with free convection heat transfer (i.e. when the storage water is static).

Their findings:

1. In an investigation of two cases of the inlet position; one the inlet is placed in the front of the collector and one in the back. The inlet position of the service water has no effect on the outlet service water temperature
2. For the collector angle, in the first ten minutes when the average storage water temperature (T_{ta}) was higher than 50^{o} C, the service water outlet temperature (T_{out}) increased, as the collector angle increased, due to the buoyancy effect. While, after ten minutes, the outlet temperature was not affected by changing the collector angle (Figure 2.1).

Their numerical model was validated against their experimental results. The experimental inputs of initial temperature of storage water, mass flow inlet and inlet temperature were used in the CFD model and there was a good agreement between the experimental and the numerical results.

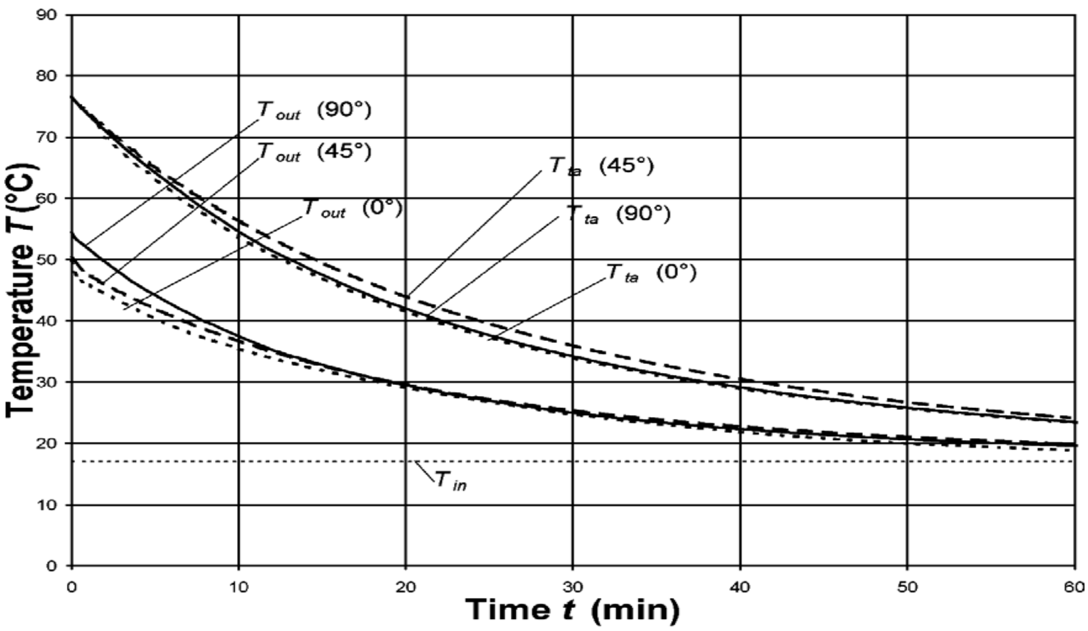

Figure 2.1: Experimental temperatures versus time for the indirect heating system at slopes 0°, 45°, 90°, without recirculation and service water flow rate of 500L/h. T_{1n} : tube water inlet (mains) temperature (Gertzos, Pnevmatikakis & Caouris 2008)

2.3 Storage Tank Construction

In the indirect heating system, thin steel metal sheets (0.8-1.2 mm thick) can be used to build the tank, without any corrosion protection (Gertzos, Caouris & Panidis 2010). This is due to the fact that the storage tank is not subjected to the high pressure similar to municipal pressure. The fluid in the tank is not connected to municipal water and it is not refreshed. The municipal water (service water) passes through a serpentine tube that is immersed in the storage tank.

According to Smyth, Eames and Norton (2006), the tank depth has an effect on the performance of the system. For example, an increase in the water depth leads to an increase in the time taken to heat the water. A decrease in the tank depth leads to a decrease in the system's capacity to store energy. Moreover, in a cold climate, a depth decrease could result in the storage water being frozen. Smyth, Eames and Norton (2006) conducted a review study in which they state that the best "volume/aperture area" ratio is 100 L/m^2 or the best tank depth is 10 cm. Tiller and Wochatz (1982) concluded that in hot weather, the performance of 102 L/m^2 is better than 51-69 L/m^2 unless the water is withdrawn fairly continuously through the daylight hours. Gertzos, Caouris and Panidis (2010) studied the indirect heating system and took the tank depth as 10 cm or the "volume/aperture area" ratio as 100 L/m^2.

2.4 Glass Cover

The glass cover has several functions:

1. It reduces convection heat losses to the surroundings
2. It protects the absorber surface from the environment
3. It reduces the radiation heat losses by reflecting the radiation emitted from the absorber surface. As the wave length of solar radiation is shorter (in the range 0.3-3 μm) than the radiation that emits from other surfaces at lower temperature, solar radiation is able to transmit through the glass cover while

the radiation emitting from the absorber surface is not able to transmit back through the glass cover.

However, the glass material has to be highly transparent for the solar radiation, since any loss in the transmittance results in a direct decrease in the collection efficiency (Smyth, Eames & Norton 2006).

Kumar and Rosen (2011) numerically investigated five strategies for reducing the top heat losses. They applied an energy balance equation for each case and solved these equations numerically using a “forward time step marching finite difference technique”. Their study aimed to find the best strategy for enhancing the thermal performance of the system. The 100 L tank capacity model and 1 m^2 absorber area was used to assess five cases:

(1) Single glass cover without night insulation.

(2) Single glass cover with a night insulation cover.

(3) Double glass cover without a night insulation cover.

(4) Transparent insulation with a single glass cover.

(5) Insulating baffle plate with a single glass cover.

Case 3 gave the highest thermal performance, while Case 5 gave the lowest. The water temperature in the storage tank for Case 3 was higher than the temperature for Case 4 and 5 by 5-7^{o} C and the thermal efficiency was higher by 12-14%. In Cases 1, 2, 3 and 5, the high and low thermal efficiency resulted from low and high heat loss respectively. However, in Case 4 the relatively low efficiency resulted from the decreased incoming solar radiation on the absorber surface due to the presence of the transparent insulation material between the absorber plate and the glass cover.

According to Kumar and Rosen (2011), using a double glass cover in the integrated collector system is an efficient strategy for reducing the top heat losses. However, the air spacing between the upper and lower glass, and between the lower glass and the absorber surface, has an effect on the amount of heat losses. Manz (2003) investigated numerically the convective heat flow through an air layer in cavities of facade elements. The Rayleigh number was varied between 1000 and 10^6 in this study. It was changed by altering the temperature difference between the walls surrounding the air or by altering the distance between the walls. The result of Manz's study suggested that the increasing Rayleigh number resulted in an increase in the velocity of the air which in turn increased the convective heat transfer. Therefore, at a high Rayleigh number the gap is not as effective in reducing the heat loss.

Mossad (2006) investigated the effect of the air gap spacing of double glassed doors in closed refrigerated vertical display cabinets. The results showed that when the size of the air gap was very small, the heat transfer was mainly due to conduction: as the gap spacing increased, air begins to move due to natural convection which leads to an increase in the convective heat loss. Therefore, the sizes of the top and lower air gap spacing have an effect on the amount of heat loss from the system.

2.5 Heat Transfer Enhancement

Previous studies in the indirect heating integrated collector system showed that the heat gained by the service water is enhanced by agitating the storage water and changing the heat exchanger design. While in the direct heating system, using a corrugated absorber surface was found to increase the heat gained. A summary of the research aimed at investigating different techniques to enhance the heat transfer in the integrated collector storage solar water heating system is given below.

2.5.1 Agitating the Storage Water

Gertzos, Pnevmatikakis and Caouris (2008) used a pump circulating the storage water to enhance the heat transfer between the storage and service water (Figure 2.2). The experimental and numerical methods of this study were summarized in Section 2.1. The inlet, outlet service water temperature and the average temperature of the storage water were measured at one second time intervals and were averaged and recorded every 30 seconds, for energy withdrawal periods of one hour.

Gertzos, Pnevmatikakis and Caouris (2008) reported that the outlet service water temperature was higher in the case with circulating pump than without circulating pump. Figures 2.3 and 2.4 present the experimental and computational temperatures of the service water inlet and outlet (T_{in}, T_{out}), storage tank (T_{ta}) and temperature in the middle of the service water tube (T_{med}) during a one hour period, for the system with and without circulating pump, respectively. When the circulating pump was used with a 923 L/h flow rate (Figure 2.3), the outlet temperature was 55^{o} C at time equals zero, but when the circulating pump was not used (Figure 2.4), the outlet temperature was 50^{o} C at time equals zero.

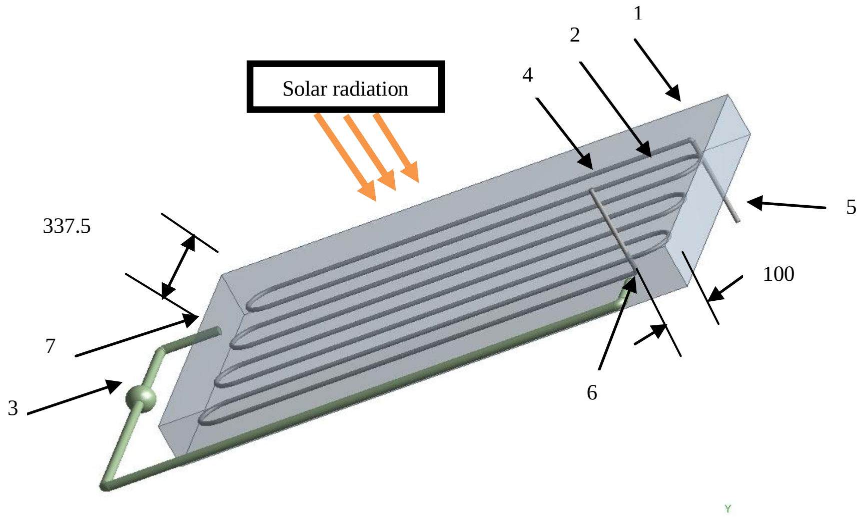

Figure 2.2: the heat exchanger in the indirect heating system with circulating pump. Key: 1. storage tank; 2. HX; 3. circulating pump; 4. service water inlet; 5. service water outlet; 6. inlet, circulating water; 7. outlet circulating water.

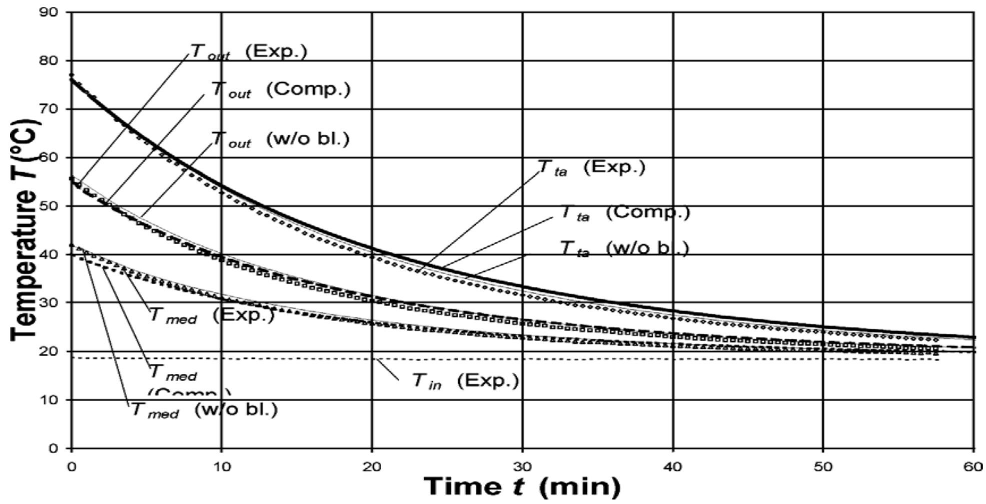

Figure 2.3: Experimental and computed temperatures versus time for the system with recirculation flow rate of 923L/hr and service water flow rate of 500L/h (Gertzos, Pnevmatikakis & Caouris, 2008)

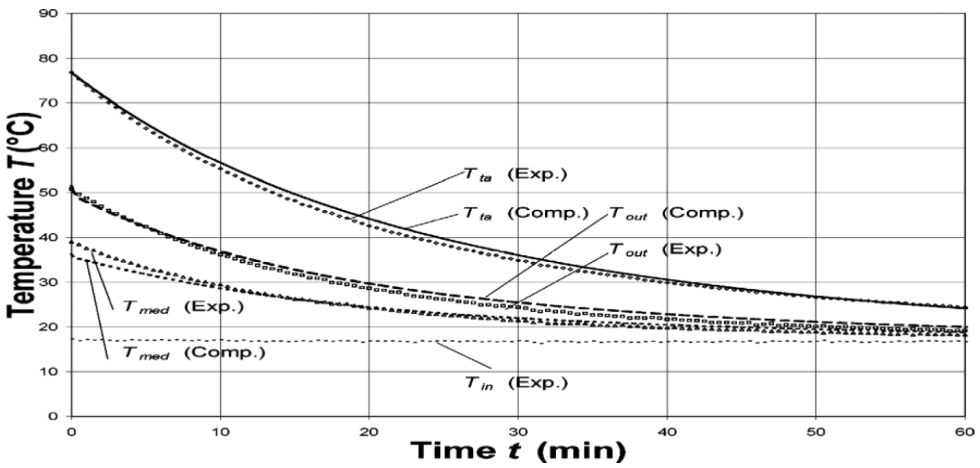

Figure 2.4: experimental and computed inlet, middle, outlet and average tank temperatures versus time, without recirculation and for service water flow rate of 500L/h (Gertzos, Pnevmatikakis & Caouris, 2008)

Gertzos & Caouris (2008) conducted a study on the same system (Figure 2.2) with circulating pump. The objective of the study was to reduce the construction cost without reducing the thermal efficiency of the system. The storage tank was constructed from thin steel material to minimise cost. However, the water weight and pressure inside the storage tank tended to deform the plate. To prevent deformation, fins were used to connect the back and front plates of the storage tank (Figure 2.5). These fins should be placed in a position that has a minimal influence on the velocity of the storage water (Gertzos & Caouris 2008).

Gertzos and Caouris (2008) investigated four parameters that have effect on the mean water velocity in the tank, and hence on the outlet service water temperature. These parameters are the inlet and outlet position of circulating pump (number 6 and 7 in Figure 2.2), the diameter of the inlet and outlet of the circulating tube and the arrangement of the interconnecting fins. The study was conducted in steady state condition assuming that the circulating water mass flow rate was 900 L/h, the storage water temperature was constant at 60^{o}C and for two service water inlet temperatures'; 15 and 20 ^{o} C.

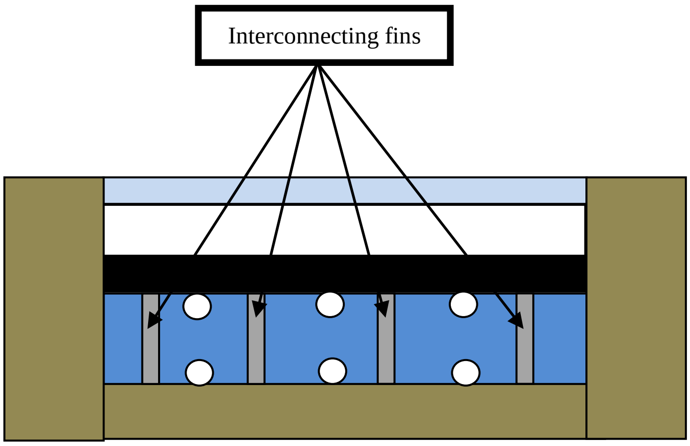

Figure 2.5: A storage tank with a fin joining the front and back surface

Gertzos and Caouris (2008) found that the influence of the inlet diameter and position of the circulating water on the storage water velocity are more important than the influence of the outlet diameter and its position. The optimum inlet diameter was 8 mm, while the optimum position was 100 mm from the top right side. The optimum position of the outlet was 337.5 mm from the lower left side (Figure 2.2). For the interconnecting fins, they found that the case using five fins of 10 cm length (f.1-f.5 in Figure 2.6) was the best option. If extra strength is required, the case of nine fins with 5 cm length (f.1-f.5 and f.6-f.9) was found to the second best option. The optimal arrangement of the interconnecting fins and the circulating pump inlet and outlet led to increase in the main storage water velocity by 65 % which in turn increased the outlet service water temperature by 8^{o} C.

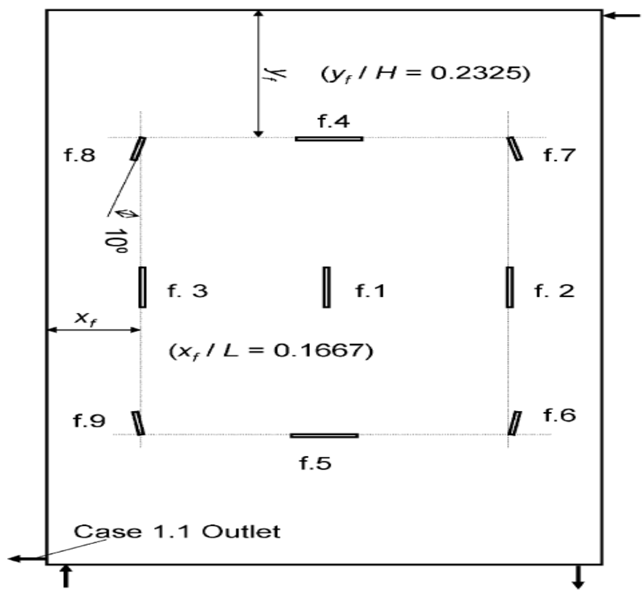

Figure 2.6: Optimal arrangement of the connecting fins position (Gertzos & Caouris 2008)

2.5.2 Heat Exchanger Design

The heat exchanger in the indirect heating system includes a storage tank which contains the storage water and the service water tube through which the service water flows. Gertzos, Caouris and Panidis (2010) investigated the effect of three parameters in the model given earlier (Gertzos & Caouris 2008), with the presence of a circulating pump (Figure 2.2). These parameters were the service water tube positions relative to the tank wall, the tube length and the tube diameter. They developed various steady CFD models to identify the optimum magnitude of these parameters.

In regard to the tube placement, they investigated five different positions for the service water tube (Figure 2.7). In Case 1, the tube was placed inside the tank touching the upper and lower walls of the tank, while in Case 2, half of the tube was placed outside the tank and half inside the tank. The advantage of Case 2 was to increase the storage water velocity inside the tank because the tube resistance to the storage water decreased in this case. As a result an increase in the heat transfer coefficient can be obtained. The tube in Case 3 was soldered to the walls with the aim of introducing better thermal conductivity. In Case 4, the tube was placed in the middle of the tank depth and in Case 5, the tube at the top plate was placed across at the middle between the tubes the lower plate of the tank.

For each case, a CFD model was developed to evaluate the outlet service water temperature which was used as a measure for the thermal efficiency. They solved the continuity, momentum and energy equation in steady state using the k-omega turbulence model and used the following assumptions:

1. The storage water temperature was fixed at 60^{o} C
2. The service water mass flow rate was chosen to be 300, 500 and 700 L/h
3. The inlet temperature was at 20^{o} C
4. The circulating water mass flow rate was varied to 100, 450 and 810 L/h,
5. The service water tube diameter and length was 13 mm, 16.26 m respectively.

Cases 1, 3 and 5 provided the same outlet service water temperature, which was higher than Cases 2 and 4. As the fabrication of Case 3 was more expensive than

Case 1 and they had the same outlet service water temperature, Gertzos, Caouris and Panidis (2010) rejected Case 3. Case 1 was found to be the optimum case because it gave a slightly better result than Case 5 and its fabrication is simpler. Moreover, the service water outlet temperature increased by 4-6^{o} C as the circulating water flow rate was increased by 350 L/h and decreased by 4-8^{o} C as the service water flow rate was decreased by 200 L/h.

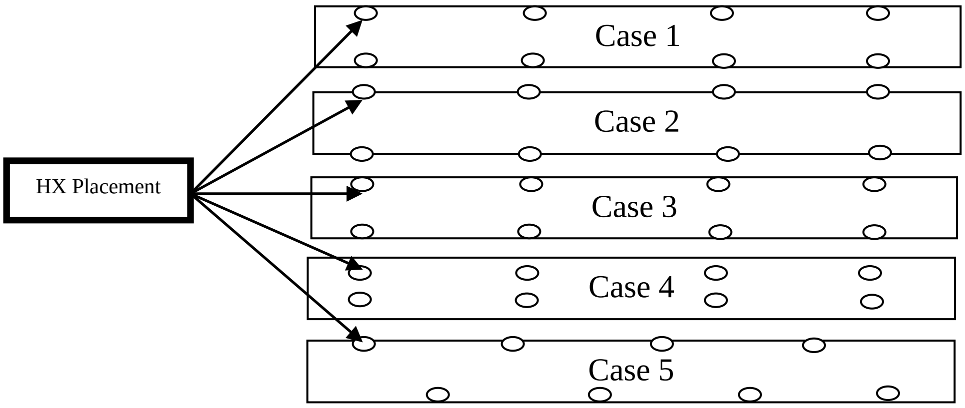

Figure 2.7: Cases for HX placement

For the service water tube diameter, Gertzos, Caouris and Panidis (2010) examined four inside diameters: 10, 13, 16 and 20 mm. They solved the continuity, momentum and energy equation in a steady state condition. They used the same assumptions for investigating the tube placement. The optimum tube diameter was found to be 16 mm, as it gave the highest outlet temperature.

In regard to the service water tube length, they examined the heat exchanger with tube lengths of 16.26 m and 21.68 m. They investigated the system in a steady state condition and found that in the case where the tube length was 21.68 m, the difference between the average temperature of storage water and the outlet service water varied between 1^o C to 6^o C for the service water mass flow rate 300 and 700 L/h, respectively. In this case, the tube diameter was 16 mm and the circulating water mass flow rate was 810 L/h. They considered this temperature difference to be acceptable for heat exchanger systems. Therefore, they concluded that there is no need for a further increase in the tube length.

Gertzos, Caouris and Panidis (2010) developed a transient CFD simulation to examine the behaviour of the system during a one hour period of the energy withdrawal. They used the following assumptions:

1. The initial temperature of the storage water was 60^o C
2. The service water mass flow rate was 500 L/h
3. The inlet temperature was 20^o C
4. The circulating water mass flow rate was 810 L/h
5. The tube length was 21.68 m
6. The tube inside diameter was 16 mm
7. The tube position was as for Case 1.

Figure 2.8 presents the outlet temperature of the service water (T_{out}), the average temperature of the storage water (T_{ta}) and the temperature of the service water in the middle of the tube length (T_{med}) for a one hour period of energy withdrawal. During this period, the difference between the average temperature of the storage water and the outlet temperature of the service water was less than 4^o C. The outlet temperature decreases to 30^o C after 20 min, whereas T_{ta} and T_{out} are equal after 50 min.

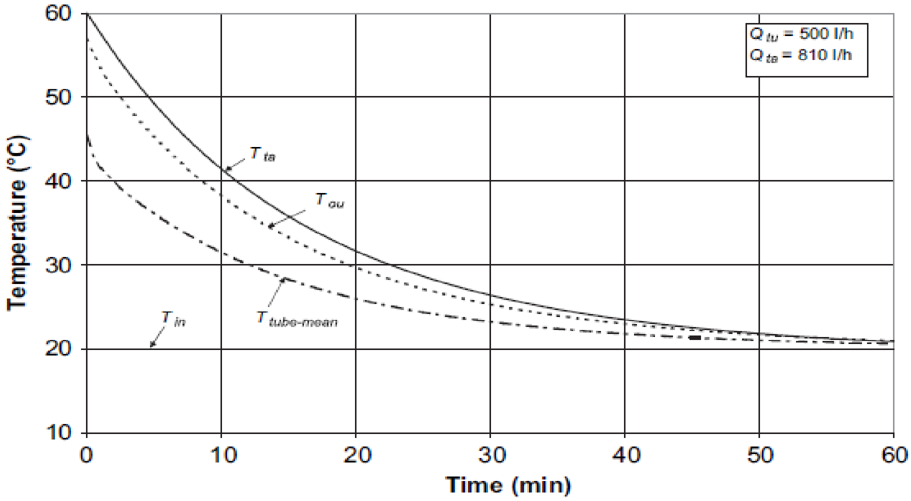

Figure 2.8: Mean tank water, mean tubes water and service water outlet temperature (Gertzos, Caouris & Panidis 2010)

2.5.3 Corrugated Absorber

In the direct heating type, the service water flows through the collector and there is no service water tube. Therfore, using a corrugated absorber instead of plain one can increase the heat transfer between the absorber and the service water. Kumar and Rosen (2010) studied the effect of introducing a corrugated absorber surface for the direct heating integrated collector storage solar water heating system. Introducing a corrugated absorber surface increased the area in contact with the service water side (Figure 2.9), and hence increased the system operating temperature and increased the useful energy converted from solar energy. When the depth of the corrugation was changed from 0.4 to 1 mm, the maximum service water temperature increased from 53 to 64^{o} C. In contrast, increasing the operating temperature resulted in an increase in heat loss, which in its turn reduced efficiency. According to this study, the efficiency reduction was marginal and could be overcome by continuous water withdrawal from the system. Kumar and Rosen (2010) concluded that the performance of the integrated solar collector is better when using a corrugated absorber than when using a plain absorber.

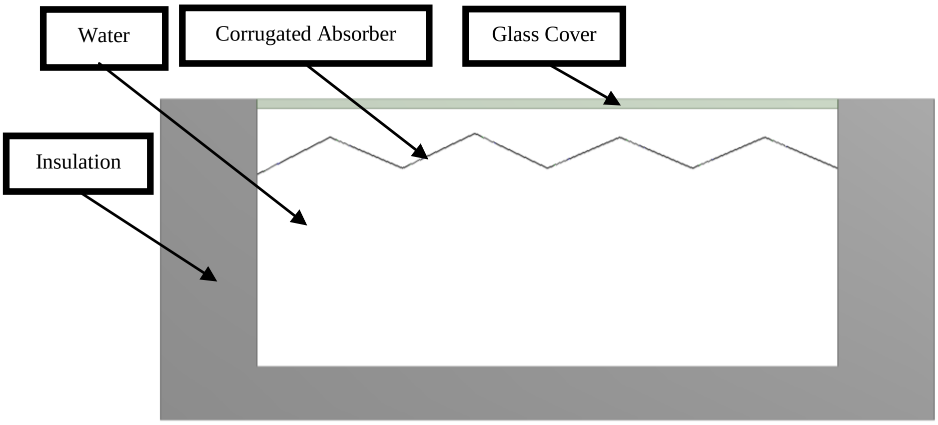

Figure 2.9: Cross-section of direct heating system with corrugated absorber

2.6 The Heat Exchanger in other Applications

As the heat exchanger is a major component in the indirect heating system, this section is devoted to summarising research conducted on general heat exchangers. The heat exchanger is defined as an apparatus in which heat transfers between a warmer and colder substance, usually fluids (Kreith, Frank & Bohn 2001, p. 485). There are two important factors when designing a heat exchanger: the economic factor which is important in every engineering design, and the thermal performance of the heat exchanger. Gebreslassie et al. (2010) proposed a general equation (equation 2.1) for a thermal system to estimate the optimal area of a heat exchanger considering both economic and thermal factors. This equation depends on parameters directly related to the heat exchanger. These parameters are cost, the overall heat transfer coefficient, the logarithmic mean temperature difference and the heat transfer rate. Thus, it indicates how the area should be changed if these parameters are modified.

The geometry of the heat exchanger, the temperature of the cold and hot fluid, and the velocity of the fluid affects the thermal performance of the heat exchanger. Prabhanjan, Raghavan and Rennie (2002) compared the heat transfer rates of a straight tube heat exchanger and a helical tube heat exchanger. They concluded that the heat transfer coefficient is also affected by the geometry of the heat exchanger.

Mellouli et al. (2007) examined experimentally the effect of using a spiral heat exchanger in a metal-hydrogen reactor (Figure 2.10). The reactor consists of a cylindrical stainless steel tank containing 1 kg of $LaNi_5$ (hydride bed). The benefit of using the spiral tube is that a centrifugal force is generated as the fluid flows through a carved tube. This force can cause a significant increase in the heat transfer rate (Mellouli et al. 2007).

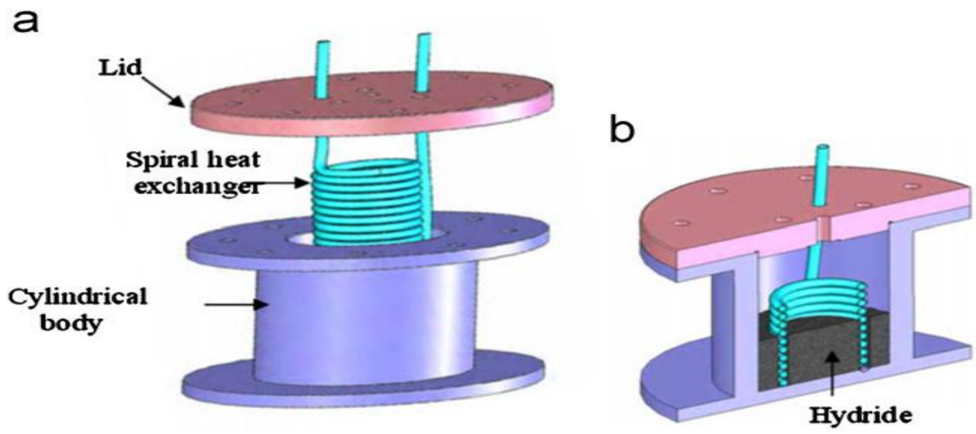

Figure 2.10: Geometrical configuration of a reactor. (a) Burst sight of the reactor; (b) Cross-section of the reactor (Mellouli et al. 2007)

2.7 Research Gap

More research is needed to improve the performance of the integrated collector storage solar water heating system, reduce its operating cost and introduce a system with a more aesthetic configuration (Smyth, Eames & Norton 2006). Studies of the indirect heating system are limited, and of these only a small number refer to the heat transfer in the indirect heating system. For example, Gertzos, Pnevmatikakis and Caouris (2008) examined experimentally and numerically the outlet service water temperature in a heat exchanger (storage and service water) of an indirect heating system with and without agitating the storage water. They found that when the storage water was static, the difference between the average temperature of the storage water and the outlet service water temperature was between 15^{o} and 20^{o} C. When the storage water was moved using a circulating pump, the temperature difference reduced to the range of 10-12^{o} C (Gertzos, Pnevmatikakis & Caouris

2008). The low temperature difference between the storage water and the outlet service water means that the heat transfer between the two fluids is high.

Gertzos and Caouris (2008) and Gertzos, Caouris and Panidis (2010) achieved the optimum value of the interconnecting fin placement, service water tube position relative to the tank wall, and the diameter and length of the service water tube for the system with circulating pump. Consequently, the temperature difference decreased to 4^{o} C, which is acceptable in heat exchanger design (Gertzos, Caouris & Panidis 2010).

Kumar and Rosen (2011) found that using a double glass cover is an effective strategy for reducing the heat losses, and that the heat gained from the solar radiation was the same whether using a single or double glass cover. To the author's best knowledge, the optimum air gap spacing in the integrated collector storage solar water heating system with double glass cover has not been investigated.

This study will investigate numerically the optimum size of the upper and lower air gap (Figure 1.12). In this investigation, the following assumptions were used:

1. The continuity, momentum and energy equations were numerically solved in a steady state condition
2. The absorber temperature was assumed to be 82^{o} C. This temperature is the maximum temperature that the absorber surface can reach when solar incident radiation is 850 W/m^2 in the flat plate collectors (Gertzos & Caouris 2007). This value was chosen mainly to identify the best air gap spacing that gives the lowest heat loss at the possible maximum absorber temperature. This was to

determine the design parameters of the exchanger at the worst case scenario (i.e. when the losses are at maximum).

3. The collector angle was chosen to be 45^o from the horizontal
4. Radiation between surfaces was calculated by using the surface-to-surface (S2S) radiation model.

The previous studies in the indirect heating system by Gertzos and Caouris (2007); Gertzos, Pnevmatikakis and Caouris (2008); Gertzos and Caouris (2008); Gertzos, Caouris and Panidis (2010) investigated heat transfer in the heat exchanger. Namely, the heat transfer between the storage and service water. They used the assumptions that the temperature of the storage water was fixed at 60^o C for the steady state investigation. While for the transient investigation, the initial temperature of the storage water of 60^o C or 80^o C was used. The present study will investigate the heat exchanger in the indirect heating system using different assumptions:

1. The whole collector (double glass covers and heat exchanger) were included in the calculations
2. A circulating pump of the storage water was not used
3. The absorber surface temperature was assumed to be 60^o C, as an average absorber temperature.

In the heat exchanger investigations, these assumptions were considered to be more realistic than the previous studies' assumptions because:

1. The absorber, rather than the storage water, is the heat source in the system

2. Based on energy balance, the absorber temperature can reach 60^o C when solar incident radiation is 650 W/m^2, but there is no evidence that the whole system can reach this temperature
3. The average absorber temperature was chosen to identify the best heat exchanger configurations at average incident radiation.

Therefore, to investigate the best heat exchanger design assuming that, the absorber temperature is constant at 60^o C and including the effect of the double glass covers with no circulating pump is a more realistic model and is expected to use less energy.

CHAPTER 3: Mathematical Model

- ***Introduction***
- ***The Governing Equations***
- ***Computational Fluid Dynamics (CFD)***
- ***The Advantages of Using CFD Approaches***
- ***Types of Flow***
- ***Turbulence Modelling***
- ***The Use of CFD Software***
- ***Chapter Conclusion***

3.1 Introduction

The objective of the present study is to numerically investigate ways to improve the thermal performance of the indirect heating system with an aim of reducing both the initial and running costs of the system. There are many numerical methods that can be used to solve fluid flow and heat transfer problems. These include finite element, finite difference, control volume, boundary element and meshless method (neural network). The main goal of all these numerical methods is to transfer the complicated differential equations that govern the flow and heat transfer, and which are not possible to solve analytically, into simple algebraic equations. These equations can then be solved using the power of computers. These methods are called computational fluid dynamics, CFD. This chapter presents the mathematical equations that must be solved and the particular method used in this research to solve them.

3.2 The Governing Equations

To evaluate the thermal performance of the indirect heating integrated collector storage solar water heating system, the velocity, temperature and pressure of the fluids involved in the system need to be evaluated. These fluids are water (in the storage tank and the service water in the pipe) and air (in the gap spacing between the glass covers). The equations that govern the fluid flow and heat transfer are the continuity, momentum and energy equations. The equations for unsteady, turbulent and incompressible flow are presented below.

1. According to Versteeg and Malalasekera (2007, pp. 62-4), the continuity equation is:

$$div\,\boldsymbol{U} = 0 \qquad (3.1)$$

where;

$\boldsymbol{U}$:fluid velocity vector (i.e.$\boldsymbol{U} = \bar{u}i + \bar{v}j + \bar{w}k$)

The continuity equation is written in rectangular coordinates as below.

$$\frac{\partial \bar{u}}{\partial x} + \frac{\partial \bar{v}}{\partial y} + \frac{\partial \bar{w}}{\partial z} = 0 \qquad (3.2)$$

2. According to Versteeg and Malalasekera (2007, pp. 62-4), momentum or Reynolds-Averaged Navier-Stokes equations are:

   a. x-momentum equation

$$\frac{\partial\overline{\rho}\,\bar{u}}{\partial t}+\ \mathrm{div}\left(\overline{\rho}\,\bar{u}\ \boldsymbol{U}\right)$$

$$=-\frac{\partial\overline{p}}{\partial x}+\ div(\mu\ grad\bar{u}\ )$$

$$+\left[-\frac{\partial\left(\overline{\overline{\rho}\,u'^2}\right)}{\partial x}-\frac{\partial(\overline{\overline{\rho}\,u'\,v'})}{\partial y}-\frac{\partial(\overline{\overline{\rho}\,u'w'\,})}{\partial z}\right]$$

$$+\ \ f_x \qquad (3.3a)$$

b. y-momentum equation

$$\frac{\partial\overline{\rho}\,\bar{v}}{\partial t}+\ \mathrm{div}\left(\overline{\rho}\,\bar{v}\,\boldsymbol{U}\right)$$

$$=-\frac{\partial\overline{p}}{\partial y}+\ div(\mu\ grad\bar{v}\ )$$

$$+\left[-\frac{\partial(\overline{\overline{\rho}\,u'\,v'})}{\partial x}-\frac{\partial\left(\overline{\overline{\rho}\,v'^2}\right)}{\partial y}-\frac{\partial(\overline{\overline{\rho}\,v'w'\,})}{\partial z}\right]$$

$$+\ \ f_y \qquad (3.3b)$$

c. z-momentum equation

$$\frac{\partial\overline{\rho}\,\bar{w}}{\partial t}+\ \mathrm{div}\left(\overline{\rho}\,\bar{w}\ \boldsymbol{U}\right)$$

$$=-\frac{\partial\overline{p}}{\partial z}+\ div(\mu\ grad\bar{w}\ )$$

$$+\left[-\frac{\partial(\overline{\overline{\rho}\,u'\,w'})}{\partial x}-\frac{\partial(\overline{\overline{\rho}\,v'\,w'})}{\partial y}-\frac{\partial\left(\overline{\overline{\rho}\,w'^2\,}\right)}{\partial z}\right]$$

$$+\ \ f_z \qquad (3.3c)$$

3. According to Nakayama (1995, pp. 73-5), the energy equation governing this type of flow is written in abbreviated form as:

$$\frac{\partial \overline{T}}{\partial t} + \frac{\partial (\overline{\mathbf{V}}_j \overline{T})}{\partial x_j} = \frac{\partial}{\partial x_j}\left(\frac{\vartheta}{Pr}\frac{\partial \overline{T}}{\partial x_j} - \overline{u_j' T'}\right) \tag{3.4}$$

Where:
$f_{x,y,z}$: Body force in the direction of x, y and z
p: Fluid pressure

$\overline{\mathbf{V}}_j$: Tensor notation of mean velocity vector of the fluid and it has three components for Cartesian coordinate, one in x direction ($\overline{\mathbf{V}}_1 = \bar{u}$), one in y direction ($\overline{\mathbf{V}}_2 = \bar{v}$) and one in z direction ($\overline{\mathbf{V}}_3 = \bar{w}$)

x_i: Cartesian coordinates (x, y, z)
$\overline{u_j' T'}$: Turbulent heat flux
Pr: Turbulent Prandtl number
ϑ: Fluid kinematic viscosity

The tool that is used to solve the above equations is described in the following sections.

3.3 Computational Fluid Dynamics (CFD)

Computational fluid dynamics (CFD) is the science of predicting fluid flow, heat and mass transfer and related phenomena such as chemical reaction, mixing flow and phase change by solving numerically the mathematical equations. These equations represent the physical laws that govern the processes. CFD approach has been used widely in industrial applications such as the design of aircraft, jet engines, internal combustion engines, combustion chambers of gas turbines and furnaces. The methods are also used in non-industrial applications like weather prediction, and simulating the blood flow through arteries and veins.

Several CFD-codes are available: CFX, FLUENT, PHOENICS and STAR-CD. The present study used FLUENT software, because of its availability to the author and because it has been used and validated in many studies including the indirect heating integrated collector storage solar water heating system (Gertzos & Caouris 2007, 2008; Gertzos, Caouris & Panidis 2010; Gertzos, Pnevmatikakis & Caouris 2008). To use FLUENT or any CFD-code successfully, the users must have a good understanding of the internal working of these codes i.e. the physics applied to the fluid flow and the fundamentals of the numerical algorithms (Versteeg & Malalasekera 2007, p. 6). The advantages of using CFD and the theory of the CFD approach are presented in the following section.

3.4 The Advantages of Using CFD Approaches

Although the experimental results are more acceptable than results obtained by using CFD methods, CFD approaches have many advantages (Versteeg & Malalasekera 2007, p. 6):

1. CFD methods are cheaper than the experimental approaches. They can be used to perform parametric studies to optimise equipment performance for lower costs and less time
2. Details of results obtained by using CFD are more than details of experiments
3. CFD approach has the ability to study systems that are very difficult to control practically, particularly very large systems
4. CFD approach has the ability to investigate systems that are too dangerous to be investigated experimentally.

3.5 Types of Flow

The fluid flow is classified into three types, laminar, transitional and turbulent flow. The ratio of the inertia forces to the viscous forces in the fluid which is known as the "Reynolds number" indicates whether the flow is laminar, transitional or turbulent. When the Reynolds number is lower than a critical value, which depends on the problem type, the flow is smooth and moves in layers past each other in an orderly fashion. This kind of flow is the laminar flow. However, when the Reynolds number exceeds the critical value, which tends to be the case in many practical problems, the flow is turbulent (Versteeg & Malalasekera 2007, pp. 40-1). The turbulent flow is characterized by a rapid mixing of fluid particles due to random three dimensional velocity fluctuations (Figure 3.1). The fluid molecules in turbulent flow fluctuate at a variable length and time scale.

The heat transfer and the friction in the turbulent flow are higher than that in the laminar flow, as the momentum and energy exchange between the molecules and the solid walls increase (Blazek 2005, p. 227). For the laminar flow, the velocity components in x, y, z direction, pressure, density and temperature of the fluid particles are simply u, v, w, p, ρ, and T respectively while the turbulent velocity components, pressure, density and temperature are represented as:

$$u = \bar{u} + u' \qquad v = \bar{v} + v'$$

$$w = \bar{w} + w' \qquad P = \bar{P} + P'$$

$$\rho = \bar{\rho} + \rho' \qquad T = \bar{T} + T'$$

where;

$u', v', w', P', \rho', T'$ are the fluctuation terms, $\bar{u}, \bar{w}, \bar{\rho}, \bar{v}, \bar{P}, \bar{T}$ are the mean value of the flow properties.

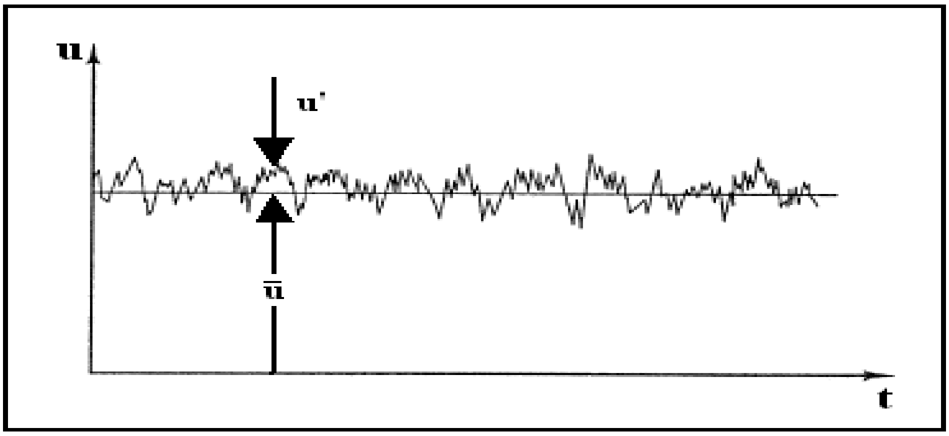

Figure 3.1: Typical point velocity measurement in turbulent flow (Versteeg & Malalasekera 2007, p. 41)

The flow in the indirect heating integrated collector system is turbulent as it is in most engineering applications.

3.6 Turbulence Modelling and Direct Numerical Simulation

Due to random three dimensional velocity fluctuations, the turbulence causes a rapid mixing of the fluid particles. The fluid molecules fluctuate at variable lengths and time scales, and they interact in a dynamically complex way (Versteeg & Malalasekera 2007, p. 65). Much research has been developed to capture the important effect of turbulence (the effect of eddies), and to solve the turbulent governing equations. The turbulent modelling approaches are classified into two groups (Versteeg & Malalasekera 2007, pp. 65-6):

1. Turbulence model for Reynolds-averaged Navier-Stokes (RANS) equations:

   This type of modelling focuses on the mean flow properties and on the effect of turbulence on these properties. The Reynolds stresses ($\rho\overline{V'_i}\overline{V'_j}$)

and the turbulent heat flux terms ($\overline{u_j' T'}$) are modelled to solve Reynolds-Averaged Navier-Stokes and energy equations. This type of turbulence modelling requires less computational time than other approaches such as large eddy simulation and direct numerical simulation because it only produces a solution of the mean values of flow pressure, temperature and velocity. However the fluctuation of these values that arise due to turbulent i.e. u′, v′, w′, T′ and p′ are estimated using different formulation. These include Mixing length, Spalart-Allmaras, k-ϵ, k-ω, Algebraic stress and Reynolds stress models

2. Large eddy simulation:

Large eddy simulation (LES) model tries to capture all flow scales. In the turbulent flow, the fluid molecules fluctuate with wide range of lengths and time scales. The Reynolds number of the large eddies (R_{el}), calculated based on length scale, is similar to the mean flow Reynolds number (R_e), while it equals to one for the small eddies (Versteeg & Malalasekera 2007, pp. 40-3). It is very computationally expensive to solve the entire turbulent length scales and it is not feasible for the high Reynolds number. In this model, the large eddies are directly resolved, but the small eddies are modelled using one of the RANS model. The large eddies are anisotropic and directly affected by geometry, boundary condition and body force. They are responsible for transporting most of the momentum, mass and energy in the turbulent flow. However, the small eddies are isotropic, especially for high R_e and less dependent on geometry. They are easily modelled by other turbulent models such as RANS models. This model requires a significantly finer mesh than RANS and it has to solve time dependent equations. As a result, more powerful hardware and more computational time are required to solve the flow with LES (ANSYS 2009)

There is another method of solving the turbulent flow equation that is direct numerical simulation (DNS). The mean flow and all turbulence velocity fluctuation are solved in this model. The unsteady turbulent equations are solved with small time step to resolve the period of the fastest fluctuations. Up to date, this method is not commonly used, as high computing resources are required and it requires much finer special grid than the other turbulence models. In turbulent flow, the ratio of the smallest to largest length scales was estimated as a proportion of $R_e^{3/4}$. As the smallest and largest turbulent length scales are solved in DNS and the turbulent flows are inherently three-dimensions, computing meshes increase by $R_e^{9/4}$. If a typical turbulent flow with 10^4 Reynolds number needs to be solved with DNS, computing meshes with 10^9 grid points are required (Versteeg & Malalasekera 2007, pp. 65-111).

In this study, the k-ϵ model was chosen to be used to identify the optimum air gap spacing. In the heat exchanger investigation, the results for the particular system using the realizable k-ϵ and standard k-ω turbulence models were compared to available experimental results to determine the appropriateness of the turbulence model choice. Both models gave good agreement with the experimental results, but the percentage error for the numerical simulation of k-ϵ model was higher than for the k-ω model (these results will be presented in chapter 4).

The reasons for choosing the k-ϵ and k-ω turbulence models in the present study are given bellow.

1. As k-ϵ and k-ω models are Reynolds-averaged Navier-Stokes (RANS) equations models, they require reasonable computational time,
2. Their accuracy is appropriate in many industrial applications, and They were used previously in the investigations of the indirect heating system and they were found to have a good agreement with experimental results such as the work by (Gertzos & Caouris 2007, 2008; Gertzos, Caouris & Panidis 2010; Gertzos, Pnevmatikakis & Caouris 2008).

Therefore, k-ϵ and k-ω models were assumed to be appropriate for this work and they are described in more details below.

The governing equations (3.1, 3.3 and 3.4) are derived by applying the Reynolds-time averaging approach (Nakayama 1995, pp. 73-5). The Reynolds-time averaging equation is given below.

$$\overline{V_i} = \lim_{T \to \infty} \frac{1}{T} \int_t^{t+T} V_i \, dt \qquad (3.5)$$

T→ ∞ means that the time interval “T” should be large as compared to the typical time scale of the turbulent fluctuations (Blazek 2005, pp. 231-2).

Due to the presence of the turbulence, there are extra components that appear in the momentum and energy equations. These components are the Reynolds stresses tensor ($\rho\overline{V'}_i\overline{V'}_j$) and the turbulent heat flux tensor ($\overline{u_j' T'}$). Additional equations other than equations (3.1, 3.3 and 3.4) are required to solve these parameters that appear due to the turbulence. The methods used in this study are presented in the next section.

3.6.1 K-ϵ Model

The k-ϵ model is a two-equation model commonly used in industrial applications, as it provides reasonable accuracy for the majority of turbulent flow computations and it is economic in terms of computational expense. The model is based on two assumptions that (a) the flow is fully turbulent and (b) the effect of molecular viscosity can be neglected. Therefore, this model is not valid, when these conditions are not met (ANSYS 2009, pp. 4-12). The method applied to derive k and ϵ equations is presented below:

According to Launder & Spalding (1972, p. 74) the kinetic energy equation (k-equation) is derived by applying the following steps:

a. Multiply x, y, and z -component of the momentum equation (3.3a, b and c) by $u^{'}, v^{'}, w^{'}$ respectively
b. Apply the Reynolds-time averaging approach on the resulting equations
c. Summing the three equations and with mathematical rearrangement result which results in the following turbulent kinetic energy, k, equation

$$\frac{\partial k}{\partial t} + \overline{\boldsymbol{V}}_{\boldsymbol{j}} \frac{\partial k}{\partial x_j} = \tau_{ij} \frac{\partial \overline{\boldsymbol{V}}_i}{\partial x_j} - \varepsilon + \frac{\partial}{\partial x_j}\left[\vartheta \frac{\partial k}{\partial x_j} - \left(\underset{[\mathrm{T.T.}]}{\frac{1}{2}\overline{u'_i u'_i u'_j}}\right) - \left(\underset{[\mathrm{P.D.}]}{\frac{1}{\rho}\overline{p' u'_j}}\right)\right] \tag{3.6}$$

where;

T.T.: Turbulent transport

P.D.: Pressure diffusion

The turbulent dissipation rate equation (ε) is derived by applying the following moment of the Navier-Stokes equation (Wilcox 2006, p. 129):

$$2\vartheta \overline{\frac{\partial u'_i}{\partial x_j} \frac{\partial}{\partial x_j} [N(u_i)]} = 0 \qquad (3.7)$$

where;

$N(u_i)$: Navier-Stokes operator which is given below:

$$N(u_i) = \rho \frac{\partial u_i}{\partial t} + \rho u_k \frac{\partial u_i}{\partial x_k} + \frac{\partial p}{\partial x_i} - \mu \frac{\partial^2 u_i}{\partial x_k \partial x_k} = 0 \qquad (3.8)$$

The exact equation of the turbulent dissipation, (3.9), is obtained by solving equations (3.7) and (3.8).

$$\frac{\partial \varepsilon}{\partial t} + \overline{\boldsymbol{V}}_j \frac{\partial \varepsilon}{\partial x_j} = -2\vartheta\left[\overline{u'_{i,k} u'_{j,k}} + \overline{u'_{k,i} u'_{k,j}}\right] \frac{\partial \overline{\boldsymbol{V}}_i}{\partial x_i} - 2\vartheta \overline{u'_k u'_{i,j}} \frac{\partial^2 \overline{\boldsymbol{V}}_i}{\partial x_k \partial x_j}$$
$$- 2\vartheta \overline{u'_{i,k} u'_{j,m} u'_{k,m}} - 2\vartheta^2 \overline{u'_{i,km} u'_{j,km}}$$
$$+ \frac{\partial}{\partial x_i}\left[\vartheta \frac{\partial \varepsilon}{\partial x_j} - \vartheta \overline{u'_j u'_{i,m} u'_{i,m}} - 2\frac{\vartheta}{\rho} \overline{p'_m u'_{j,m}}\right] \qquad (3.9)$$

Three types of the k-ϵ model are available in the FLUENT software, including Standard, RNG and Realizable k-ϵ. The Realizable k-ϵ model was chosen to be used in the optimization of the air gap spacing because it outperforms the standard and

RNG k-ϵ models of predicting the flows involving rotation, separation and recirculation (ANSYS 2009, pp. 4-18). Therefore, this model is presented in the next section and the author refers to the ANSYS-FLUENT help for more information about the other models.

Realizable k-ϵ Model

A realizable k-ϵ model is developed by Shih et al. (1995). The term "realizable" means the model satisfies certain mathematical constraints on the Reynolds stresses and is consistent with the physics of turbulent flows (ANSYS 2009, pp. 4-18). The model is characterised by a new formula for the turbulent viscosity that is derived based on the realizability constrains. The modelled kinetic energy, k, equation, (3.10), is derived from the exact kinetic energy equation, equation (3.6). The dissipation rate, ε, equation (3.13), is also derived from the exact dissipation rate equation, (3.9), by developing a model equation for the dynamic equation of the mean-square vorticity fluctuation. These two equations are given below:

The k-equation:

$$\frac{\partial(\rho k)}{\partial t}+\frac{\partial\left(\rho k\overline{\boldsymbol{V}}_{\boldsymbol{i}}\right)}{\partial x_i}$$

$$=\frac{\partial}{\partial x_j}\left[\left(\mu+{}^{\mu_t}/_{\sigma_k}\right)\frac{\partial k}{\partial x_j}\right]+\left[\underset{[I]}{-\rho\overline{u_i'u_j'}\,\frac{\partial u_j}{\partial x_i}}\right]+\left[\underset{[II]}{\beta g_i\,\frac{\mu_t}{Pr_t}\,\frac{\partial T}{\partial x_i}}\right]-\rho\varepsilon$$

$$-\begin{bmatrix}2\rho\varepsilon M_t^2\\ [III]\end{bmatrix}+S_k \qquad (3.10)$$

where; Pr_t is turbulent Prandtl number for energy, g_i is the component of the gravitational vector in i direction, σ_k is turbulent Prandtl number for k and its default value is 1.0, S_k is the kinetic energy source term, and β, which is the coefficient of thermal expansion, is defined as:

$$\beta = -\frac{1}{\rho}\left(\frac{\partial \rho}{\partial T}\right) \qquad (3.11)$$

M_t is defined as turbulent Mach number

$$M_t = \sqrt{\frac{k}{a^2}} \qquad (3.12)$$

where; $a = \sqrt{\gamma R T}$ speed of sound.

The term [I] in equation (3.10) presents the generation of turbulent kinetic energy due to the mean velocity gradients, [II] the generation of turbulence energy due to buoyancy and [III] the effects of compressibility on turbulence which is neglected in the present study because the flow was assumed to be incompressible.

The ϵ-equation:

$$\frac{\partial(\rho\varepsilon)}{\partial t} + \frac{\partial\left(\rho\varepsilon\overline{\boldsymbol{V}}_{\boldsymbol{i}}\right)}{\partial x_i} = \frac{\partial}{\partial x_j}\left[\left(\mu + {}^{\mu_t}/_{\sigma_\varepsilon}\right)\frac{\partial \varepsilon}{\partial x_j}\right] + \rho C_1 S_\varepsilon - C_2\rho\frac{\varepsilon^2}{k+\sqrt{\vartheta\varepsilon}} + C_{1\varepsilon}\frac{\varepsilon}{k}C_{3\varepsilon}\left[\beta g_i\frac{\mu_t}{Pr_t}\frac{\partial T}{\partial x_i}\right] + S_\varepsilon \qquad (3.13)$$

where;

$$C_1 = max\left[0.43, \frac{\text{ב}}{\text{ב} + 5}\right], \qquad \text{ב}? = S\frac{k}{\varepsilon}, \qquad S = \sqrt{2S_{ij}S_{ij}},\ S_{ij} = \frac{1}{2}\left(\frac{\partial u_j}{\partial x_i} + \frac{\partial u_i}{\partial x_j}\right)$$

$$C_{1\varepsilon} = 1.44, \qquad C_2 = 1.9, \qquad \sigma_\varepsilon = 1.2, \qquad \sigma_k = 1.0$$

The turbulent viscosity, μ_t, is modelled as below:

$$\mu_t = \rho C_\mu \frac{k^2}{\varepsilon} \qquad (3.14)$$

Equation (3.14) is also used to calculate the turbulent viscosity in the standard k-ϵ model. The difference between the two models is that C_μ is constant in the standard k-ϵ model, while in the Realizable k-ϵ model it is modelled as below.

$$C_\mu = \frac{1}{A_o + A_s\frac{kU^*}{\varepsilon}} \qquad (3.15)$$

where;

$$U^* = \sqrt{S_{ij}S_{ij} + \tilde{\Omega}_{ij}\tilde{\Omega}_{ij}} \qquad (3.16)$$

$$\tilde{\Omega}_{ij} = \Omega_{ij} - 2\varepsilon_{ijk}\omega_k, \qquad \Omega_{ij} = \overline{\Omega}_{ij} - \varepsilon_{ijk}\omega_k$$

S_ε: Energy dissipation source term

$\overline{\Omega}_{ij}$: mean rate of rotation tensor

ω_k: the angular velocity

$A_o = 4.04,\ \ A_s = \sqrt{6}cos\phi,\ \ \phi = \frac{1}{3}cos^{-1}\left(\sqrt{6}W\right), W = \frac{S_{ij}S_{jk}S_{ki}}{\tilde{S}^3}, \tilde{S} = \sqrt{S_{ij}S_{ij}},\ S_{ij} = \frac{1}{2}\left(\frac{\partial u_j}{\partial x_i} + \frac{\partial u_i}{\partial x_j}\right)$

It should be noted that the effect of mean rotation is included in the definition of the turbulent viscosity, equation (3.15) and (3.16). This can result in non-physical turbulent viscosities when the domain contains both rotational and stationary zones (ANSYS 2009).

3.6.2 K-ω Model

Like k-ϵ model, k-ω model is known as a two-equation model. One equation is the turbulent kinetic energy and the other is ω-equation which is defined as a rate of dissipation of energy in unit volume and unit time. The ω-equation, which is presented below, was derived by Kolmogorov in 1942 using dimensional analysis technique (Wilcox 2006, pp. 124-5).

$$\frac{\partial \omega}{\partial t} + \overline{\boldsymbol{V}}_{\boldsymbol{j}} \frac{\partial \omega}{\partial \boldsymbol{x}_{\boldsymbol{i}}} = -\beta \omega^2 + \frac{\partial}{\partial x_j}\left[\sigma \vartheta_t \frac{\partial \omega}{\partial x_i}\right] \tag{3.17}$$

In FLUENT software, two types of the models are available; standard and shear-stress transport (SST) k-ω model. The standard model was chosen to be used in the optimization of the heat exchanger design because it is good at predicting the flow near the walls. Therefore, it is described in more details below.

Standard k-ω Model

This model was developed by Wilcox (in 1998) who improved equation (3.17) for a low Reynolds number, compressibility and shear flow spreading. According to Wilcox (2006, p. 125), equation (3.17) has the following deficiencies:

1. There is no production of kinetic energy term

2. This equation can only be applied for the domain with a high Reynolds number because there is no molecular diffusion term.

The accuracy of the model was improved for predicting free shear flows, as the production term has been added to the k and ω equations. The equations of the standard k-ω model are given below (ANSYS 2009).

The k-equation:

$$\frac{\partial(\rho k)}{\partial t}+\frac{\partial\left(\rho k\overline{\boldsymbol{V}}_i\right)}{\partial x_i}=\frac{\partial}{\partial x_j}\left[\Gamma_k\frac{\partial k}{\partial x_j}\right]+\left[\underset{[I]}{-\rho\overline{u_i'u_j'}\frac{\partial u_j}{\partial x_i}}\right]-\left[\underset{[II]}{\rho\beta^* f_{\beta^*}k\omega}\right]+S_k \qquad (3.18)$$

where;

The term [I] presents the turbulent production and the term [II] presents the turbulent dissipation of k.

The ω-equation:

$$\frac{\partial(\rho\omega)}{\partial t}+\frac{\partial\left(\rho\omega\overline{\boldsymbol{V}}_i\right)}{\partial x_i}$$

$$=\frac{\partial}{\partial x_j}\left[\Gamma_\omega\frac{\partial\omega}{\partial x_j}\right]+\left(\underset{[i]}{\alpha\frac{\omega}{k}\left[-\rho\overline{u_i'u_j'}\frac{\partial u_j}{\partial x_i}\right]}\right)-\left[\underset{[ii]}{\rho\beta f_\beta\omega^2}\right]+S_\omega \qquad (3.19)$$

where;

The term $[i]$ presents the generation of ω and the term $[ii]$ is the dissipation of ω. Γ_k and Γ_ω present the effective diffusivity of k and ω, respectively, that are computed as below.

$$\Gamma_k=\mu+\frac{\mu_t}{\sigma_k} \qquad (3.20)$$

$$\Gamma_\omega=\mu+\frac{\mu_t}{\sigma_\omega} \qquad (3.21)$$

σ_k and σ_ω are the turbulent Prandtl number for k and ω, respectively. The turbulent viscosity is modelled as below:

$$\mu_t = \alpha^* \frac{\rho k}{\omega} \qquad (3.22)$$

$\alpha^*$is defined as a low-Reynolds number correction and computed as below:

$$\alpha^* = \alpha_\infty^* \left(\frac{\alpha_0^* + {}^{R_{et}}/_{R_k}}{1 + {}^{R_{et}}/_{R_k}} \right) \qquad (3.23)$$

$$R_{et} = \frac{\rho k}{\mu\omega}, R_k = 6, \alpha_0^* = \frac{\beta_i}{3}, \beta_i = 0.072$$

For a high Reynolds number $\alpha^* = \alpha_\infty^* = 1$.

$$\alpha = \frac{\alpha_\infty}{\alpha^*} \left(\frac{\alpha_0 + {}^{R_{et}}/_{R_\omega}}{1 + {}^{R_{et}}/_{R_\omega}} \right), R_\omega = 2.95 \qquad (3.24)$$

$$f_{\beta^*} = \begin{cases} 1 & x_k \leq 0 \\ \dfrac{1 + 680x_k^2}{1 + 400x_k^2} & x_k > 0 \end{cases} \qquad (3.25)$$

$$x_k = \frac{1}{\omega^3}\frac{\partial k}{\partial x_j}\frac{\partial \omega}{\partial x_j}, \beta^* = \beta_i^*[1 + \zeta^* F(M_t)], \beta_i^* = \beta_\infty^* \left(\frac{{}^4/_{15} + \left({}^{R_{et}}/_{R_\beta} \right)^4}{1 + \left({}^{R_{et}}/_{R_\beta} \right)^4} \right), \zeta^*$$

$$= 1.5, R_\beta = 8, \beta_\infty^* = 0.09 \qquad (4.26)$$

$$f_\beta = \frac{1+70x_\omega}{1+80x_\omega}, x_\omega = \left|\frac{\Omega_{ij}\Omega_{ik}S_{ki}}{\beta_\infty^* \omega}\right|, \Omega_{ij} = \frac{1}{2}\left(\frac{\partial u_i}{\partial x_j} - \frac{\partial u_i}{\partial x_i}\right), S_{ki} = \frac{1}{2}\left(\frac{\partial u_i}{\partial x_k} - \frac{\partial u_k}{\partial x_i}\right), \beta = \beta_i\left[1 - \frac{\beta_i^*}{\beta_i}\zeta^* F(M_t)\right] \quad (3.27)$$

$F(M_t)$ is defined as the compressibility correction function and is given as below

$$F(M_t) = \begin{cases} 0 & M_t \leq M_{t0} \\ M_t^2 - M_{t0}^2 & M_t > M_{t0} \end{cases} \quad (3.28)$$

where;

$$M_t^2 = \frac{2k}{a^2}, M_{t0} = 0.25, a = \sqrt{\gamma RT} \quad (3.29)$$

Note: $\beta_i^* = \beta_\infty^*$ for a high Reynolds number and $\beta^* = \beta_i^*$ for incompressible flow. The model constants are given below:

$$\alpha_\infty^* = 1, \alpha_\infty = 0.52, \alpha_0 = \frac{1}{9}, \beta_\infty^* = 0.09, \beta_i = 0.072, R_\beta = 8, R_k = 6, R_\omega = 2.95,$$

$$\zeta^* = 1.5, M_{t0} = 0.25, \sigma_k = 2.0, \sigma_\omega = 2.0$$

After presenting the CFD equations and the methods used to solve them, the next section presents the process of any commercial CFD-code.

3.7 Wall treatment for wall bounded turbulent flow

The walls have important effect on the turbulent flow, as the wall no-slip condition affects the mean flow velocity. The fluid molecular fluctuation is also changed by the presence of walls. In the near-wall region, the tangential velocity fluctuations are reduced by viscous damping, while the normal fluctuations are reduced by kinematic blocking. As the velocity is largely increased toward the turbulent core, the production of kinetic energy rapidly augments the turbulence. Therefore, accurate modelling is very necessary to resolve the flow in the near-wall region where the velocity has large gradients (ANSYS 2009).

The near-wall region is divided into three layers including viscous sublayer in which the flow is almost laminar, molecular layer in which the viscosity plays important role in momentum and heat or mass transfer, and the fully turbulent layer in which the turbulence plays a significant role. Two methods are applied to model the flow near walls, including "wall function" and "near-wall-modelling". In the wall function approach, semi-empirical formulas are used to calculate the viscosity-affected region (viscous sublayer and molecular layer). This approach is less computationally expensive than the near-wall-modelling approach. In the near-wall-modelling approach, the turbulence models are modified to resolve the viscosity-affected region (ANSYS 2009).

When k-ϵ turbulence model is used, three types of wall functions are available in FLUENT, including standard wall function, non-equilibrium wall function and enhanced wall function (See FLUNT theory guide for more information about these functions). However, when k-ω turbulence model is used, FLUENT treats the boundary condition near the walls by using enhanced wall function and for the fine meshes low-Reynolds number boundary condition is applied (ANSYS 2009).

3.8 The Use of CFD Software

The fluid flow governing equations are solved, using ANSYS-FLUENT software which is a commercial CFD package. FLUENT and all commercial CFD packages contain three main elements for the input of the problem parameters to solve the problem and examine the results. These are (a) a pre-processor, (b) a solver and (c) a post-processor (Versteeg & Malalasekera 2007, pp. 2-4).

a) Pre-processor

In this step, a representative model of the flow problem is created before the numerical solution process. This step involves the following:

1. Create the computational domain
2. Grid generation: divide the domain into a number of elements
3. Choose the physical and chemical phenomena that need to be solved
4. Define the fluid properties
5. Specify the boundary condition

In the pre-processor step, the shape and size of the elements in a flow domain play an important role for the accuracy of the solution and for the computational time required to solve the problem. In the three dimensional simulation, the perfect shape is a hexahedron of aspect ratio equal to one, because the number of elements is the lower than if tetrahedron elements are used and the elements are laid perpendicular to the fluid flow. As a result, a significant reduction in the simulation time and more accurate results are achieved. Furthermore, as the size of the elements is reduced, the accuracy of the solution increases. However, the increased number of cells means more computational time and more powerful computer hardware are required.

Therefore, the shape and cell size must be optimized to obtain physically realistic results in less time.

b) Solver

The governing equations for the fluid flow which are presented in Section 3.2 are non-linear partial differential equations and the analytical solution is impossible except for very few simple cases. CFD-codes solve these equations numerically. The numerical solution is an approximate way of solving the differential equations, leading to the evaluation of velocities, pressures, and temperatures at predetermined locations within the nodes (Anderson 1995, pp. 23-79). Different numerical methods are used to solve the fluid flow equations, including finite difference, finite element, finite volume, boundary element and the meshless method (neural network). FLUENT software uses the control volume approach and the numerical algorithm of this method consists of three main steps:

1. The governing equations of the fluid flow are integrated over a number of control volumes about the cell centres or vertices to form set of discrete equations
2. The non-linear equations are linearised and the resulting equations are converted into a system of algebraic equations
3. Iterative process is performed to solve the set of algebraic equations.

c) Post-processor

Post-processor step is a way of presenting the predicted flow data and producing the CFD images and animations. There are many methods of presenting the results in the

CFD approaches and these include vector plot, contour plots, 2D and 3D surface plot.

3.9 Chapter Conclusion

In order to have a basic knowledge of the CFD-codes, this chapter presented the fundamental physics of the fluid flow and heat transfer. The continuity, momentum and energy equations that govern the fluid flow are non-linear partial differential equations, so that they must be solved numerically. Due to the appearance of eddies in the turbulent flow; the equations are more complex in turbulent flow than in laminar flow. Therefore, an approximating approach is applied to solve the governing equations for turbulent flow i.e. turbulence modelling. The Reynolds-average Navier-Stokes (RANS) equations method is appropriate in many industrial applications and requires less computational expense than large eddy and direct numerical simulation approaches. The most famous RANS models are the k-ϵ and k-ω models, and these are used in this study. The realizable k-ϵ model is simply the standard k-ϵ model being improved to predict the flows involving rotation, separation and recirculation. Furthermore, the k-ω model is very good at predicting flow near the surfaces.

CHAPTER 4: System Modifications using the CFD Approach

- ***Introduction***
- ***Optimisation of the Air Gap Spacing***
- ***Optimisation of the Heat Exchanger***
- ***Chapter Conclusion***

4.1 Introduction

As indicated in Chapter 1, the indirect heating system is the most economical solar water heating system. In this project, CFD approach was used to enhance the efficiency of the indirect heating system. The objectives of this study are to increase the heat gain from the sun, minimise the heat loss from the system, and reduce both the initial and operating costs. The optimum air gap size was investigated to reduce the heat losses to the ambient atmosphere through radiation and convection heat transfer. The optimum heat exchanger design was also investigated to enhance the heat gained by the service water. The chosen system has the following parameters:

1. Double glass covers with glass thickness of 3 mm
2. Absorber area of 0.7 m × 1.35 m with 10 mm thickness of metallic nickel chrome (M-N-chrome)

3. Storage tank volume of 81 x 135 x 10 cm (containing about 109l of water) with 2 mm thickness of iron sheet
4. Insulation walls of wood with 50 mm thickness
5. Copper service water tubes of 1 mm thickness.

The physical properties used in the simulation of these materials are given in Table 4.1.

Table 4.1: Physical properties of material

Material name	Density (ρ) kg/m^3	Specific heat (C_p) J/ (kg. K)	Thermal conductivity (k) W/(m. K)	Emittance (ϵ)
M-N-chrome	7865	460	19	0.94
Glass	2800	800	0.81	0.93
Wood	700	2310	0.173	0.9
Copper	8978	381	387.6	Not included*
Iron	7832	434	63.9	Not included

**** The participation of Copper and Iron was not enabled in the radiation calculations.***

The following two sections describe the parametric study of the system to achieve the objectives of this study.

4.2 Optimisation of the Air Gap Spacing

The function of the air gap spacing is to insulate the absorber surface. However, the effectiveness of this insulation depends on the size of the air gap spacing (Manz 2003; Mossad 2006). Thus, the choice of the size of these gaps will have an impact on the performance of the solar collector. The system chosen in this work has a double air gap spacing, because it was found to have an efficient thermal performance (Kumar & Rosen 2011). L_1 is the lower air gap spacing between the absorber and the lower glass cover and L_2 is the upper gap between the upper and lower glass covers. L_1 and L_2 were varied within the range of 15-50 mm to investigate which combination of gap sizes would result in minimum total heat losses; including radiation and convection (Figure 4.1).

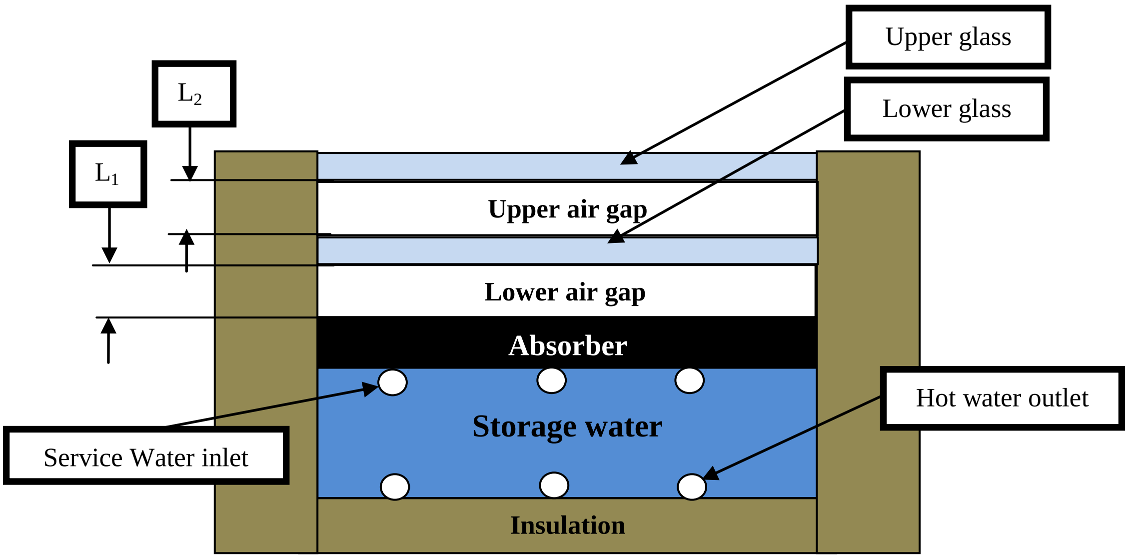

Figure 4.1: Cross section of the indirect heating integrated collector storage solar water heating system with double glass cover

4.2.1 CFD Model

3D CFD models for the absorber with the double glass cover (i.e. without the storage water and the heat exchanger) were developed to evaluate the radiation and convection losses (Figure 4.2). L_1 was changed to 15, 25 and 40 mm. For each value of L_1, L_2 was changed to 15, 25, 35 and 50 mm (i.e. combinations of 12 cases were investigated). The geometry and the computational grid were generated, using

ANSYS 13.0-Workbench. To validate the grid independency, three computational grids were developed for the model of L_1 equals 25 mm and L_2 equals 50 mm for 100,000, 162,000 and 227,500 elements. The elements shape were hexahedral for all models and finer mesh was chosen close to the walls (Figure 4.3). The 162,000 and 227,500 elements provided the same results which had ∓1 to 1.5% differences from the results of the 100,000 model. Therefore; the element size for all other models was kept similar to those models of 162,000 and 227,500 elements.

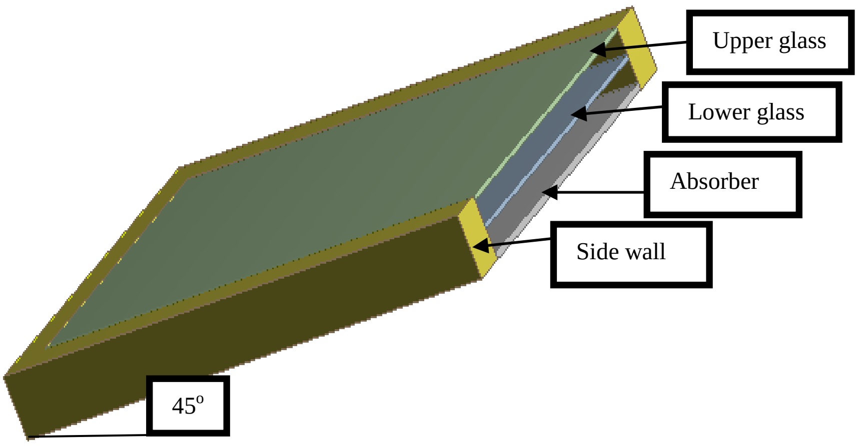

Figure 4.2: 3D model of the air spacing of the integrated collector system

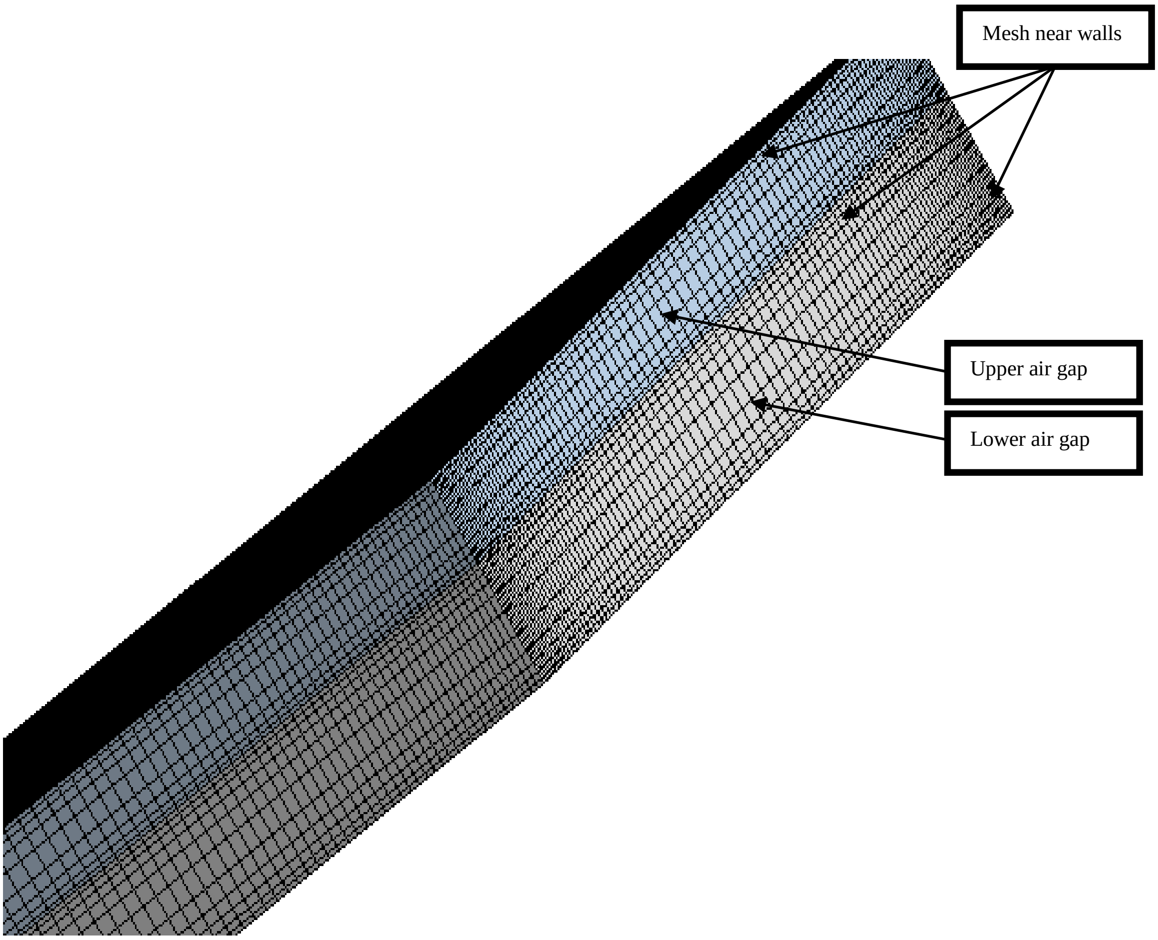

Figure 4.3: The computational grid for the air gap spacing

To predict the heat losses from the solar collector, the velocity and temperature of the air in the gap spacing and the temperature of the upper and lower glass covers require evaluation, since the heat loss depends on these values. The continuity, momentum and energy equations applied to the air in the gaps were solved in a steady state condition using FLUENT software. The pressure-based type solver and the Realizable k-ϵ turbulence model were used. The flow near the walls was treated by using the Non-Equilibrium wall function. The velocity-pressure coupling was treated by using the SIMPLE algorithm and a first order upwind scheme for Momentum, Turbulent Kinetic Energy and Turbulence Dissipation. For the residual, 10^{-4} was used as a convergence criterion for: x-velocity, y-velocity, z-velocity, kinetic energy, epsilon and continuity. For the energy, 10^{-8} was used.

The radiation heat transfer between surfaces and to the sky was included in the CFD model. The following two sections describe the radiation model.

a- Radiation model

The radiation heat loss to the sky was included in the boundary condition of the side wall and upper glass cover. The sky temperature was calculated by using the equation of Akhtar and Mullick (2007) as $0.0552\ T_a^{1.5}$. The sky temperature of 272.6 K was used, because ambient temperature, T_a, was taken as 290 K.

A Surface-to-Surface (S2S) radiation model was used to calculate the radiation heat transfer between surfaces. The radiation process was started by estimating the view factors between the surfaces. At every tenth iteration (the FLUENT default), throughout the solution, the radiosity of the surfaces was updated based on the new surfaces' temperature through another iterative process, in order to produce greater accuracy of the radiation heat transfer calculations.

In the S2S model, only surface to surface radiation is significant. The following assumptions are used in this model:

1. The absorption, emission or scattering of radiations are neglected
2. The surfaces are assumed to be gray and diffuse
3. The effect of air in the gap spacing is ignored

4. The surfaces are opaque (transmissivity is zero). The glass cover can be opaque in this case, because the wavelength of the surfaces radiation is ≥ 9.3 µm (Kreith, Frank. 2010, pp. 564-5).

b- The S2S model equations

As transmissivity is neglected, ($\tau = 0$), the energy flux leaving a given surface ($q_{out,k}$) includes two parts:

1. Directly emitted energy
2. Reflected energy

$$q_{out,k} = \boldsymbol{\varepsilon}_k \sigma T_k^4 + \boldsymbol{\rho}_k q_{in,k} \qquad (4.1)$$

where;
k: A surface involved in the model
$\boldsymbol{\sigma}$: Boltzmann's constant
$\boldsymbol{\rho}$: Reflectivity, (it is calculated as $\boldsymbol{\rho} = 1 - \boldsymbol{\varepsilon}$)
$\boldsymbol{\varepsilon}$: Emissivity ($\alpha = \varepsilon$)
$\boldsymbol{\alpha}$: Absorptivity
$q_{in,k}$: Energy flux incident on surface k from the surrounding surfaces which is calculated as:

$$q_{in,k} = \sum_{j=1}^{N} q_{out,j} F_{jk} \qquad (4.2)$$

where;
F_{jk}: View factor between surface k and
N: Number of surrounding faces
$q_{out,j}$: Energy flux leaving surface j

Therefore, in the S2S the energy flux leaving a surface (k) is calculated as the below equation (ANSYS 2009; Chhanwal et al. 2010).

$$q_{out,k} = \varepsilon_k \sigma T_k^4 + \rho_k \sum_{j=1}^{N} q_{out,j} F_{jk} \qquad (4.3)$$

4.2.2 Boundary Condition and Operating Parameters

The boundary condition on the side wall and upper glass cover was taken as convection with a heat transfer coefficient of 10 W/(m^2 K) to an ambient temperature, T_a, of 17^o C and radiation to the sky at a temperature which was taken according to Akhtar and Mullick (2007) as 0.0552 $T_a^{1.5}$. As previously mentioned, the service and storage water were not included in the model, so a constant temperature of 82^o C was assumed for the absorber surface in all cases. This was considered to be the maximum absorber temperature, assuming the solar incident radiation of 850 W/m^2. Therefore, the best gap spacing, which gives the minimum heat loss at maximum absorber temperature, can be identified. The collector angle was chosen to be 45^o from the horizontal (Figure 4.2). The interfaces between the glass covers, side walls and the air were defined as walls with coupled condition to allow the heat to transfer through these walls.

4.3 Optimisation of the Heat Exchanger

To enhance the performance of the heat exchanger, different pipe diameters, locations and shapes were chosen and modelled to identify the optimum configuration that is economically efficient and produces a high outlet service water temperature. The CFD model was firstly validated against an existing experiment to be sure that the CFD results were reliable.

4.3.1 Validating the CFD Model

In order to get confidence of the chosen model used in the CFD, the experimental work of Gertzos, Pnevmatikakis and Caouris (2008) was chosen to validate the CFD model.

4.3.1.1 Experimental procedure

Gertzos, Pnevmatikakis and Caouris (2008) examined heat transfer between the storage and service water with and without using circulating pump for the storage water. The system without circulating pump was used in this study to validate the CFD model. Their system consisted of a storage water tank and serpentine tube immersed in the storage water (Figure 4.4). The storage tank was made of iron (k= 63.9 W/m K and 1.7mm thick) and its inner dimensions were 81 x 135 x 10 cm containing about 109 l of water. It was insulated using glass wool (k= 0.041W/m K and 5 cm thickness). The tube was made of iron with 2 mm thickness and 10mm inside diameter (k = 63.9 W/m K). The total length of the tube inside the tank was 16.2 m. The part of the tube outside the storage tank was insulated by 1.9 cm thickness of conventional foam with 0.037 W/ m K thermal conductivity.

Experimental data of temperature was provided during a one hour period. The temperatures were monitored using six thermocouples which have an accuracy of ±1^{o} C. Four of these thermocouples were used to measure the storage water temperature (T_1, T_2, T_3 and T_4) and they were placed as shown in Figure 4.4. The other two were used to monitor the inlet and outlet service water temperature. A flow meter type buoyant was used to measure and regulate the inlet mass flow rate. The outlet flow rate was measured using electromagnetic flow meter with an accuracy ±0.35% of the measured value.

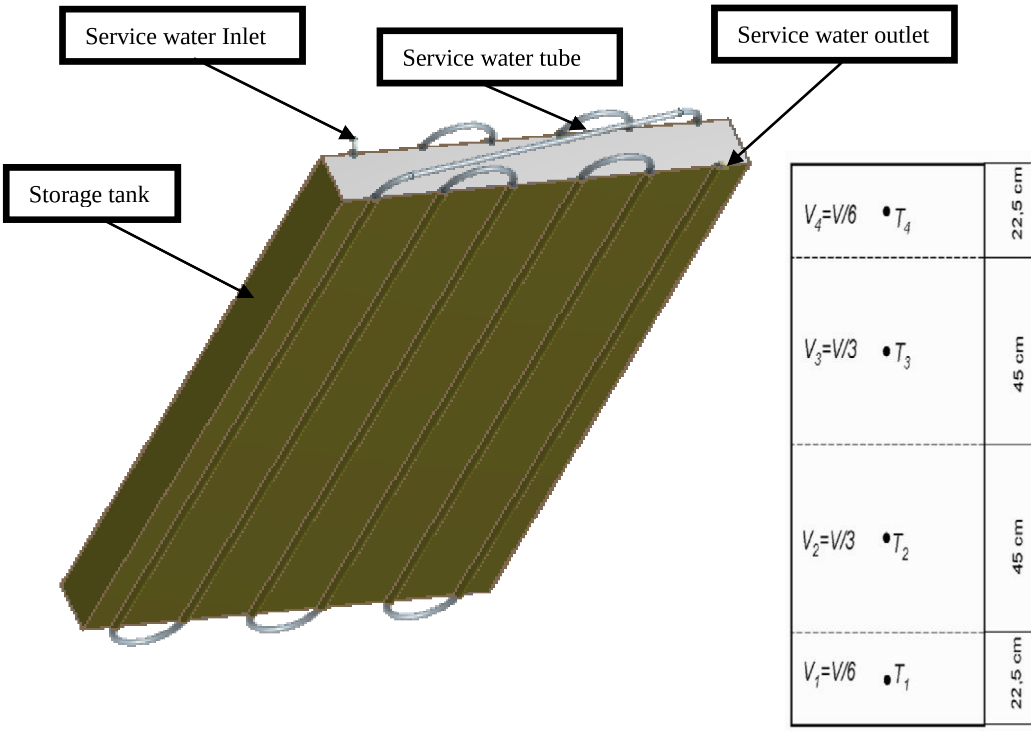

Figure 4.4: The system investigated in the experiment of Gertzos, Pnevmatikakis and Caouris (2008)

The experimental procedure took place indoors. The angle of the tank was 45^o from the horizontal plane. The inlet service water temperature was in the range of 16.5-17.8^o C and the mass flow rate was 500 L/h. The procedure was as follows. The storage water was heated, using successive passages through an external heater. When the temperature of the storage water reached 80^o C, the heating process stopped and the service water started to flow through the tube. The temperatures of the inlet and outlet service water were measured at one second time intervals. The storage water temperature was measured at four different positions (T_1, T_2, T_3 and

T_4); also at one second time intervals. These temperatures were averaged and recorded every 30 seconds, for energy withdrawal periods of one hour.

4.3.1.2 CFD Model for the Experimental Setup

A computational grid was developed for the same setup as Gertzos, Pnevmatikakis and Caouris (2008) using ANSYS 13.0 software. The number of elements was 1,130,000 and most of these were hexahedral (Figure 4.5). The continuity, momentum and energy equations were solved in transient conditions (for a one hour period). A pressure-based type solver was used and the effect of gravity was included with full buoyancy effect. The velocity-pressure coupling was treated, using the SIMPLE algorithm (Semi-Implicit Method for Pressure Linked equation). A first order upwind scheme was used for Momentum, Turbulent Kinetic Energy and Turbulence Dissipation. For the residual, 10^{-4} was used as a convergence criterion for: x-velocity, y-velocity, z-velocity, kinetic energy, epsilon and continuity. For the energy, 10^{-8} was used. The standard k-ω and the realizable k-ϵ turbulence models were chosen to identify the model that best produces results comparable to the results obtained by Gertzos, Pnevmatikakis and Caouris (2008).

The properties of water were varied as a function of temperature, according to the following equations recommended by Gertzos, Pnevmatikakis and Caouris (2008).

$$\rho = -1.3187 * 10^{-7} T^4 + 1.8447 * 10^{-4} T^3 - 9.9428 * 10^{-2} T^2 + 23.28T - 1113.5 \qquad (4.4a)$$

$$\mu = 3.533 * 10^{-11} T^4 - 4.8141 * 10^{-8} T^3 + 2.4637 * 10^{-5} T^2 - 0.0056188T + 0.48281 \qquad (4.4b)$$

$$C_p = 3.321729 * 10^{-6}T^4 - 4.459811 * 10^{-3}T^3 + 2.248733T^2 - 5.041488 * 10^2\, T + 4.654524 * 10^4 \qquad (4.4c)$$

$$k = 6.2068 * 10^{-10}T^4 - 8.0897 * 10^{-7}T^3 + 3.8437 * 10^{-4}T^2 - 7.7569 * 10^{-2}T + 6.1019 \qquad (4.4d)$$

The variation of properties of air with temperature was included by using the incompressible ideal gas equation to estimate the density and by using the kinetic theory equation to estimate the specific heat, thermal conductivity and viscosity. Equation (4.5a) is the equation to calculate air viscosity using the kinetic theory. The reader is referred to ANSYS (2009) for more details about the incompressible ideal gas equation, kinetic theory equations for specific heat and thermal conductivity.

$$\mu = 2.67 \times 10^{-6} \left[\frac{\sqrt{M_W T}}{\sigma^2\, \Omega_\mu}\right] \qquad (4.5a)$$

$$\Omega_\mu = \Omega_\mu(T^*) \qquad (4.5b)$$

$$T^* = \frac{T}{\varepsilon/k_B} \qquad (4.5c)$$

where;

M_W: Air molecular weight

T: Air temperature in Kelvin

σ and ε/k_B: Lennard-Jones parameters

A B

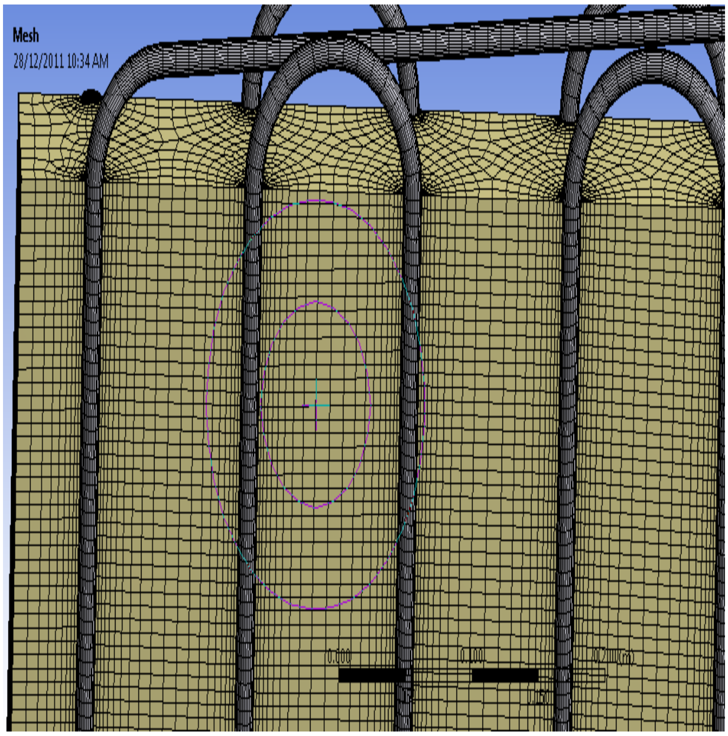

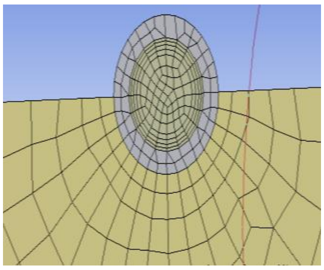

Figure 4.5: (A) Computational grid for the system, (B) The shape and distribution of the elements near the tube wall

4.3.1.3 Boundary Conditions and Operating Parameters

The boundary condition at the inlet was taken as "velocity-inlet". The velocity was 1.768 m/s (500 L/h flow rate), hydraulic diameter 0.01 m, turbulence intensity, I, 4.6% which is a function of the Reynolds number, R_e, and was computed from $I = 0.16(R_e)^{-1/8}$ (Gertzos, Caouris & Panidis 2010) and temperature 16.9^o C which was the average of the experimental inlet temperatures during the whole period. The boundary condition at the outlet was taken as "pressure-outlet" with atmospheric pressure. The interface between the tube wall and the water was defined as wall with coupled condition to allow the heat to transfer from the storage water to the tube wall and from the tube wall to the service water. The part of the service water tube outside the storage tank was assumed to be fully insulated. The boundary condition at the outer wall of the storage tank was taken as radiation to the laboratory wall with temperature of 20^o C and convection to the surrounding air with heat transfer coefficient, h_c=5 W/m^2K, and 20^o C temperature. The convective heat transfer coefficient for natural convection (h_c) was estimated using Kreith's equations (5.13) and (5.14) (2010, pp. 309-10), assuming that the tank wall temperature is 80^o C.

4.3.1.4 Validation Results

Two transient CFD simulations (for a one hour period) were studied; a Realizable k-ϵ turbulence model was used first and a standard k-ω second. At every five seconds of the solution, the average temperature at the outlet, T_out, average temperature of the storage water, T_ta, and the temperature at points T_1, T_2, T_3 and T_4 were recorded.

Figures 4.6 and 4.7 present the service water outlet temperature and the average storage water temperature for k-ϵ and k-ω models respectively, against the experimental results. Figures 4.8, 4.9, 4.10 and 4.11 show the numerical and experimental temperatures of the points T_1, T_2, T_3 and T_4 for both models. There was good agreement between the experimental and the numerical results using both models. However, the percentage error, which was calculated from equation (4.6), for k-ϵ model was higher than k-ω model. It varied between zero (no errors) and 15 percent for k-ϵ and zero to 8.5 percent for k-ω model. For both models, the maximum percentage of error appeared in the outlet temperature. This finding agrees with the finding of Gertzos and Caouris (2007) who also tested different turbulence models. Therefore, k-ω model was used in the optimization of the heat exchanger.

$$percentage\ error = \frac{T_{CFD} - T_{exp}}{T_{exp}} \times 100 \qquad (4.6)$$

where;

T_{CFD}: Temperature from CFD simulation

T_{exp}: Temperature from experiment

It is important to notice that there are other sources of error, resulting in a difference between the experimental and numerical results. These sources can be summarized as follows:

1. Thermocouple accuracy was ±1^{o} C and flow meter accuracy was ± 0.35%
2. In the experiment, the inlet service water temperature was in the range of 16.5-17.8^{o} C. For simplicity, in the numerical simulation, the inlet service water temperature was assumed to be 16.9^{o} C which was calculated by taking the average of the experimental inlet temperatures during the whole period
3. The heat transfer coefficient was assumed to be constant at 5 W/m^{2}K for the outer wall of the tank during the whole simulation period, because it was calculated with the assumption that the temperature of the tank wall as 80^{o} C. Due to the decrease in the storage water temperature, the temperature of the wall decreased as the time progressed.

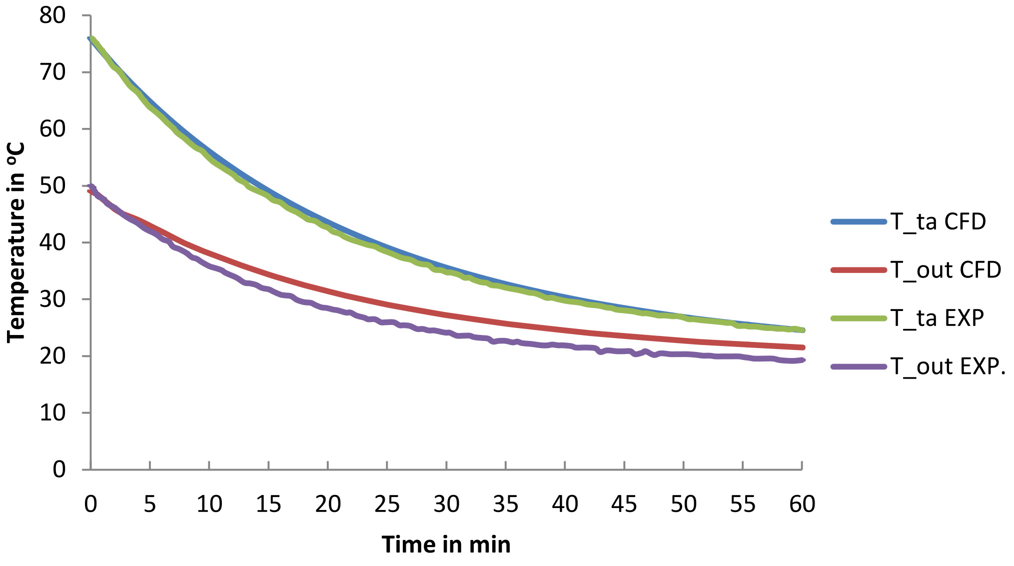

Figure 4.6: Comparison of the experimental outlet and storage temperatures with the numerical temperatures using the k-ϵ turbulence model

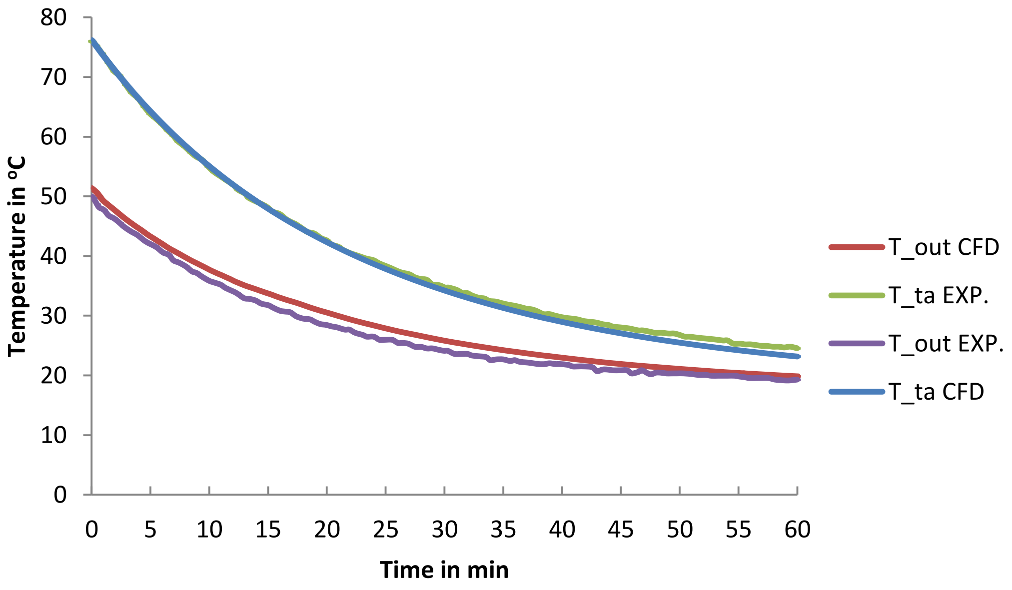

Figure 4.7: Comparison of the experimental outlet and storage temperatures with the numerical temperatures using the k-ω turbulence model

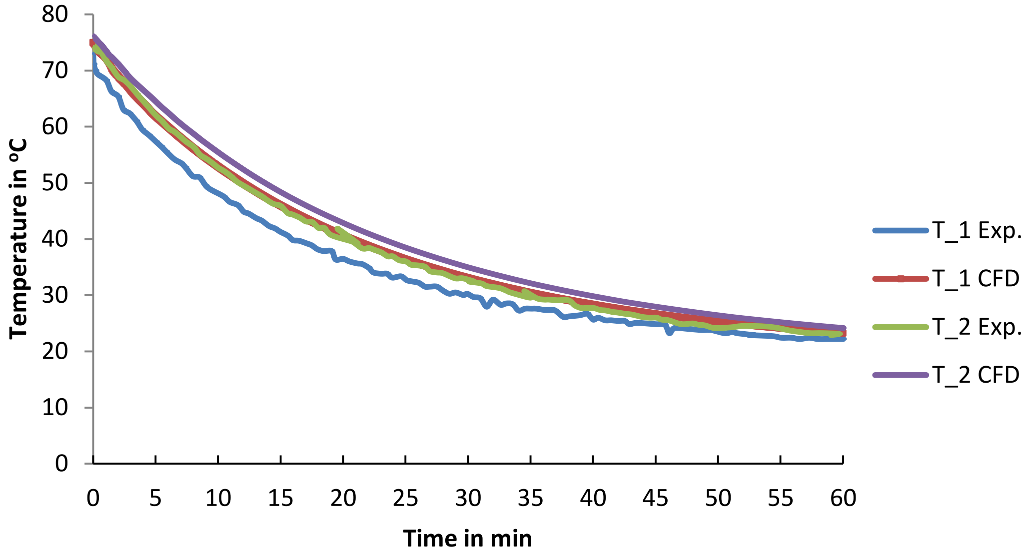

Figure 4.8: Comparison of the experimental temperatures at points T_1 and T_2 with the numerical temperatures using the k-ϵ turbulence model

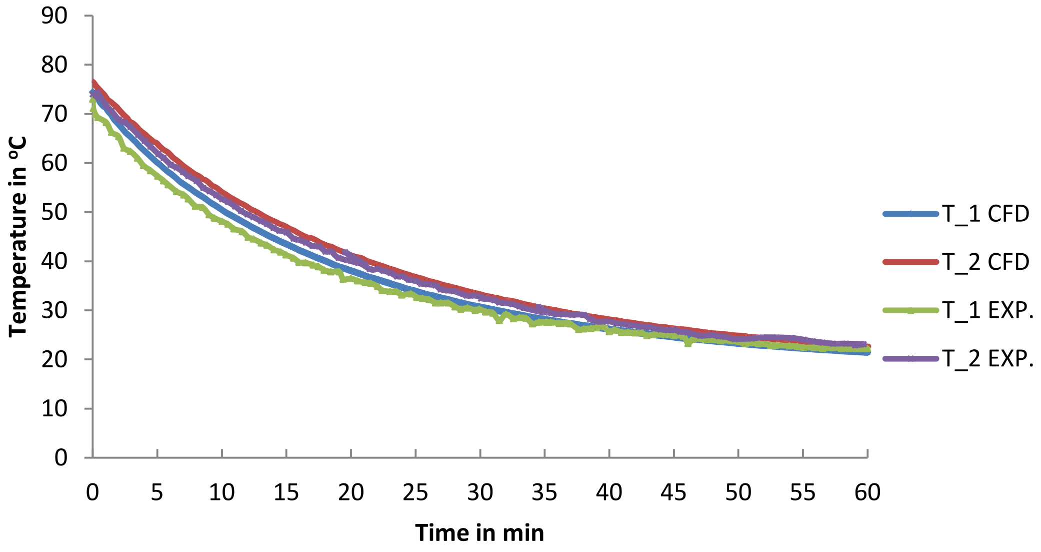

Figure 4.9: Comparison of the experimental temperatures at points T_1 and T_2 with the numerical temperatures using the k-ω turbulence model

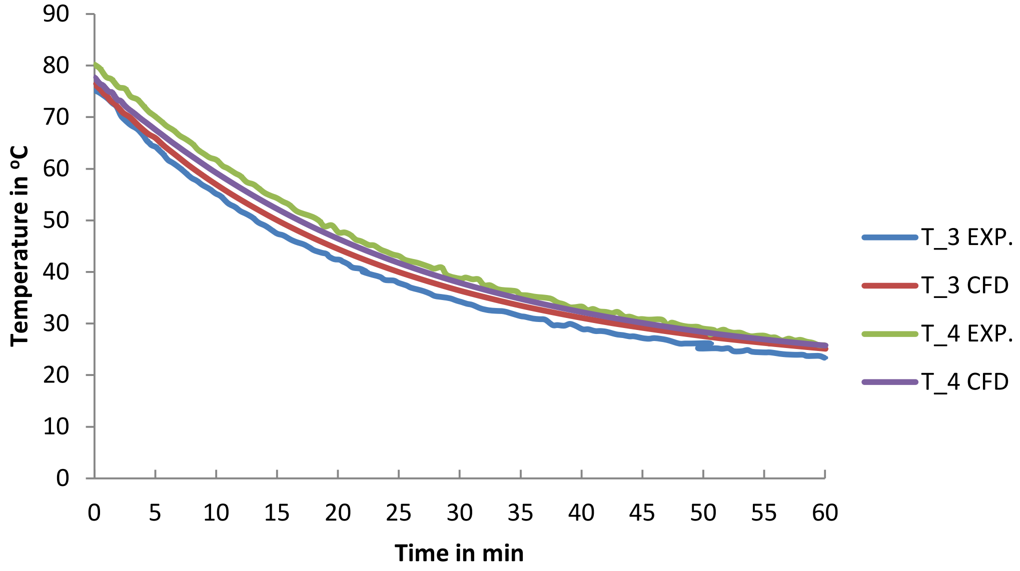

Figure 4.10: Comparison of the experimental temperatures at points T_3 and T_4 with the numerical temperatures using the k-ϵ turbulence model

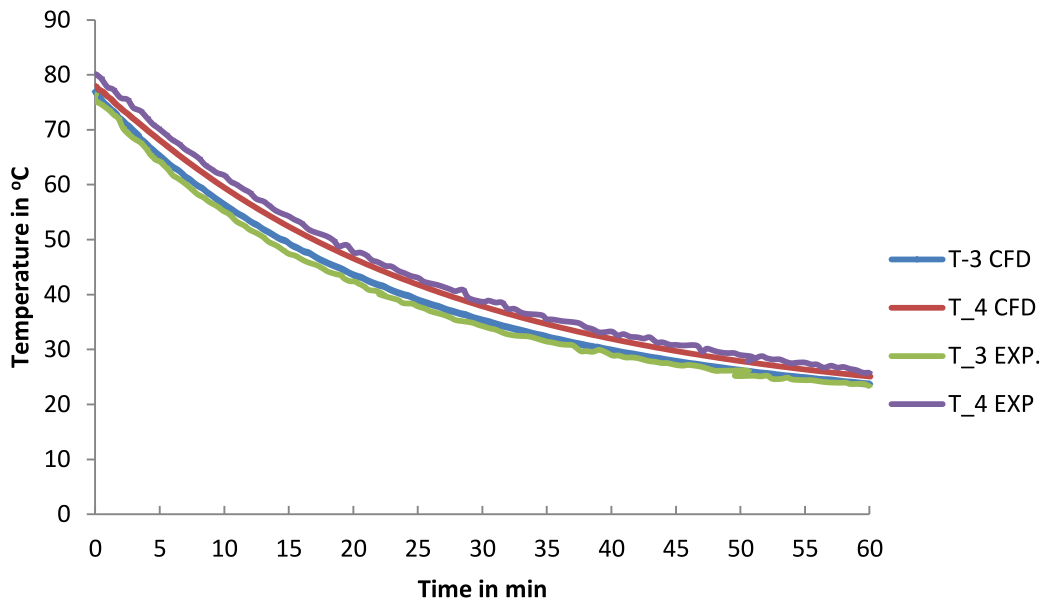

Figure 4.11: Comparison of the experimental temperatures at points T_3 and T_4 with the numerical temperatures using the k-ω turbulence model

The good agreement between the experimental and the numerical results, using the k-ω model confirms that the model can be used in this study with more confidence. The next step is to investigate different configurations of the heat exchanger to identify the optimum design.

4.3.2 Optimising the Heat Exchanger

The previous studies of the indirect heating system (Gertzos & Caouris 2007, 2008; Gertzos, Caouris & Panidis 2010; Gertzos, Pnevmatikakis & Caouris 2008) investigated the heat transfer between the storage and service water (without including the glass cover) and assumed that the temperature of the storage water was fixed at 60^{o} C for the steady state investigation. For the transient investigation, the initial temperature of the storage water was 60^{o} C or 80^{o} C. These studies also used a pump to circulate the storage water. The present study investigated the whole collector consisting of the double glass covers and the heat exchanger and without using circulating pump. This study used the assumption that the temperature of the absorber surface is constant at 60^{o} C which was considered to be more realistic than the previous assumptions (see Section 2.7).

The objective of this investigation was to identify the best tube position, length, diameter and shape that enhance the performance of the heat exchanger, while reducing both the initial and operating costs of the system. Enhancing the performance of the heat exchanger leads to maximising the energy acquired from solar radiation and reducing the pumping power. The following service water tubes were modelled:

1. Tube of double row heat exchanger (Figure 4.12) with length of 16.2 m
2. Tube of single row heat exchanger (Figure 4.13) with length of 8.1 and 10.8 m.

Three following tubes were chosen:

1. A circular copper tube type A DN 15 (1/2”) with an inside diameter of 10.7 mm and a wall thickness of 1 mm
2. A circular copper tube type B DN 20 (3/4”) with an inside diameter of 17.1 mm and wall thickness of 1 mm
3. A copper elliptical cross-sectional tube. The cross section area of the elliptical tube was equivalent to the area of a circular tube of 17.1 mm inside diameter with an aspect ratio of 2:1; i.e. the major radius of 12.092 mm, the minor radius of 6.046 mm, and the hydraulic diameter of 15.295 mm.

The service water volume flow rate was 500 and 650 L/h. Half of the tube was placed in the absorber surface and half in the storage water to enhance the heat transfer between the absorber and the service water (Figure 4.14). The hypothesis for using the elliptical tube was to increase the area of contact with the heat source, i.e. the absorber surface and with the service water. This can enhance the heat transfer between the absorber and the service water.

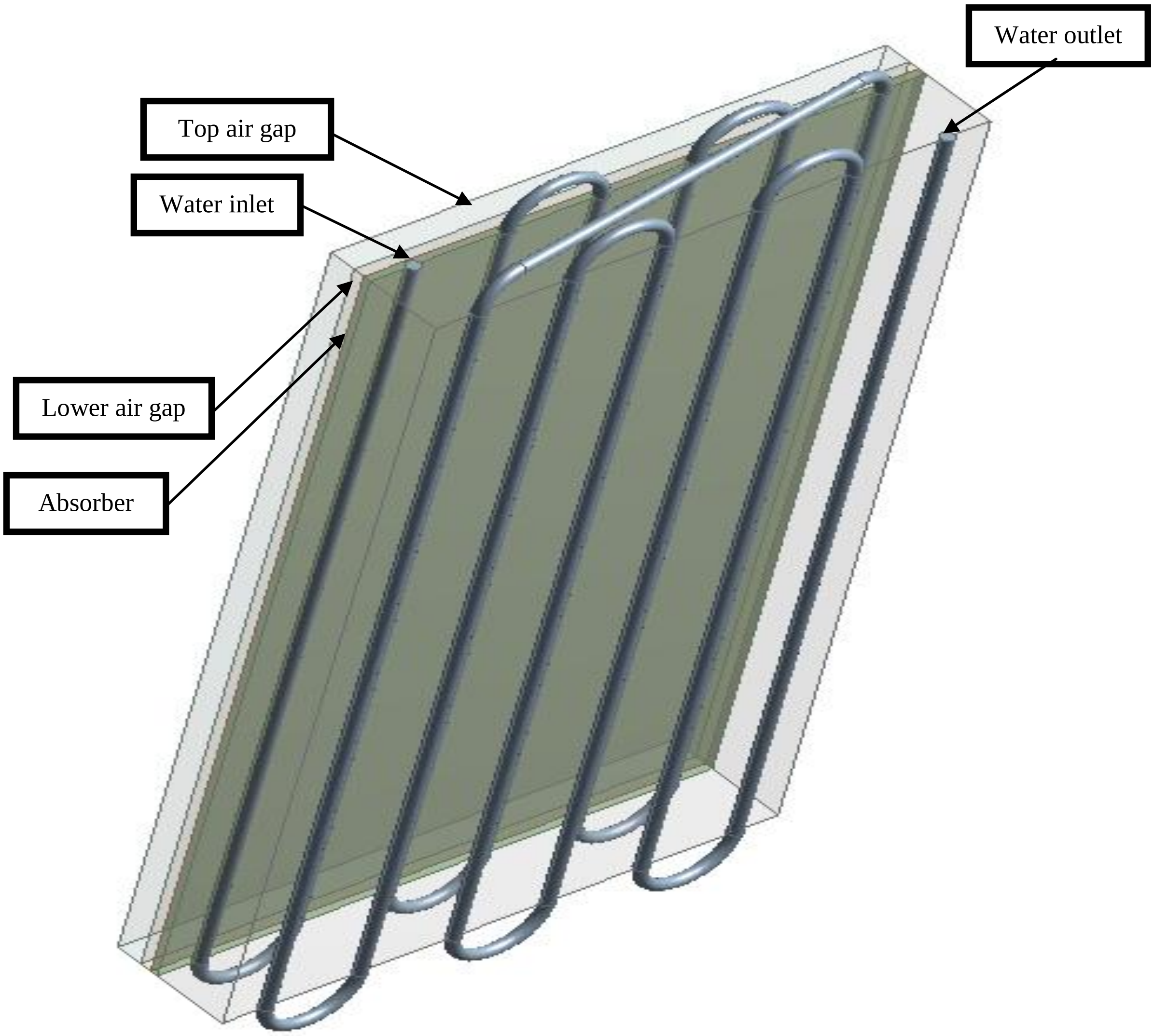

Figure 4.12: Indirect heating system with double row HX (16.2 m)

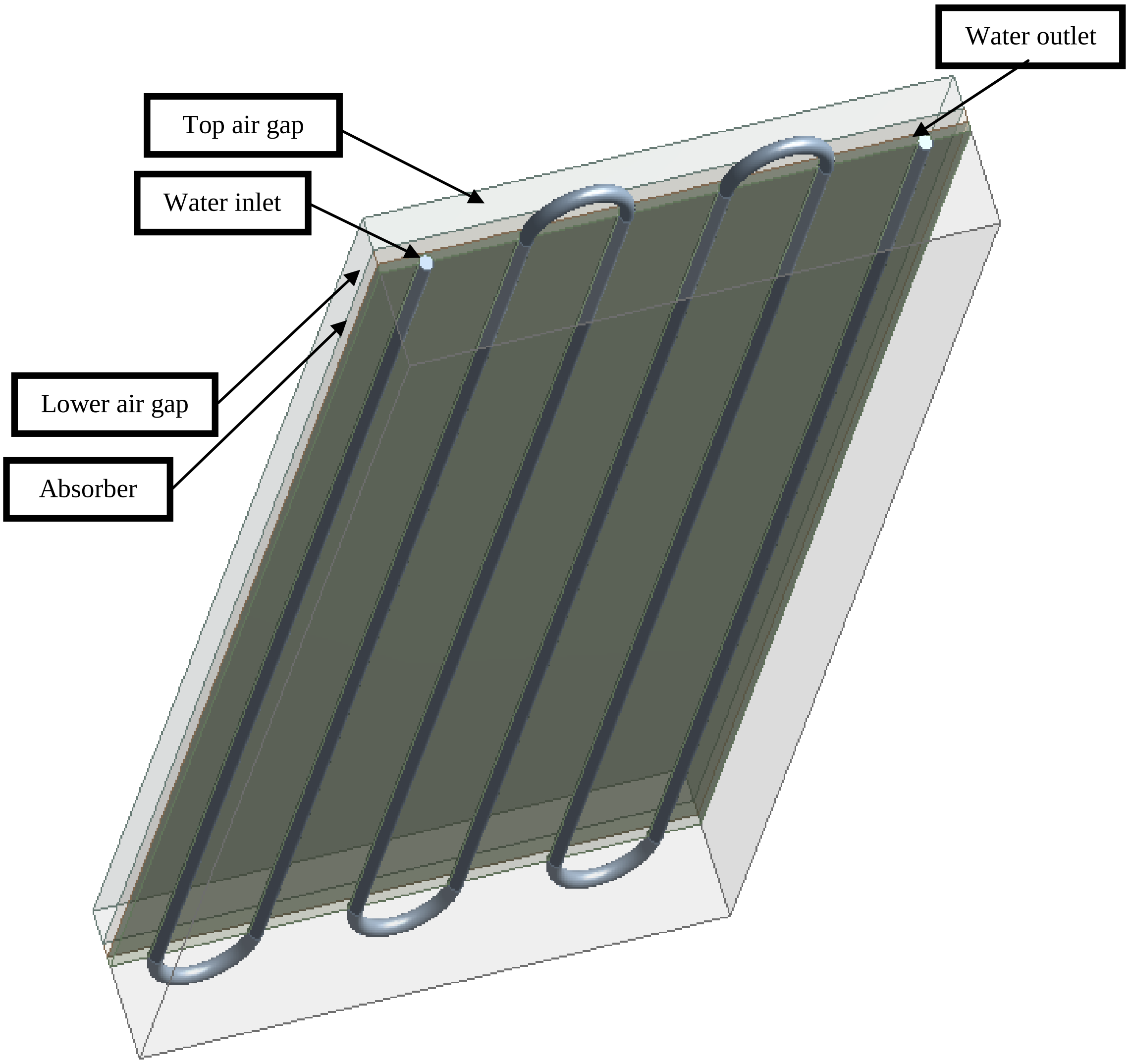

Figure 4.13: Indirect heating system with single row HX (8.1 m)

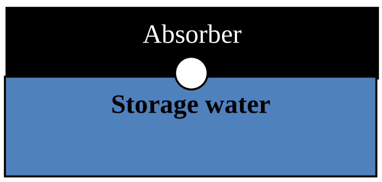

Figure 4.14: Tube placement in the collector

4.3.2.1 CFD Model

Steady 3D CFD models for two different configurations of the indirect heating integrated collector system have been developed to evaluate the heat gained by the service water. The geometry and computational grid were modelled using ANSYS-FLUENT 13.0 software. To validate the grid dependency, three computational grids were developed for the model of type A tube with double row HX; 2.5 million, 2.74 million and 3.125 million elements. The results of all three models were almost the same, but the model of 2.74 million elements converged faster than the others because the mesh quality was better. Therefore; the same methods used to generate the computational grid in the model of 2.74 million was applied for all other models.

The steady state continuity, momentum and energy equations were solved for the fluids involved in the model, i.e. the air in the gaps and the water inside the storage tank as well as inside the service water tubes. As the standard k-ω model gave a good agreement with the experiment, it was used in all of these cases. Surface-to-surface radiation model was included. The service water tube and tank wall were not included in the S2S model calculations.

4.3.2.2 Boundary condition and operating parameters

The boundary conditions on the upper glass cover were taken as convection with a heat transfer coefficient of 10 W/(m^2 K) to the ambient temperature, T_a=17^o C and radiation to the sky at a temperature which was calculated as T_s= 0.0552 $Ta^{1.5}$. A constant temperature of 60^o C was assumed for the absorber surface in all cases. The velocity of the service water at the inlet was varied to 0.604, 0.786, 1.544 and 2.00 m/s, as the mass flow rate and tube diameter varied and the inlet temperature was constant at 17^o C. The pressure at the outlet was taken as atmospheric pressure. The following interfaces were defined as wall with coupled condition to allow the heat to transfer through the walls:

1. Between the absorber and the service water tube
2. Between the absorber and the storage water
3. Between the service water tube and the storage water
4. Between the service water tube and the service water.

The collector angle was chosen to be 45^o. The upper and lower air gap spacing was taken as 35 and 15 mm, respectively, since it was found to be the most efficient combination (AL-Khaffajy & Mossad 2011).

4.4 Chapter Conclusion

The present study used ANSYS-13-FLUENT software to investigate the optimum air gap spacing and heat exchanger design in order to achieve an efficient system that possesses maximum heat gain by the service water, minimum heat loss, and low initial and running costs. The next chapter will present the results and a discussion of these investigations.

CHAPTER 5: Results and Discussion

- ***Introduction***
- ***Optimisation of the Air Gap Spacing***
- ***Optimisation of the Heat Exchanger***
- ***Chapter Conclusion***

5.1 Introduction

As previously mentioned, the objectives of this work are to enhance the thermal performance and to reduce both the initial and operating costs of the indirect heating integrated collector storage solar water heating system. ANSYS-13-FLUENT software was used to investigate the optimum air gaps sizes for the system of double glass cover, and the optimum heat exchanger configurations (i.e. service water tube position; length, diameter and the shape). The methods used for system modification were presented in Chapter 4. The results and discussion of these modifications are presented in two sections of this chapter:

1. Optimisation of the air gap spacing
2. Optimisation of the heat exchanger.

5.2 Optimisation of the Air Gap Spacing

Combinations of twelve cases were modelled as the lower air gap, L_1, and the upper air gap, L_2, were changed. L_1 was chosen to be 15, 25 and 40 mm and for each value of L_1, L_2 was chosen as 15, 25, 35 and 50 mm. Detailed velocity and temperature distributions for the air within the gaps and temperatures of the glass surfaces were obtained. Figures 5.1 and 5.2 present the velocity vectors for a horizontal plane in the middle of the top gap spacing for the case with L_1 equals to 15 mm and L_2 equals to 15 and 50 mm, respectively. These figures show that the air velocity increases as the gap spacing increases. However, to facilitate comparison, centre lines (in the z direction) were chosen at which these results are plotted in figures 5.4, 5.5 and 5.6.

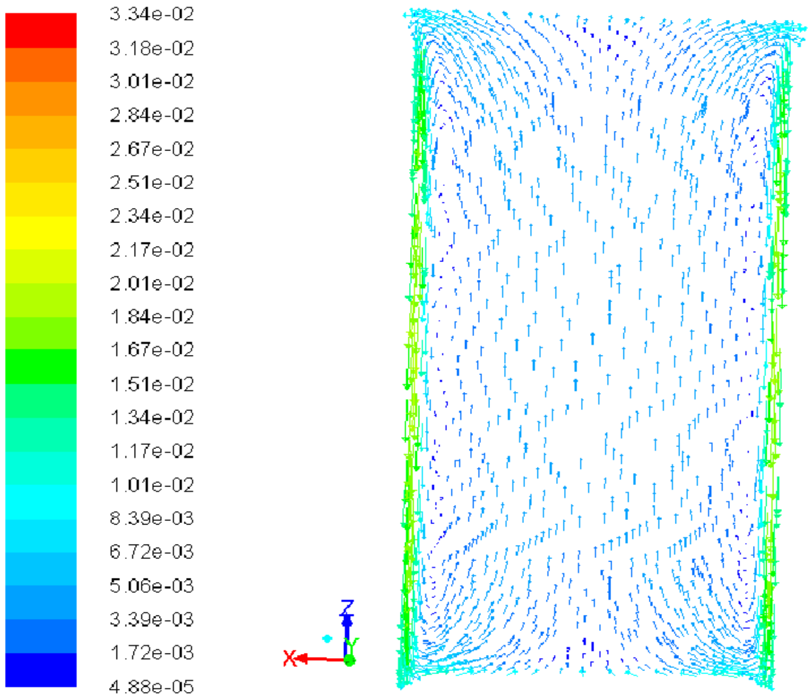

Figure 5. 1: Velocity vector (m/s) for a horizontal plane in the middle of top gap spacing for L_1=L_2= 15 mm

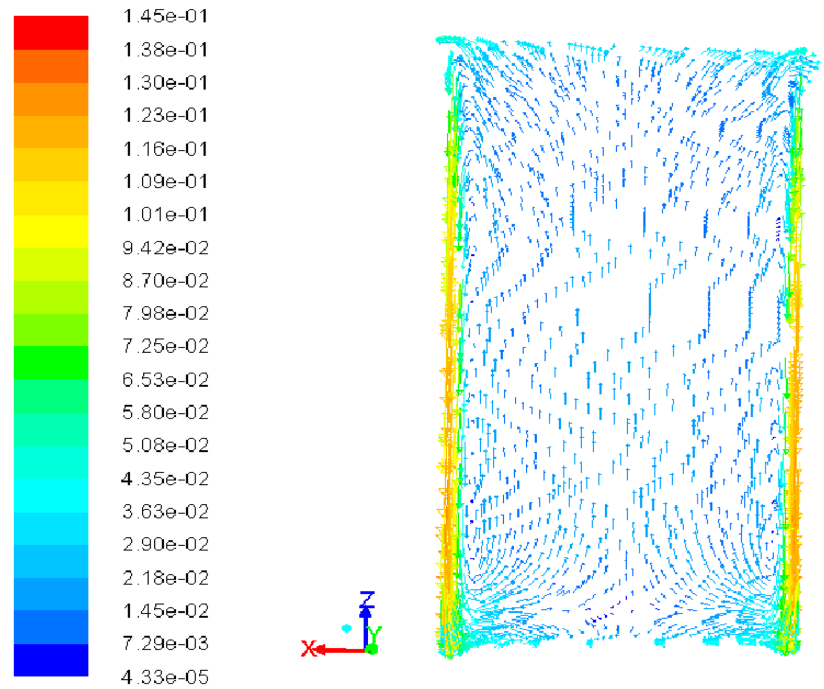

Figure 5. 2: Velocity vector (m/s) for a horizontal plane in the middle of top gap spacing for L_1=15 mm and L_2= 50 mm

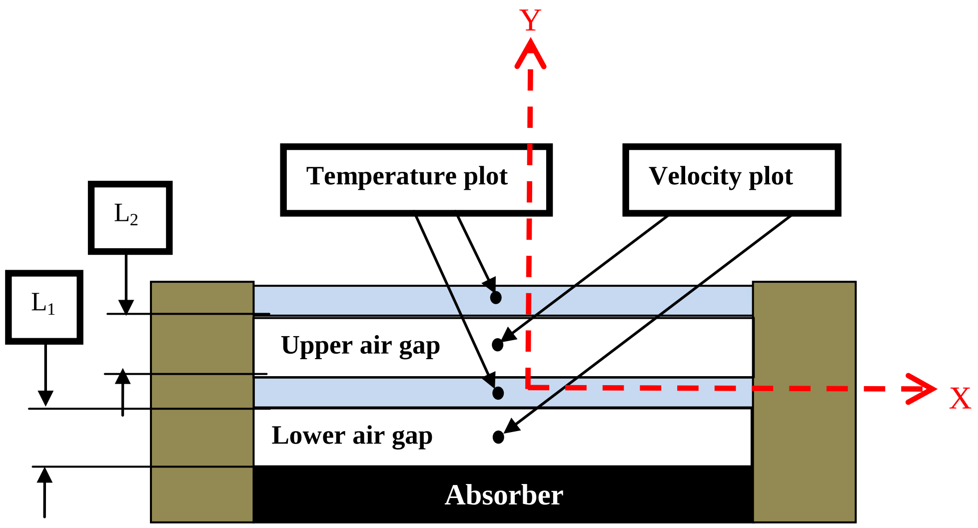

Figure 5.3: The points in which the velocity and temperature are plotted I prefer you bring this before the last two figures

For each case of changing L_1 and L_2, the velocity of the air in the middle of the upper and lower air gaps along the collector (in the z direction) was presented. The figures of these cases are as follows:

1. Figures 5.4 presents the air velocity for the case of 15 mm L_1 and 15, 25, 35 and 50 mm L_2
2. Figure 5.5 presents the air velocity for the case of 25 mm L_1 and 15, 25, 35 and 50 mm L_2
3. Figure 5.6 presents the air velocity for the case of 40 mm L_1 and 15, 25, 35 and 50 mm L_2.

The results showed that as the upper gap spacing was changed, there was no change in the air velocity of the lower gap. The air velocity in the lower gap did not change as the top gap spacing was changed (Figure 5.4 A). This behaviour was the same for the air velocity in the upper gap which did not change, when the lower gap spacing was changed (Figures 5.4B, 5.5B and 5.6B).

The upper and lower air velocity became higher as the upper and lower gap spacing increased, respectively. Comparing Figures 5.4a and 5.5a, one can observe that as the lower gap spacing changed from 15 to 40 mm, the velocity in the lower gap spacing increased from 0.009 m/s to 0.016 m/s. Similarly, as the upper gap spacing increased, the air velocity in the upper gap increased (Figure 5.4b, 5.5b and 5.6b).

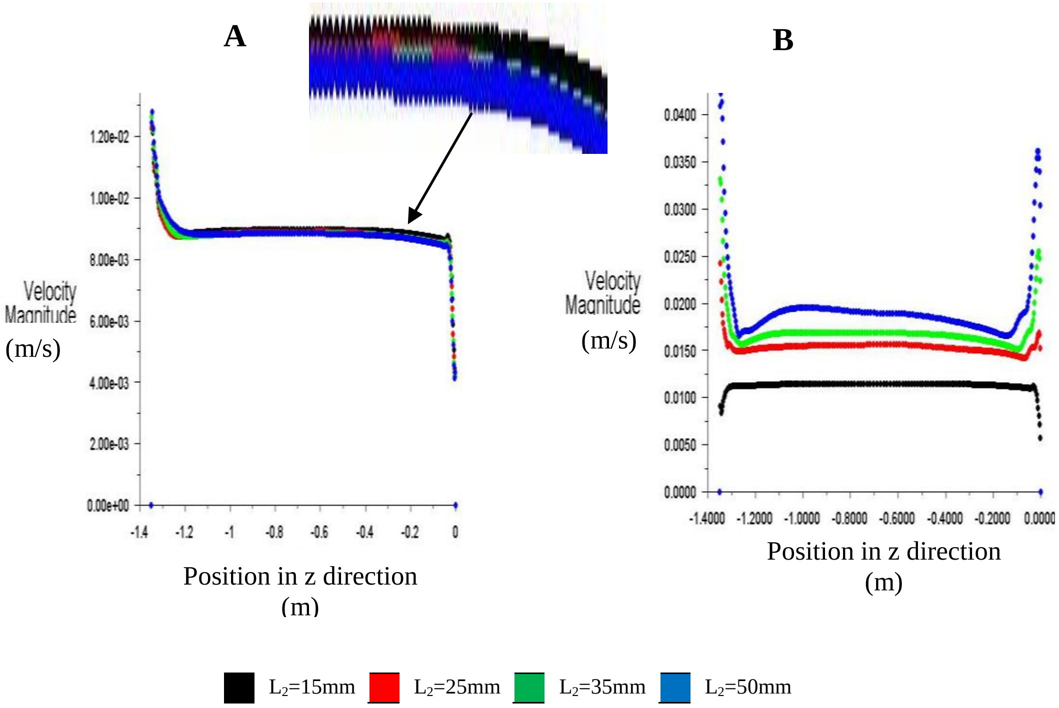

Figure 5.4: (A) Velocity in the middle of lower gap L_1=15 mm and different L_2, (B) Velocity in the middle of upper gap as L_2 changed and L_1=15 mm

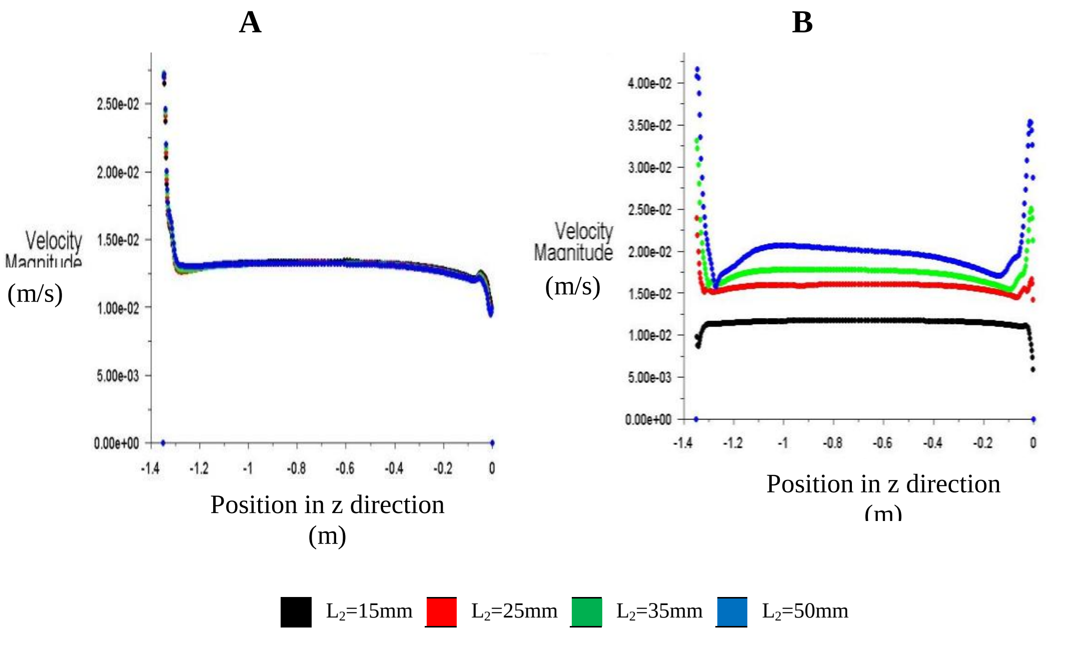

Figure 5.5: (A) Velocity in the middle of lower gap L1=25 mm and different L_2; (B) Velocity in the middle of upper gap as L_2 changed and L_1=25 mm

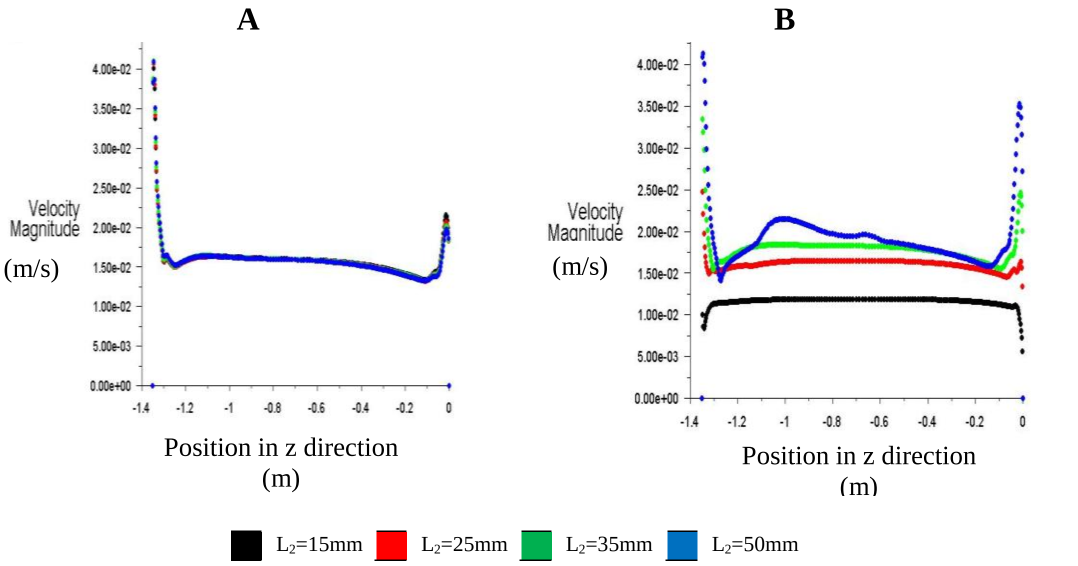

Figure 5.6: (A) Velocity in the middle of lower gap L_1=40 mm and different L_2; (B) Velocity in the middle of upper gap as L_2 changed and L_1=40 mm

Figures 5.7 and 5.8 present the temperature contours for plane in the middle of the lower and top gap spacing, respectively, for the case of L_1 =15 mm and L_2= 50 mm. From these figures, it is observed that the air close to the side walls has much lower temperature than in the middle. This is due to the effect of the low ambient temperature and the heat losses due to convection to the ambient air and radiation to the sky as per the thermal boundary condition applied at the side walls.

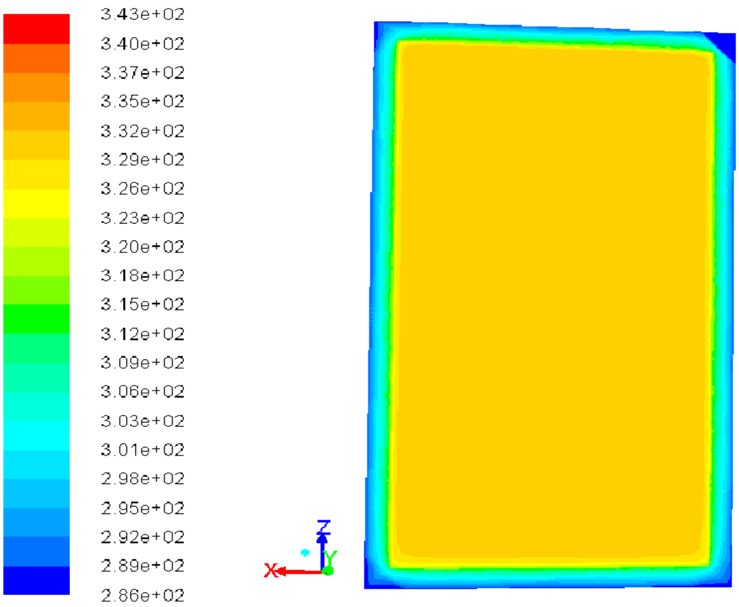

Figure 5. 7: Temperature contours (K) for a plane in the middle of lower gap spacing for L_1=15 mm and L_2= 50 mm

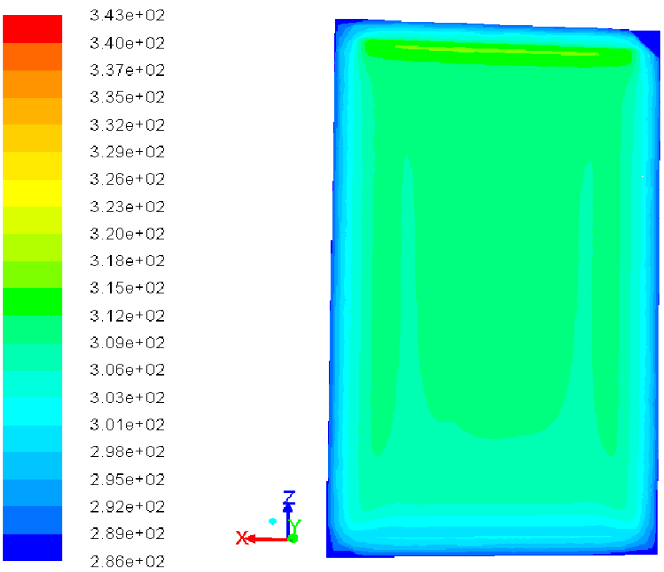

Figure 5. 8: Temperature contours (K) for a plane in the middle of top gap spacing for L_1=15 mm and L_2= 50 mm

To facilitate comparison, the temperatures of a line in the centre (in the z direction) of the upper and lower glass cover for each case of changing L_1 and L_2 are presented. The figures of these cases are as follows:

1. Figure 5.9 presents the temperatures of upper and lower glass covers for the case of 15 mm L_1 and 15, 25, 35 and 50 mm of L_2
2. Figure 5.10 presents the temperatures of upper and lower glass covers for the case of 25 mm L_1 and 15, 25, 35 and 50 mm L_2
3. Figure 5.11 presents the temperatures of upper and lower glass covers for the case of 40 mm L_1 and 15, 25, 35 and 50 mm L_2.

The temperature of the lower glass for all of L_1 values increased when L_2 increased from 15 to 25 mm and remained constant as L_2 increased further (Figures 5.9a, 5.10a and 5.11a). The increase in the temperature of the lower glass may be due to the heat transfer within the upper gap at the 15 and 25 mm which was dominated by conduction, as can be seen by the low air speeds (Figures 5.4b, 5.5b) and this enhanced the insulation effect as the gap increased in size. The further increase in the upper gap size, L_2, caused some natural convection to take place. This added to the effect of the conduction and caused a reduction in the insulation effect. As a result, no more increase in the lower glass temperature was absorbed.

From Figures 5.9b, 5.10b and 5.11b, the temperature of the upper glass decreased as L_2 increased for all L_1 values. As the distance between the surfaces i.e. absorber, lower and upper glass increased, the view factor between them decreased (Figure 5.12) and hence the radiation heat transfer decreased. Moreover, as L_1 and L_2

increased the heat losses from the side walls increased as their area increased. These two factors led to the reduction of the temperature of the upper glass cover.

The convection current in the air gap is affected by the temperature difference across the gap and the size of the gap. As the size of the upper gap, L_2, increased, the upper glass temperature decreased. Consequently, the temperature difference between the upper and lower glass increased. This can explain the increase in the air velocity within the gap, as the gap spacing increased (Figures 5.4b, 5.5b and 5.6b).

Figure 5.4 A is connected to figure 5.9A. As the lower glass temperature increases, the temperature difference between the absorber and lower glass decreases (the absorber temperature is fixed). This leads to decreased velocity in the lower air gap because the velocities are driven by the natural convection. This behaviour can be seen in these two figures. When L_2 was 15 mm the lower glass temperature was the lowest (Figure 5.9A), while the velocity was the highest (Figure 5.4 A).

To see whether the flow is laminar or turbulent, the Rayleigh number was estimated and found to be 1.4×10^7 when the gap was 15 mm. The Rayleigh number increased to 7.8×10^7 when the gap became 50 mm. This indicates a fully turbulent flow (Kreith, Frank. 2010, p. 318). The fully turbulent flow condition is one of the requirements to use k-ϵ model, as mentioned in Chapter 3. These results also confirm Manz's (2003) findings that increasing the Rayleigh number leads to increased velocity of the air in the gap.

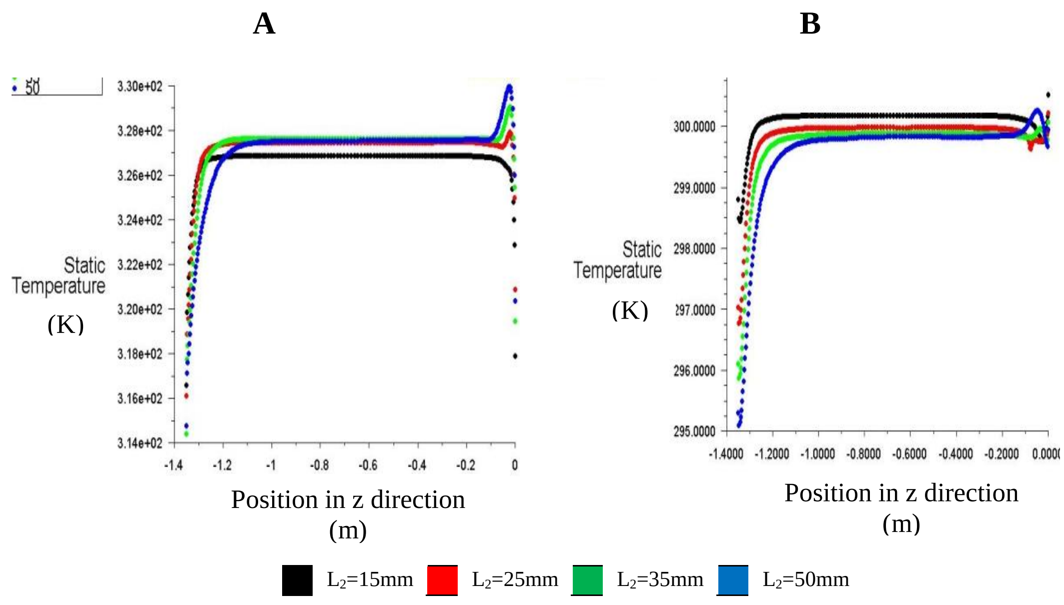

Figure 5.9: (A) Temperature of lower glass (middle of the glass) for L_1=15 mm as L_2 changed; (B) Temperature of top glass for L_1=15 mm and L_2 changed

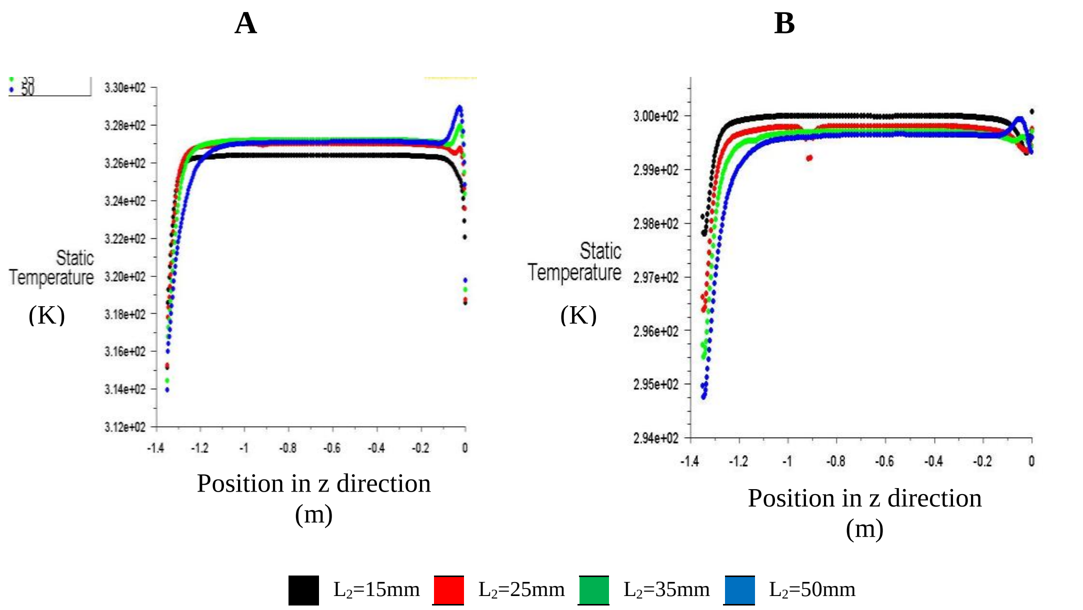

Figure 5.10: (A) Temperature of lower glass (middle of the glass) for L_1=25 mm as L_2 changed; (B) Temperature of top glass for L_1=25 mm and L_2 changed

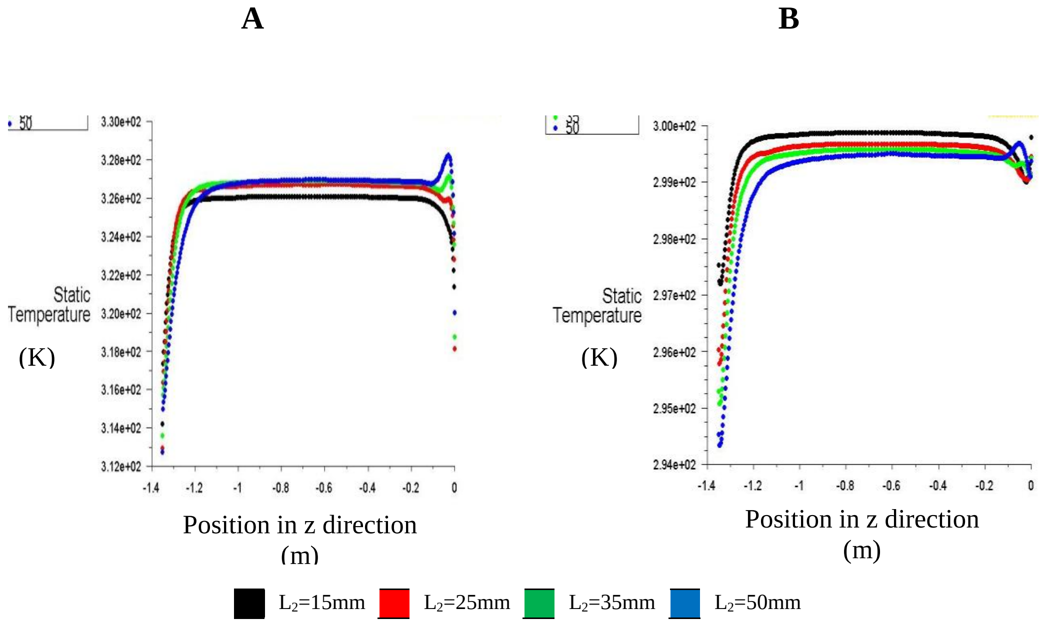

Figure 5.11: (A) Temperature of lower glass (middle of the glass) for L_1=40 mm as L_2 changed; (B) Temperature of top glass for L_1=40 mm and L_2 changed

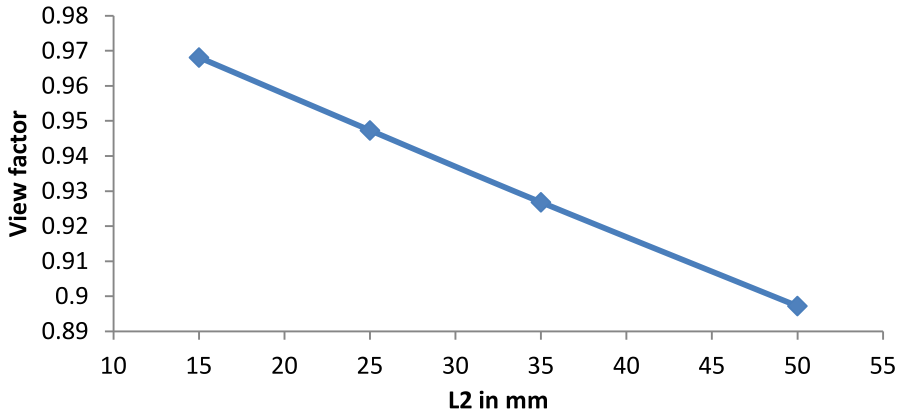

Figure 5. 12: View factor between the lower and upper glasses as L_2 changed

As mentioned previously, the solar collector effectiveness will be enhanced if heat loss is reduced. In order to estimate the effectiveness of the glass covers in reducing the heat losses, the total heat loss from the upper glass and the side walls were estimated for all modelled cases. The heat losses include convection to the ambient air and radiation to the sky. The total heat loss from the upper glass, as L_1 and L_2 were changed, is given in Figure 5.13. The heat loss from the side wall is given in Figure 5.14. The heat loss from the upper glass dropped as the air gap spacing increased because of its reduction in temperature (Figure 5.9b, 5.10b and 5.11b). The heat loss from the side wall increased as the gap spacing increased due to the increasing wall area.

The total heat losses from the upper glass and side walls are given in Figure 5.15. To identify the optimum air gap spacing, it is important to consider the total heat loss from the system which equals the heat loss from the upper glass due to convection and radiation plus the heat lost through the side walls (both the lower and upper parts). The total heat loss increased as L_1 increased for all L_2 cases, while it decreased when L_2 increased from 15 to 35 mm for all L_1 cases and increased when L_2 becomes higher than 35 mm.

The effect of the side wall on the amount of heat was small when L_2 and L_1 were lower than 35 mm because the curve follows the same behaviour of the top glass losses, i.e. heat loss decreased as the gap spacing increased (Figure 5.13). However, the effect of the side wall on the amount of heat started to be crucial when L_1 and L_2 became higher than 35 mm. This can explain the big jump in the amount of heat losses when L_1 increased from 25 to 40 mm (Figure 5.15).

For L_2, The minimum heat loss was achieved in the range of 30 and 35 mm (Figure 5.15). However, the result showed that the heat loss decreased as L_1 was decreased.

For this reason, L_1 was reduced to 10 mm to investigate the heat loss behaviour. A case of 10 mm for L_1 and 35 mm for L_2 was developed. The results showed that the heat loss increased as L_1 reduced to 10 mm (Figure 5.16). The increase in the heat loss was due to the increase in the view factor as the distance between the lower glass and the absorber decreased. This increased the radiation heat transfer from the absorber to the lower glass cover, as previously mentioned. The heat transfer due to convection had no effect on the total heat loss in the case of small gap spacing because the convection heat transfer was very small in comparison to the radiation. Therefore, the optimum lower gap spacing was found in the range of 15 and 20 mm and the optimum upper gap was found in the range of 30 and 35 mm.

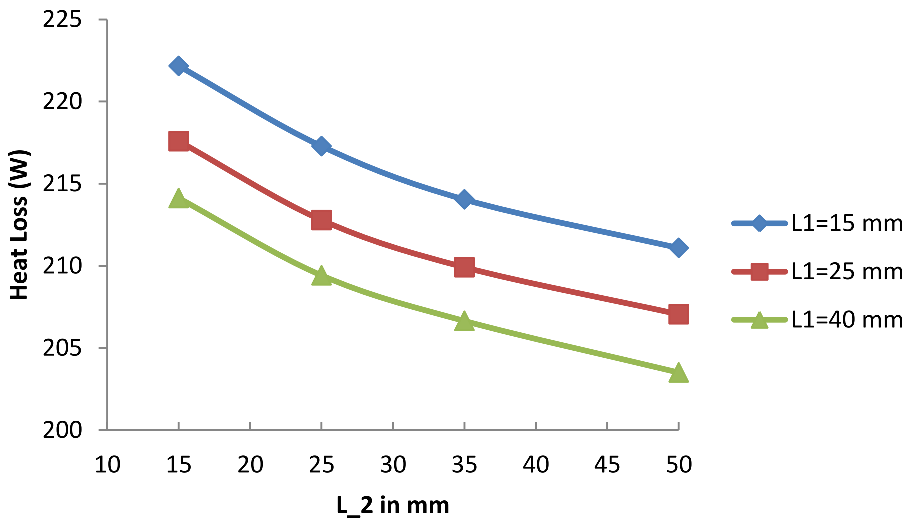

Figure 5.13: Heat loss from upper glass

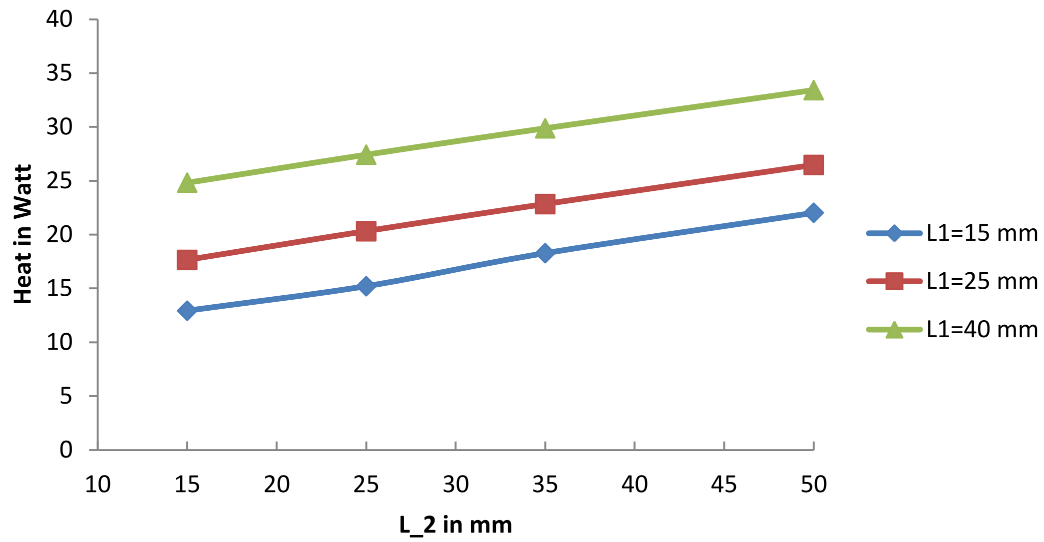

Figure 5. 14: Heat loss from side wall

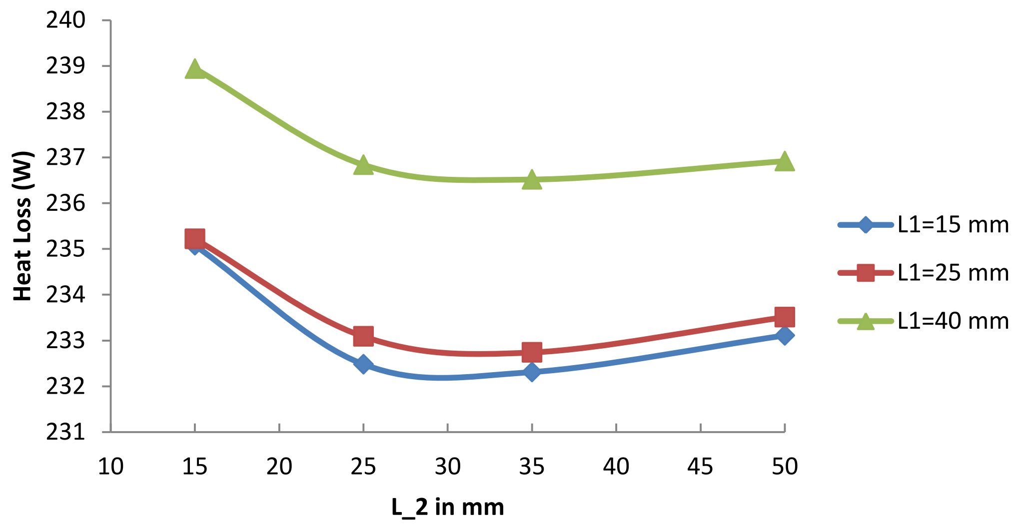

Figure 5.15: Total heat loss from upper and side wall

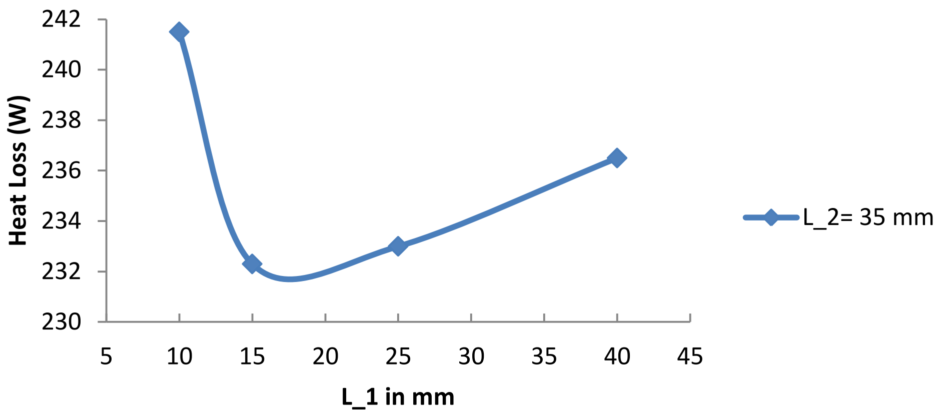

Figure 5.16: Total heat loss from upper and side wall (L_1 changed and L_2 constant)

5.3 Optimisation of the Heat Exchanger

Two configurations of the HX were investigated: double and single row HX. The effective length (of the tube inside the collector) for the tube in the double row HX was 16.2 m (Figure 4.12), in a single row HX was changed to 8.1 m and 10.8 m (Figure 4.13). Two circular pipe sizes were modelled; a copper tube type A DN 15 (1/2”) with an inside diameter of 10.7 mm and a wall thickness of 1 mm, type B DN 20 (3/4”) with an inside diameter of 17.1 mm and a wall thickness of 1 mm. An ellipse cross-sectional copper tube was also studied. The cross sectional area of the elliptic tube was equivalent to the area of a circular tube of 17.1 mm with an inside diameter and with an aspect ratio of 2:1; i.e. the major radius is 12.092 mm, the minor radius is 6.046 mm, and the hydraulic diameter is 15.295 mm. These cases were modelled, using ANSYS-13-FLUENT software. The results and discussion of these cases are given in this section.

Table 5.1 presents the service water outlet temperature; heat gained by the service water (q), power required to run the system and initial cost of the service water tube for all cases investigated. It was observed that heat gained increased as the mass flow rate increased, while the outlet temperatures for the higher flow rate was less than for the lower flow rate. This means that the increase in flow rate enhanced the heat exchange process, which is expected. The increase in the heat gained by the service water means increase in the energy acquired from solar radiation. Moreover, there was not much temperature difference (1-2^{o} C) between type A and B tubes, but there was up to 70 percent reduction in the power required when tube B was used. The elliptical tube gave higher outlet temperature than the circular one for the same length and same cross sectional area.

To choose the optimum HX configuration, many factors must be taken into consideration. These are: (1) the outlet service water temperature (2) power required to run the system as well as (3) the initial cost of the system. The tube cost and power required to run the system with single row HX and 8.1 m tube length for types A and B tube were almost half of the case for the system with double row HX, while the outlet temperature was the same (Table 5.1). Moreover, the temperature of the service water increased only in the front row of the double row HX and there was no increase in the temperature in the back row. This can be seen in the temperature contours of the service water for the double row HX type A and B tubes (Figure 5.17, 5.18, 5.19 and 5.20). The temperature behaviour was the same for both mass flow rates when type A and B tubes were investigated. Thus, the double row HX is not considered to be an efficient design because of the high initial and running costs with little thermal gain.

Table 5.1: Outlet temperature, heat gained by the service water (q), power required and cost for different tubes for inlet water temperature of 17^o C and absorber temperature of 60^o C

	Outlet Temp. and q for 500 L/h	Outlet Temp. and q for 650 L/h	Power required (W)		Tube Cost (AUD)
			500 L/h	650 L/h	
Double row HX type A tube of 16.2 m length	56^o C q= 22.6 W	54^o C q= 27.9 W	8.2	16.95	126
Single row HX type A tube of 8.1 m length	56^o C q= 23.7 W	54^o C q= 27.9 W	4.1	8.4	61
Single row HX type A tube of 10.8 m length	58^o C q=23.7 W	56.9^o C q=30 W	5.4	11.3	81
Double row HX type B tube of 16.2 m length	54^o C q=21.45 W	52.3^o C q=26.6 W	1.3	2.4	188
Single row HX type B tube of 8.1 m Length	54^o C q=21.45 W	52^o C q=26.3 W	0.86	1.4	90
Single row HX type B tube of 10.8 m Length	57^o C q=23.2 W	55.75^o C q=29.2 W	1	1.82	121
Elliptical tube of 8.1 m length	55.7^o C q=22.4 W	54^o C q=27.9 W	0.9	1.5	N/A
Elliptical tube of 10.8 m length	57.9^o C q=23.7 W	56.8^o C q=30 W	1	1.8	N/A

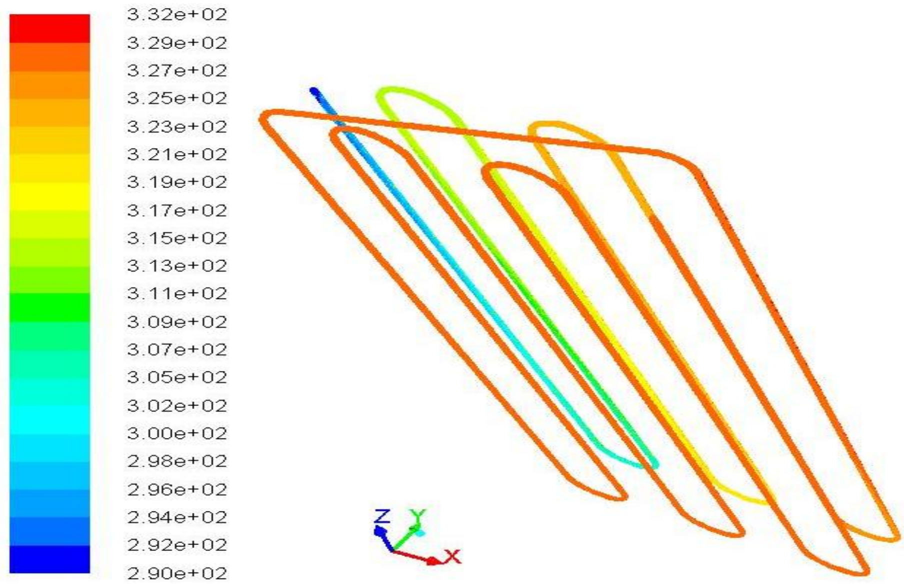

Figure 5.17: Temperature contours (K) of service water for tube A and flow rate 500L/h

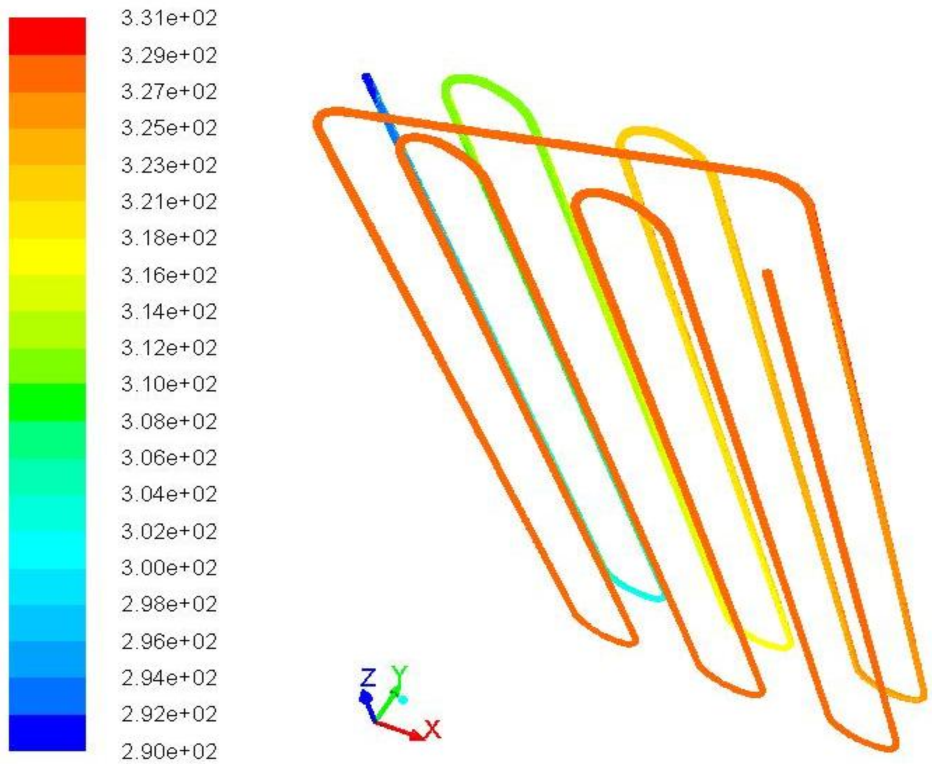

Figure 5.18: Temperature contours (K) of service water for tube A and flow rate 650 L/h

Figure 5.19: Temperature contours (K) of service water for tube B and flow rate 500 L/h

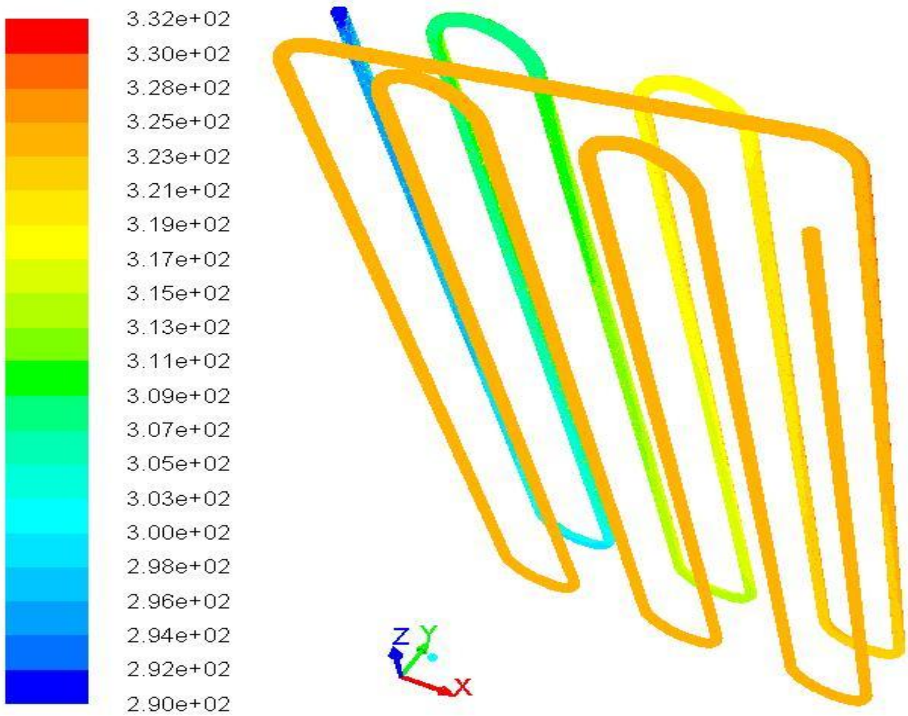

Figure 5.20: Temperature contours (K) of service water for tube B and flow rate 650 L/h

To increase the outlet temperature and hence reach an acceptable temperature for domestic use, 2.7 m was added to the tube in the front row (i.e. in the absorber side). As a result, the temperature increased by 2-3 degree for type A and B tubes (Table 5.1). However, pumping power, initial costs and running costs also increased. The increase in the power required for type B tube (0.4 W) was lower than for type A tube (3 W), as type B tube has a bigger diameter. For both mass flow rates and for a tube length of 10.8 m, the outlet temperature for type B tube was one degree lower than type A tube. The running cost for the type A tube was five times higher than for the type B tube, but the initial cost of type B tube was slightly higher than A. The advantages of lower initial cost for the type A tube systems is expected to be quickly overtaken by the high cost of operating these systems. As a result, type B tube systems are more economical than type A tube systems. Furthermore, adding 2.7 m to the front row (i.e. single row HX) was more effective than adding 8.1 m to the back row, i.e. double row HX.

For the elliptical tube, the outlet temperature was higher than the circular one for the same length and same cross section area (Table 5.1). This can be attributed to the area in contact with the absorber surface being bigger. The power required for the system of elliptic tube was similar to the system of type B tube, because the service water velocity was similar in both tubes. The elliptical tube with 10.8 m length gave the outlet temperature of 57.9 and 56.8^{o} C for Re=1.27 x 10^4 and Re=1.658 x 10^4 respectively. This gave a very small temperature difference (2-3 degree) between the absorber and the service water outlet temperature, while still running with low operating power (1 and 1.8 W, Table 5.1). Therefore, using the elliptical tube increased the outlet temperature by one degree without any increase in the running cost.

Figures 5.21, 5.22, 5.23, 5.24, 5.25 and 5.26 present the temperature contours of the service water for the cases of the single row heat exchanger, for the three types of tube and for both investigation flow rates. In these cases, the tube length was proved to be efficient because the temperature continued to increase along the tube.

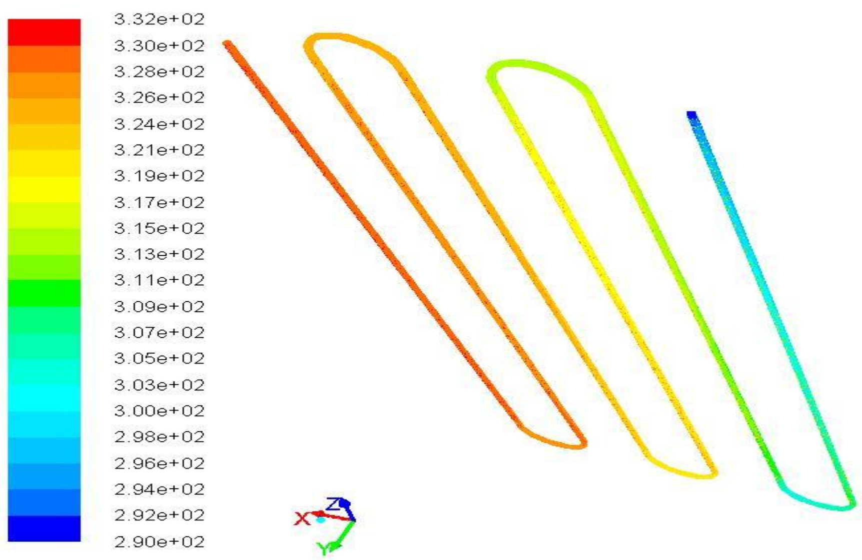

Figure 5.21: Temperature contours (K) of service water for single row HX, tube A and length 8.2 m and flow 500 L/h

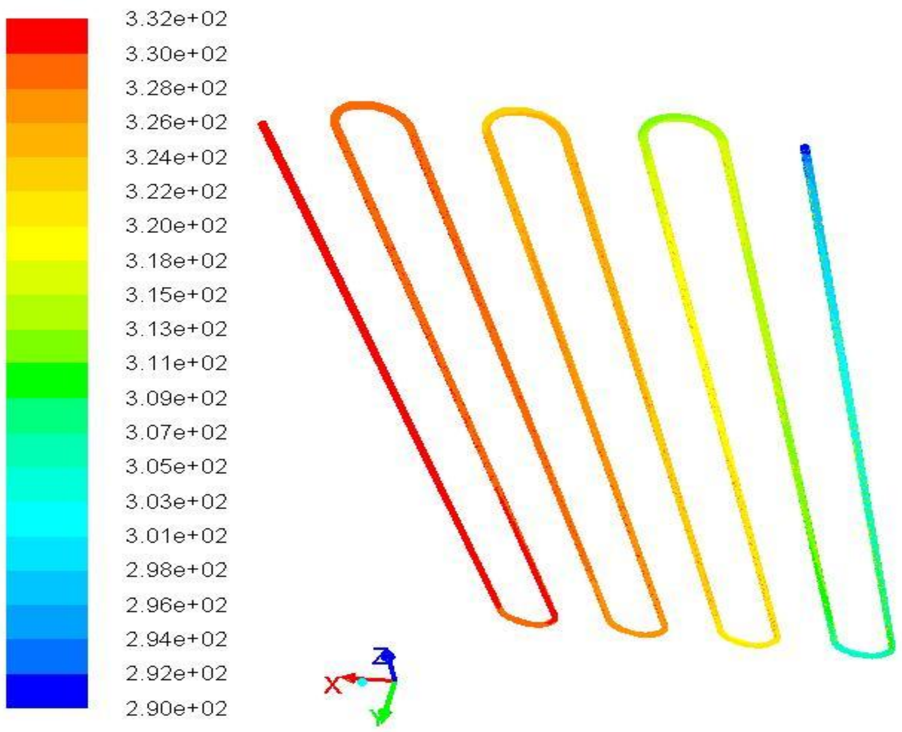

Figure 5.22: Temperature contours (K) of service water for single row HX, tube A and length 10.8 m and flow 500 L/h

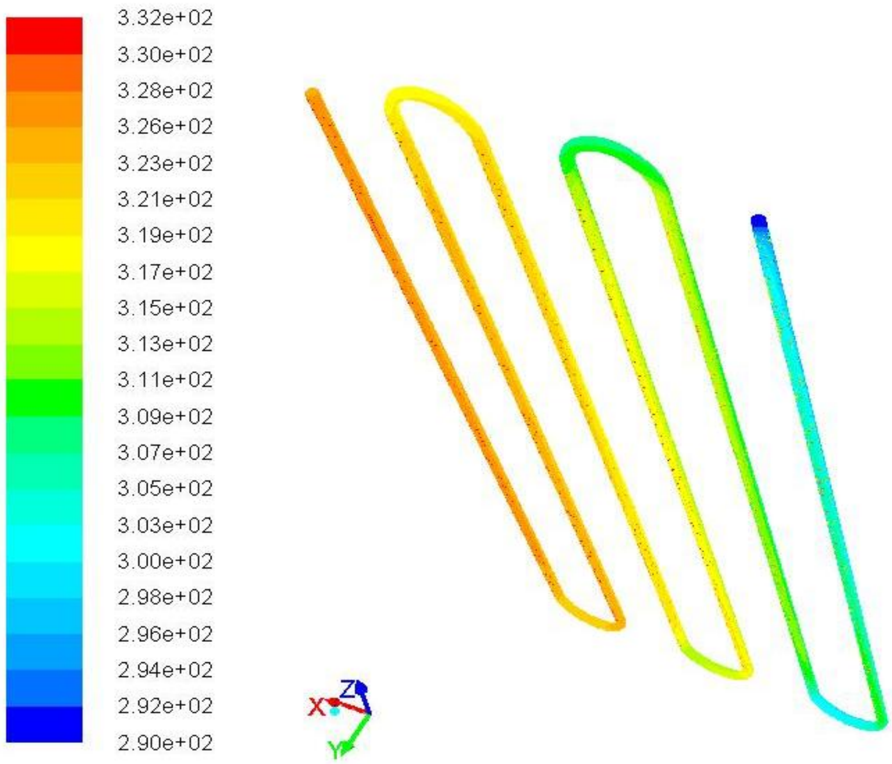

Figure 5.23: Temperature contours (K) of service water for single row HX, tube B and length 8.2 m and flow 650 L/h

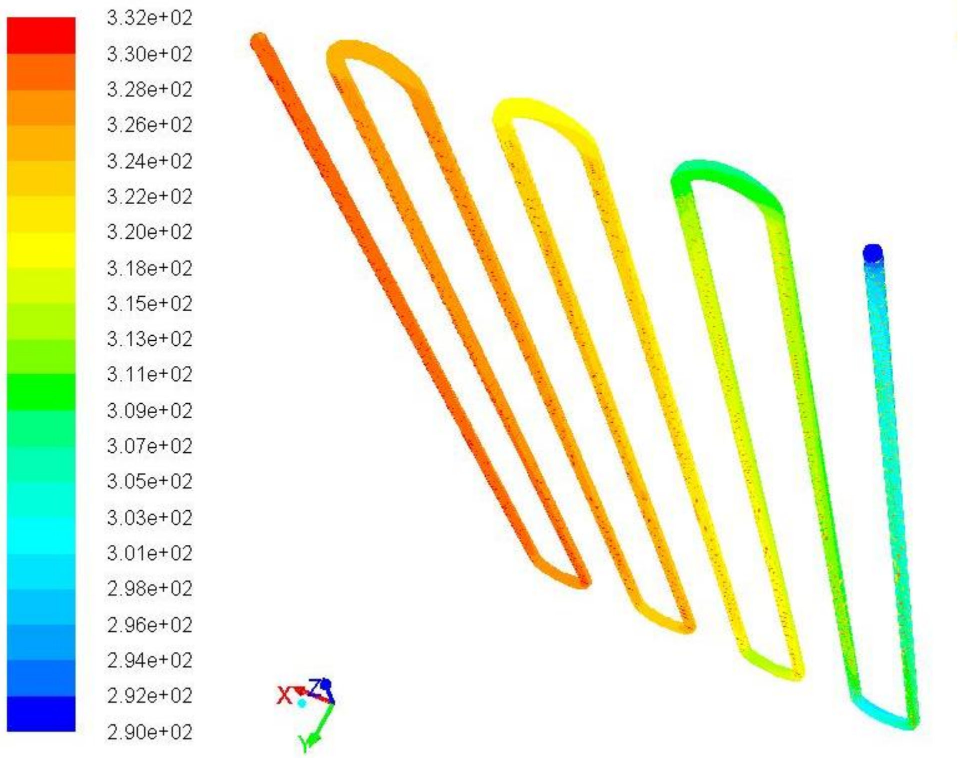

Figure 5.24: Temperature contours (K) of service water for single row HX, tube B and length 10.8 m and flow 650 L/h

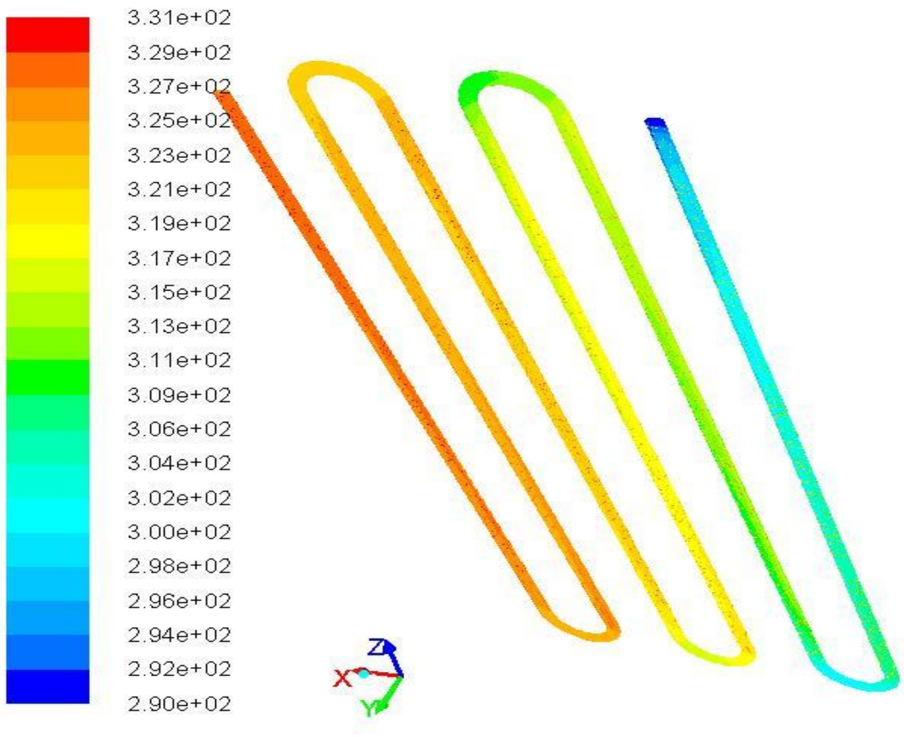

Figure 5.25: Temperature contours (K) of service water for single row HX, elliptical tube and length 8.2 m and flow 650 L/h

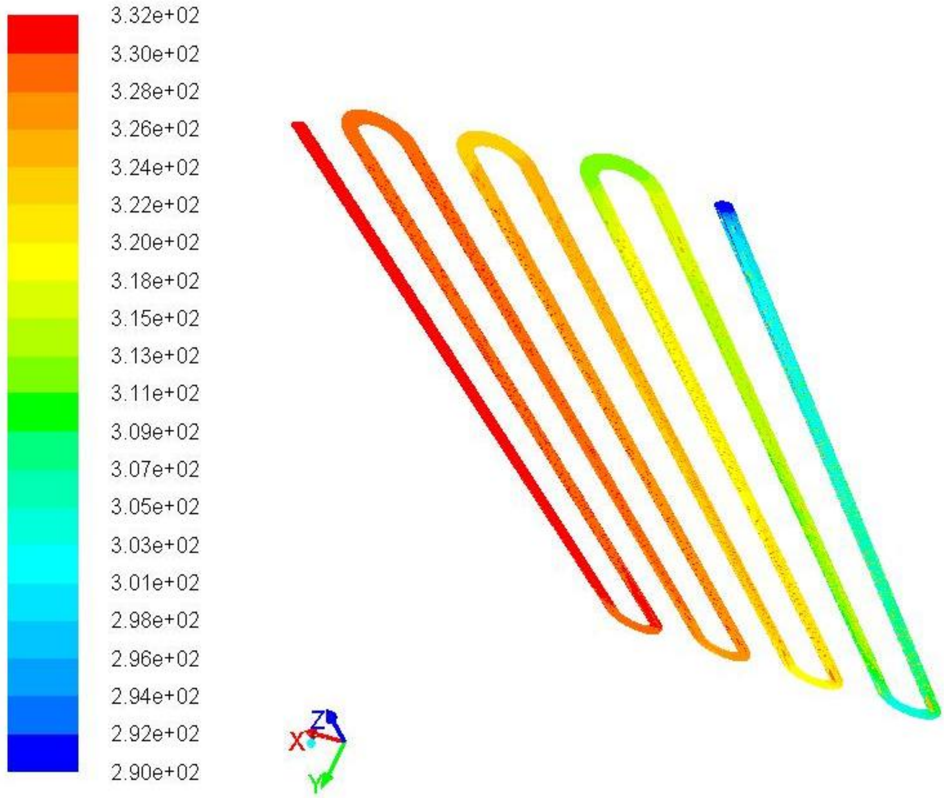

Figure 5.26: Temperature contours (K) of service water for single row HX, elliptical tube, length 10.8 m and flow 500 L/h

Figures 27 and 28 present a vector plot for the velocity in the z-x plane and z-y plane, respectively for the case with type B tube, 10.8 m length and 650 L/h flow rate. These figures show the storage water circulation due to natural convection. Due to the high absorber temperature, the water near the absorber showed the highest velocity reaching 0.3 m/s (Figure 28).

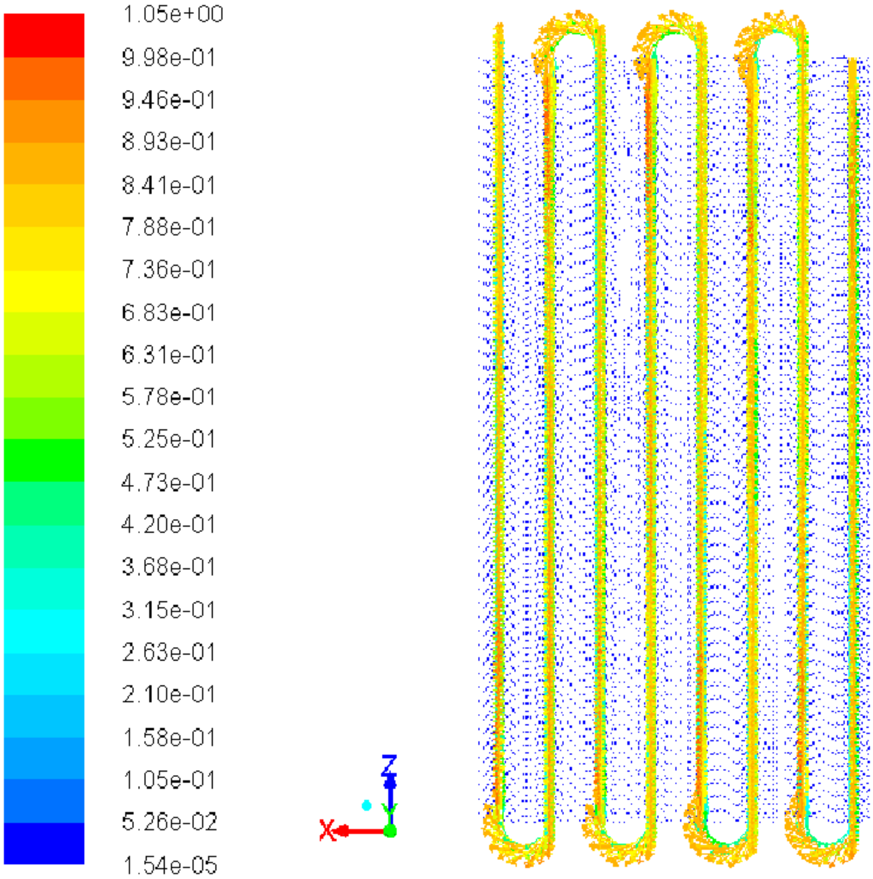

Figure 5. 27: Z-X plane of velocity vector (m/s) for tube type B with 10.8 m and 650 L/h mass flow rate

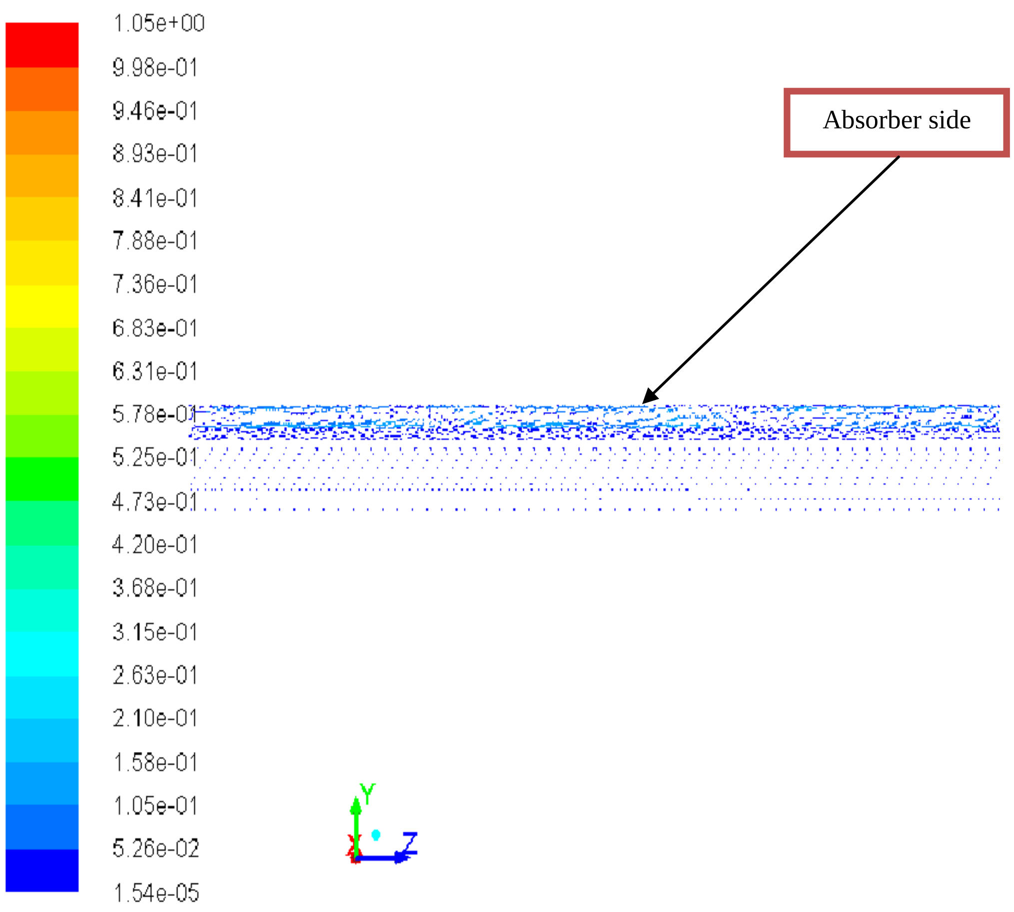

Figure 5. 28: Z-Y plane of velocity vector (m/s) for tube type B with 10.8 m and 650 L/h mass flow rate

The system of single row heat exchanger with tube length of 10.8 m and with type A, B and elliptical tubes produced high outlet temperature without a circulating pump. In heat exchanger systems, when the temperature difference between the cold and hot fluids is reduced to lower than 6 degrees, the heat exchanger configurations are acceptable (Gertzos, Caouris & Panidis 2010). In this study, the difference between the absorber temperature (the heat source) and the service water outlet temperature (cold fluid) was reduced to a range of 2.1^{o} and 6^{o}, without using a circulating pump for the storage water. As the pump requires electricity and maintenance, eliminating the circulating pump reduced both the initial and the running costs.

The initial and operating costs were also minimized by reducing the service water tube length. According to Gertzos, Caouris and Panidis (2010), the optimum tube length was 21.68 m for the system with circulating pump (Section 2.5.2). However, the present study shows that the service water tube length can be reduced to 10.8 m, and the heat exchanger remains efficient because it produced an acceptable temperature difference. The absorber area and the volume of the storage water tank was the same for both the present study and previous studies (Gertzos & Caouris 2008; Gertzos, Caouris & Panidis 2010). Thus, the initial cost of the system was less, as the tube length was minimized and the running cost of the system was less, as the pumping power was reduced.

5.4 Chapter Conclusion

The efficiency of the indirect heating system was improved as:

1. The heat loss from the system was minimized. For the lower gap spacing, the optimum distance was found in the range of 15 and 20 mm and for the upper gap, the optimum size was found in the range of 30 and 35 mm.
2. The initial and running costs are reduced. The system of a single row heat exchanger with tube length of 10.8 m and with type A, B and elliptical tubes produced an acceptable temperature without the use of circulating pump
3. The service water outlet temperature increased. Adding 2.7 m tube length to the front row was more effective than adding 8.1 m in the back row, as the outlet temperature of the system with tube length of 10.8 m (single row heat exchanger) was higher than of 16.2 m (double row heat exchanger).

CHAPTER 6: Conclusion

Due to the increase in the world's population, human development, the increase in individual income, and the aspiration for more comfortable lifestyles, power consumption has increased significantly over the last three decades resulting in an increase in carbon emissions which was 25.5 $GtCO_2$ in 2003. Achieving the Millennium Development Goals for 2030 will require that the average carbon emissions for each individual be reduced to 3.7 tCO2/ year. Thus, the percentage of the energy generated by the renewable sources, including solar energy, must be increased and consumers must be encouraged to use renewable energy rather than other non-environmentally friendly resources. This can be achieved by introducing a more economical and efficient solar collector.

ANSYS 13.0-FLUENT software was used to identify the optimum configuration of the indirect heating integrated collector storage solar water heating system which is one of the most economical solar water heating systems. The continuity momentum and energy equations were solved in a steady state condition. The realizable k-ϵ and standard k-ω turbulence models, which are based on the Reynolds-average Navier Stokes equations, were used. The realizable k-ϵ model was used in the optimisation of the air gap spacing. The results for the particular system using the realizable k-ϵ and standard k-ω turbulence models were compared to available experimental results to determine the best model to use in the heat exchanger investigation. The percentage error for the numerical simulation of k-ϵ model was higher than for the k-ω model. The error varied between zero (no errors) and 15 per cent for k-ϵ, and zero to 8.5 per cent for k-ω model. Therefore, the standard k-ω model was used in the heat exchanger investigation.

Minimizing the heat loss and increasing the outlet service water temperature were the main objectives of this study, and were used as a measure of improving the thermal performance. The power required to operate the system was used as a measure of the running cost. The performance of the indirect heating system was enhanced in the following ways:

1. **Reduced heat loss from the system:**

   The heat loss from the system was reduced by identifying the optimum combination of the upper and lower air gap spacing. The lowest radiation and convection heat losses from the system were achieved in the range of 30 and 35 mm for the upper gap, and 15 and 20 mm for the lower gap

2. **Increased outlet temperature:**

   The heat gain by the service water was maximized by identifying the best cross-sectional shape of the tube and the placement of the tube. To meet the required temperature of the typical household, 2.7 m was added to the tube for both types A and B in the front row (i.e. in the absorber side). As a result, the temperature increased by 2-3 degrees. This gave an acceptable difference between the absorber surface temperature and the service water outlet temperature

The temperature was also increased when an elliptical tube was used. The elliptical tube gave a slightly higher outlet service water temperature (1^{o} C) than the circular tube for the same length and the same cross-sectional area. Thus, the service water tube area of contact with the absorber surface has important effect on the outlet temperature and hence on the thermal efficiency of the system.

3. **Reduced initial cost:**

   The chosen system gives high outlet temperature (that suits domestic household use) without a circulating pump and with a shorter service water tube. According to Gertzos, Caouris and Panidis (2010), the optimum tube length was 21.68 m for the system with a circulating pump for the storage water. However, the present study showed that the service water tube length of the system can be reduced to 10.8 m and the circulating pump is not required. The required temperature difference for an efficient heat exchanger design ($\leq 6^{o}$) was achieved in this study without using a circulating pump for the storage water. The absorber area and the volume of the storage water tank was the same for both the present study and previous studies (Gertzos & Caouris 2008; Gertzos, Caouris & Panidis 2010). Thus, the initial cost of the system is less because the circulating pump is not required and the service water tube length is shorter

4. **Reduced operating cost:**

   Using shorter tubes require less pumping power. The running cost in the single row heat exchanger was half that of the double row, and the outlet temperature for both configurations was the same. Extra length was added to the tube in the single row heat exchanger to meet the required outlet temperature. This slightly increased the pumping power. To overcome this problem, a bigger diameter tube was used (type B tube), reducing the pumping power by one fifth of type A tube. Thus, the high initial cost of the bigger diameter tube is quickly overtaken by a much lower operating cost. Moreover, as the system of this study runs without a circulating pump, it does not require electricity to operate the pump and pump maintenance.

The result of this study showed that the users of the indirect heating integrated collector storage solar water heating system can use the system with high thermal efficiency and low initial and operating costs. Consequently, consumers will be encouraged to use solar water heating system instead of the electrical systems.

6.1 Research limitations and recommendations

This study has some limitation, thus the author recommends the following:

1- This study was based on the assumption that the absorber temperature is constant, while in reality the temperature depends on the solar intensity and the rate of energy extraction. This study recommends investigating the system with more realistic assumption, including actual data for solar radiation in a particular location and flow rate of water for a medium family size

2- As the time of the study is limited, the experimental investigation of the optimum (final) system was not conducted. It is worthwhile to investigate this system experimentally

3- Another hypothesis need to be investigated that if the area of the absorber surface change, what will the optimum parameters be for the heat exchanger such as the tube length and diameter

4- Investigate an economical mechanism to change the angle of the solar heater to capture the solar energy in more efficient way. This will have to be able to sense the direction of the sun as it moves in the horizon at the particular location.

References

286W 2009, *Optimum-Energy Communities: Moving Towards Zero Dirty Energy!*, viewed 28 April 2011, <http://edro.wordpress.com/energy/286w/>.

Akhtar, N & Mullick, SC 2007, 'Computation of glass-cover temperatures and top heat loss coefficient of flat-plate solar collectors with double glazing', *Energy*, vol. 32, no. 7, pp. 1067-74.

AL-Khaffajy, M & Mossad, R 2011, 'Optimization of the Air Gap Spacing In a Solar Water Heater with Double Glass Cover', paper presented to 9th Ausralasian Heat and Mass Transfer Conference - 9AHMTC, Monash University, Melbourne, Vectoria, Australia 2-4 November

Anderson, JD 1995, *Computational fluid dynamics : the basics with applications*, McGraw-Hill series in mechanical engineering, McGraw-Hill, New York.

Ang, BW & Zhang, FQ 2000, 'A survey of index decomposition analysis in energy and environmental studies', *Energy*, vol. 25, no. 12, pp. 1149-76.

ANSYS 2009, *ANSYS FLUENT 12.0; Theory Guide*, ANSYS, Inc., United States, 20 July 2011, <http://www.ansys.com/>.

Blazek, J 2005, *Computational fluid dynamics : principles and applications*, 2nd ed. edn, Elsevier, Amsterdam.

BP 2011, *Reneable Energy*, viewed 28 April 2011, <http://www.bp.com/sectiongenericarticle.do?categoryId=9023767&contentId=7044196>.

Chakravarty, S, Chikkatur, A, de Coninck, H, Pacala, S, Socolow, R & Tavoni, M 2009, 'Sharing global CO2 emission reductions among one billion high emitters', *Proceedings of the National Academy of Sciences*, vol. 106, no. 29, pp. 11884-8.

Chen, Z, Gu, M, Peng, D, Peng, C & Wu, Z 2010, 'A Numerical Study on Heat Transfer of High Efficient Solar Flat-Plate Collectors with Energy Storage', *International Journal of Green Energy*, vol. 7, no. 3, pp. 326-36.

Chhanwal, N, Anishaparvin, A, Indrani, D, Raghavarao, KSMS & Anandharamakrishnan, C 2010, 'Computational fluid dynamics (CFD) modeling of an electrical heating oven for bread-baking process', *Journal of Food Engineering*, vol. 100, no. 3, pp. 452-60.

Department of Energy, US 2010, *Where Does My Money go?*, viewed 28 April 2011, <http://www.energystar.gov/index.cfm?c=products.pr_pie>.

Dreamstime 2012, *Stock Photography: Parabolic dish solar collectors*, Dreamstime viewed 12 April 2012, <http://www.dreamstime.com/stock-photography-parabolic-dish-solar-collectors-image16773042 >.

Duffie, JA 1991, *Solar engineering of thermal processes*, 2nd ed. edn, Wiley, New York.

Duffie, JA 2006, *Solar engineering of thermal processes*, 3rd ed. edn, Wiley, Hoboken, NJ.

Duffie, JA & Beckman, WA 2006, *Solar Engineering Of Thermal Processes*, 3rd edn, John Wiliam & Sons, INC New Jersey.

Elminir, HK, Ghitas, AE, El-Hussainy, F, Hamid, R, Beheary, MM & Abdel-Moneim, KM 2006, 'Optimum solar flat-plate collector slope: Case study for Helwan, Egypt', *Energy Conversion and Management*, vol. 47, no. 5, pp. 624-37.

Fotosearch 2010, *Solar panel stock photos and images*, Foto search Stock Photography and Stock Footage, viewed 5 May 2010, <http://www.fotosearch.com/photos-images/solar-energy.html>.

Gebreslassie, BH, Medrano, M, Mendes, F & Boer, D 2010, 'Optimum heat exchanger area estimation using coefficients of structural bonds: Application to an absorption chiller', *International Journal of Refrigeration*, vol. 33, no. 3, pp. 529-37.

Gertzos, KP & Caouris, YG 2007, 'Experimental and computational study of the developed flow field in a flat plate integrated collector storage (ICS) solar device with recirculation', *Experimental Thermal and Fluid Science*, vol. 31, no. 8, pp. 1133-45.

Gertzos, KP & Caouris, YG 2008, 'Optimal arrangement of structural and functional parts in a flat plate integrated collector storage solar water heater (ICSSWH)', *Experimental Thermal and Fluid Science*, vol. 32, no. 5, pp. 1105-17.

Gertzos, KP, Pnevmatikakis, SE & Caouris, YG 2008, 'Experimental and numerical study of heat transfer phenomena, inside a flat-plate integrated collector storage solar water heater (ICSSWH), with indirect heat withdrawal', *Energy Conversion and Management*, vol. 49, no. 11, pp. 3104-15.

Gertzos, KP, Caouris, YG & Panidis, T 2010, 'Optimal design and placement of serpentine heat exchangers for indirect heat withdrawal, inside flat plate integrated collector storage solar water heaters (ICSSWH)', *Renewable Energy*, vol. 35, no. 8, pp. 1741-50.

Gunerhan, H & Hepbasli, A 2007, 'Determination of the optimum tilt angle of solar collectors for building applications', *Building and Environment*, vol. 42, no. 2, pp. 779-83.

Khalifa, AJN & Abdul Jabbar, RA 2010, 'Conventional versus storage domestic solar hot water systems: A comparative performance study', *Energy Conversion and Management*, vol. 51, no. 2, pp. 265-70.

Kreith, F 2010, *Principles of heat transfer*, 7th ed., SI ed. edn, Nelson Engineerng, Clifton Park NY.

Kreith, F & Bohn, MS 2001, *Principles of Heat Transfer*, 6th edn, Brooks/Cole, USA.

Kumar, R & Rosen, MA 2010, 'Thermal performance of integrated collector storage solar water heater with corrugated absorber surface', *Applied Thermal Engineering*, vol. 30, no. 13, pp. 1764-8.

Kumar, R & Rosen, MA 2011, 'Comparative performance investigation of integrated collector-storage solar water heaters with various heat loss reduction strategies', *International Journal of Energy Research*, vol. 35, no. 13, pp. 1179-87.

Launder, BE & Spalding, DB 1972, *Lectures in mathematical models of turbulence*, Academic Press, London.

Lovegrove, K & Luzzi, A 2001, 'Solar Thermal Power Systems', in AM Robert (ed.), *Encyclopedia of Physical Science and Technology*, Academic Press, New York, pp. 223-35.

Manz, H 2003, 'Numerical simulation of heat transfer by natural convection in cavities of facade elements', *Energy and Buildings*, vol. 35, no. 3, pp. 305-11.

Mellouli, S, Askri, F, Dhaou, H, Jemni, A & Ben Nasrallah, S 2007, 'A novel design of a heat exchanger for a metal-hydrogen reactor', *International Journal of Hydrogen Energy*, vol. 32, no. 15, pp. 3501-7.

Mossad, R 2006, 'Numerical simulation to optimize the design of double glazed doors for closed refrigerated vertical display cabinets', paper presented to 13th International Heat Transfer Conference IHTC-13, Redding, CT, USA, 2006/08//.

Nakayama, A 1995, *PC-aided numerical heat transfer and convective flow*, CRC Press, Boca Raton.

Prabhanjan, DG, Raghavan, GSV & Rennie, TJ 2002, 'Comparison of heat transfer rates between a straight tube heat exchanger and a helically coiled heat exchanger', *International Communications in Heat and Mass Transfer*, vol. 29, no. 2, pp. 185-91.

Shih, T-H, Liou, WW, Shabbir, A, Yang, Z & Zhu, J 1995, 'A new k-[epsilon] eddy viscosity model for high reynolds number turbulent flows', *Computers & Fluids*, vol. 24, no. 3, pp. 227-38.

Smyth, M, Eames, PC & Norton, B 2006, 'Integrated collector storage solar water heaters', *Renewable and Sustainable Energy Reviews*, vol. 10, no. 6, pp. 503-38.

Steinberger, JK & Roberts, JT 2010, 'From constraint to sufficiency: The decoupling of energy and carbon from human needs, 1975-2005', *Ecological Economics*, vol. 70, no. 2, pp. 425-33.

Tiller, JS & Wochatz, V 1982, *Performance of Integral Passive Solar Water Heaters (Breadbox-Type) under Varying Design Condition in the Southeast U.S.*, Knoxville, USA.

Versteeg, HK & Malalasekera, W 2007, *An introduction to computational fluid dynamics: the finite volume method*, 2nd edn, Pearson Prentice Hall, Sydney.

Wilcox, DC 2006, *Turbulence modeling for CFD*, 3rd ed. edn, DCW Industries, La Cãnada Calif.